EXTERNAL FEEDBACK OPERATION

OF

SEMICONDUCTOR LASERS

EXTERNAL FEEDBACK OPERATION

OF

SEMICONDUCTOR LASERS

by

PAUL H. G. KEMPF, B.ENG.

A Thesis

Submitted to the School of Graduate Studies

in Partial Fulfillment of the Requirements

for the Degree

Master of Engineering

McMaster University

August 1984

MASTER OF ENGINEERING (1984) MCMASTER UNIVERSITY
(Engineering Physics) Hamilton, Ontario.

TITLE: EXTERNAL FEEDBACK OPERATION OF SEMICONDUCTOR LASERS

AUTHOR: Paul H. G. Kempf, B.Eng. (McMaster University)

SUPERVISOR: Professor B.K. Garside

NUMBER OF PAGES: vii, 158

ABSTRACT

The aim of this thesis is to contribute to the understanding of the dynamics of semiconductor lasers on a 10 to 100 ps time scale when their output is altered by external feedback. The optimization of parameters involved in optoelectronic feedback results in a reduction in the measured minimum pulse FWHM relative to previous work, and gives the conditions necessary to produce 25 ps FWHM optical pulses using this technique. To aid in the understanding of the modelocking of diode lasers, the CW spectral and threshold characteristics of a diode laser coupled to a mirror external cavity are examined. It is found that multiple reflections in the compound cavity cause an increase in mode linewidth with increasing bias current up to a maximum for a particular level of feedback for an external mirror coupled laser, but not for a grating coupled laser. As a result of the CW optical feedback analysis, grating feedback is utilized as a probe of the laser gain in a refinement of a previously reported technique for direct gain measurement. Also, the total loss reduction induced by external optical feedback is found to be made up of the sum of mirror loss and mode propagation loss reductions. This has significance in simulations of active modelocking and injection locking tuning characteristics carried out in this work. Simulations for active modelocking of a diode laser with low residual facet reflectivity in an external mirror cavity account for the previously unexplained

extreme sensitivity of the modelocking process to oscillator stability. Grating external cavity injection locking experiments and simulations present a new scheme for obtaining nearly transform limited optical pulses using semiconductor lasers.

ACKNOWLEDGEMENTS

I would like to express my appreciation for the help received from my supervisor, Dr. B. K. Garside, during the course of this thesis. Also, I would like to acknowledge the efforts of Dr. J. C. Goodwin whose earlier work provided the basis for most of the simulations done in this work. A special thanks to my friends at McMaster for just being, and to my parents for just caring.

TABLE OF CONTENTS

CHAPTER I

INTRODUCTION

Interest in the use of semiconductor lasers as picosecond optical sources for the investigation of ultrafast processes, the development of high speed optoelectronics, and specifically for their application in optical communications has resulted in extensive research concerning their operating characteristics. High data rate optical communications systems make use of the large bandwidth available at optical frequencies. Semiconductor lasers are appropriate light sources for optical communications because of their small size, reliability, and high drive efficiency. Their output wavelength dependence on composition also allows a matching of the near infrared operating wavelength to the low loss wavelength regions in communications grade glass fibres. Modern graded index single mode fibre causes losses of fractions of a dB per kilometer, and gives dispersion of tens of picoseconds per kilometer per nanometer of spectral width. A limitatation on maximum data rates and repeater spacing is imposed by the broad pulse spectrum typically associated with short, intense optical pulses from semiconductor lasers. Understanding the dynamic characteristics of semiconductor lasers and altering their output characteristics on a 10 to 100 ps time scale is therefore important in achieving higher data rate optical communications.

The work presented here is roughly divided into two sections. The first experimental part of this thesis is concerned with the optimization of the optical pulse full width at half maximum (FWHM) and intensity available from an optoelectronic feedback scheme. Regenerative pulsing using optoelectronic feedback provides a train of gain switched optical pulses at an inherently stable repetition frequency. The remainder of this thesis then deals with both continuous wave (CW) and pulsed operation of diode lasers coupled to external resonators. Knowledge of the effects of external feedback on the CW characteristics of diode lasers allows use of the feedback as a probe of the diode gain, and is crucial to the understanding of injection locked diode lasers in external resonators.

Chapter 2 briefly reviews the development of semiconductor lasers and gives background theory necessary to the discussions later in this thesis. A previously developed [1] rate equation model of the laser dynamics used as a basis for many of the simulations carried out in this work is also introduced in Chapter 2.

Chapter 3 presents an analysis of the optimum circuit parameters necessary to obtain short, intense optical pulses using optoelectronic feedback. This analysis includes experimental refinement of previous workers' attempts, and simulations which estimate the shortest possible optical pulses using this scheme.

Chapter 4 introduces CW optical feedback effects on semiconductor lasers. The spectral and threshold characteristics are measured for both

plane mirror and diffraction grating feedback, and are compared to a theory which includes the effects of multiple reflections in the external resonator. The results of this chapter are relevant to the discussion of CW and dynamic optical feedback effects in the remainder of this thesis.

In Chapter 5, CW grating external feedback is used as a probe of the optical gain of the laser diode. Interpretation of experimental results clarifies misconceptions in earlier work relating to the representation of the diode gain using a significant wavelength dependent absorption loss term. An effort is also made to investigate the agreement between the gain measured directly using grating feedback and a theoretical equation which gives the curvature of the gain.

Chapter 6 discusses oscillator stability considerations for active modelocking in a plane mirror external resonator using sinusoidal modulation at approximately 1 GHz. The change of optical pulse position with respect to the current modulation for the shortest, most intense optical pulses is investigated for various chip facet reflectivities using both experiments and simulations. The relative size of the mode propagation loss reduction to the actual mirror loss reduction induced by the external feedback is significant in the simulations of the tuning characteristics. It is found that strict oscillator stability requirements are necessary to obtain very short optical pulses ($\leq$ 10 ps) when a laser with low residual facet reflectivity ($R \simeq 0.01$) is used for active modelocking.

In Chapter 7, a comb generator which gives short (≃ 80 ps), high peak (≃ 10 V) pulses at a repetition frequency of 500 MHz is used in conjunction with several optical feedback schemes to find the conditions for producing short, high peak power, and spectrally narrow optical pulses. Grating external feedback injection locking is found to satisfy the above requirements. Simulations using a non-iterative approach to find self consistent injection locking solutions are shown to be in good agreement with measurements of the modulation tuning behaviour. Consideration of the actual magnitude of the mirror loss reduction relative to the total loss reduction using grating feedback is again shown to be important in simulations of the injection locking tuning characteristics.

A summary of the results of this thesis is given in Chapter 8.

CHAPTER 2

BACKGROUND

2.1 Introduction

This chapter is intended to give the reader who is unfamiliar with semiconductor lasers a brief history of their development and an overview of the principles involved in their operation.

2.2 Development of Laser Diodes

Interest in using semiconductor materials for lasers began in 1958. It was not until 1961, when Bernard and Duraffourg developed the conditions necessary for obtaining stimulated emission in a semiconductor, that a quantitative understanding of the necessary conditions was made possible. The achievement of close to 100 percent efficiency for electroluminescence in GaAs was the starting point for rapid experimental progress in semiconductor lasers [2].

In September 1962, coherent light emission was observed from a forward biased GaAs $p\text{-}n$ junction at 77 K. The first homostructure laser was made up of a chip of GaAs with polished ends perpendicular to the plane of the diffused p-n junction [3]. Further work made use of cleaving the crystal along the natural [110] cleavage planes to make the end facets

of the 0.2 to 1.0 mm long Fabry Perot cavity [4]. Since the typical threshold current density required for lasing was very high at room temperature ($\geq$ 50,000 A cm^{-2}) for the homostructure laser, continuous wave (CW) operation at room temperature was not possible. A stripe contact was used along the length of the diode to reduce the total current required, but this was not enough to allow room temperature CW operation. Room temperature operation of homostructure lasers was restricted to short current pulses at low duty cycles.

The development of heterostructure lasers was necessary to obtain CW room temperature operation. A heterojunction is made up of two semiconductors with different energy gaps. A useful property of a heterojunction is that the diffusion of injected minority carriers can be contained in the narrow energy gap material to give efficient radiative recombination there. An important technological step in 1967 was the growth of $Al_xGa_{1-x}As$ on GaAs by liquid phase epitaxy (LPE). Since the lattice parameters of GaAs and AlAs are nearly identical, good epitaxial layers were possible. The energy gap of AlGaAs can be varied by changing the AlAs content. A laser with decreased room temperature threshold density was made up of an epitaxially grown layer of Zn doped p-type AlGaAs on an n-GaAs substrate. Annealing of the LPE grown layer causes Zn to diffuse into the GaAs substrate and form a p-n homojunction approximately 2 μm from the heterojunction. The single heterostructure laser confines injected electrons to the p-GaAs region of the p-n junction.

The double heterostructure (DH) laser shown in Figure 2.1 was developed in 1969. A thin p-GaAs layer (0.5 μm) between higher energy gap n and p-GaAs layers grown on a GaAs substrate gives a structure which confines both light and carriers. The SiO_2 insulation defines a stripe contact which limits both the spread of injected carriers and light in the plane parallel to the junction.

The first room temperature CW operation of the DH laser allowed further consideration of practical optical communication systems employing semiconductor lasers and glass fibres. The improvement in LPE techniques to reduce the amount of non-radiative recombination at the heterojunctions has allowed the increase of device lifetime to about 10^5 hours [5]. Parallel reduction in optical fibre losses to fractions of a dB per kilometer has made high data rate communication systems possible.

2.3 Double Heterostructure Lasers

An energy band diagram for a double heterostructure laser with a p-type active region is shown in Figure 2.2. Let us consider the characteristics of the p-p heterojunction. The two semiconductors have different band gaps, E_g, and electron affinities. The electron affinity is defined as the energy necessary to raise an electron from the bottom of the conduction band to the vacuum level. The difference in electron affinities gives a step in the conduction band at the junction, as well as a complementary step in the valence band. Since the composition of the semiconductor is graded to some extent at the boundary, the space charge effects which give the band bending at the

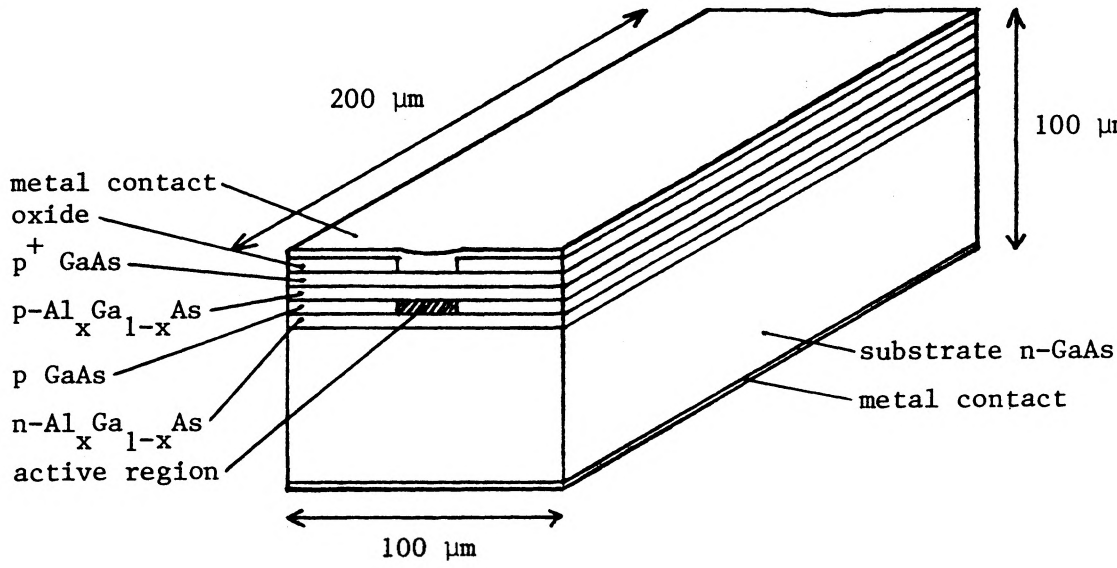

FIGURE 2.1 Double heterostruture (DH) GaAs laser.

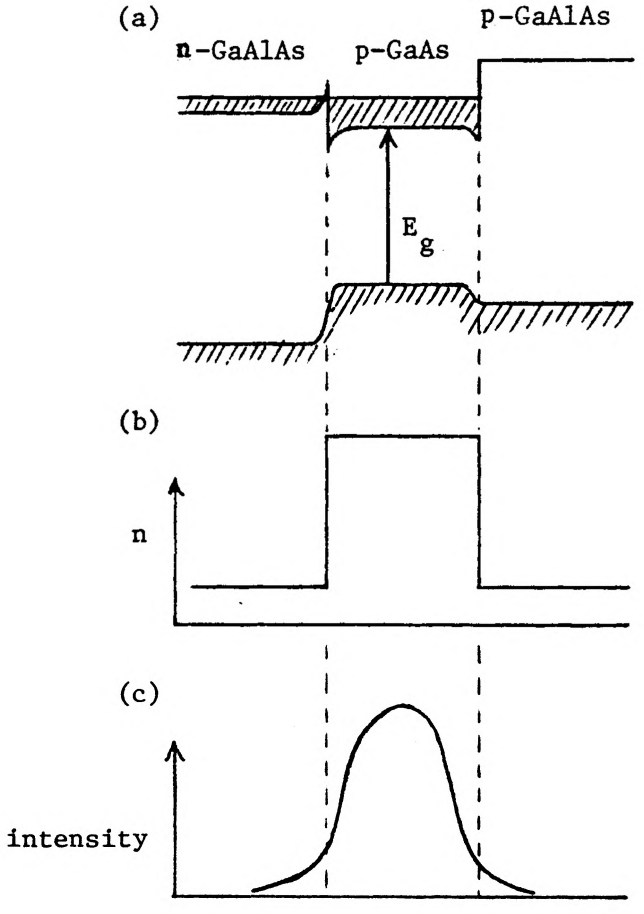

FIGURE 2.2 Potential of the energy bands (a), refractive index step (b), and optical confinement (c) for a double heterostructure.

junction cause the valence band to be nearly flat. The conduction band does have a significant potential step which confines electrons to the p-GaAs region. The confinement of holes in the valence band at the n-p heterojunction is as effective as the confinement of electrons at the p-p heterojunction. The space charge region which builds up at the n-p heterojunction can provide an undesirable barrier for electrons. Slight grading of the junction reduces the barrier height to less than the thermal energy of the carriers (kT) when the junction is strongly forward biased.

The larger bandgap material on either side of the active region has a lower refractive index. The typical refractive index step, Δn, of 0.1 to 0.5 is intended to reduce the coupling loss which occurs whenever the optical field spreads beyond the confining layers. The critical difference in refractive index required for good optical confinement varies inversely as the thickness of the central layer. The central layer thickness is usually small enough that only a single transverse laser mode can oscillate. Parallel to the junction, the lasing region is limited to less than 10 μm by the width of the stripe contact where carriers are injected. Multi-lateral modes are possible, but are usually eliminated by making the strip narrow enough, or by employing a more complicated laser structure to confine carriers and light in the lateral direction as well.

The spacing of the longitudinal modes is dependent on the effective cavity length, which in turn varies with the refractive index.

Since the refractive index is dependent on wavelength, temperature, and carrier density, the position of the longitudinal modes will vary with these parameters. The variation of refractive index with carrier density has a significant effect on the output spectrum of a modulated diode. This effect will be discussed later in this thesis. A large number of longitudinal Fabry-Perot modes fall within the broad gain spectrum of the semiconductor. A typical laser 200 μm in length will have a mode spacing of about 4 Å and a gain spectrum at threshold with a width of approximately 170 Å.

Because the confinement of light is to a small region in both transverse and lateral directions, diffraction will occur which introduces a propagation loss in the cavity. However, the gain profile in the lateral direction gives more amplification to light which propagates down the axis of the cavity, rather than to light which propagates off axis. This gain guiding compensates for the diffraction losses and gives the light leaving the cavity a curved phase front, which places the virtual source of the emitted light inside the cavity. The dependence of the gain guiding on the injection level is of importance when coupling light out of or into the active region since the virtual source of the light changes with the level of gain [6].

2.4 Optical Processes and Gain in Semiconductors

In a direct band gap semiconductor, such as GaAs, the maximum valence band energy states and the minimum conduction band energy states have the same momentum. This is not the case for an indirect band gap

semiconductor, such as Si or Ge, where photon absorption and emission processes require interaction of a phonon to conserve momentum. The probability of such interactions is therefore much lower for an indirect than for a direct band gap semiconductor.

For an undoped direct band gap semiconductor in thermal equilibrium, most valence band states are full while most conduction band states are empty. The small number of electrons in the conduction band available to make a transition to the valence band and emit a photon determines the low spontaneous emission rate. A photon of suitable energy present in the semiconductor can either be absorbed and raise an electron from the valence to the conduction band, or it can stimulate the transition of an electron from the conduction to the valence band. The stimulated transition causes emission of a second photon with the same frequency and phase as the initial photon. For stimulated emission to become the dominant process, the number of electrons in the conduction band must be large enough to make the probability of stimulated emission higher than the probability of absorption. When net gain is achieved, the spontaneous emission rate also increases due to the large number of electrons in the conduction band which can participate in random recombination.

The condition required for net stimulated emission can best be described by referring to Figure 2.3 which shows the relation between electron energy and density of states for a pumped, undoped semiconductor. The difference in the curvature of the valence and conduction bands

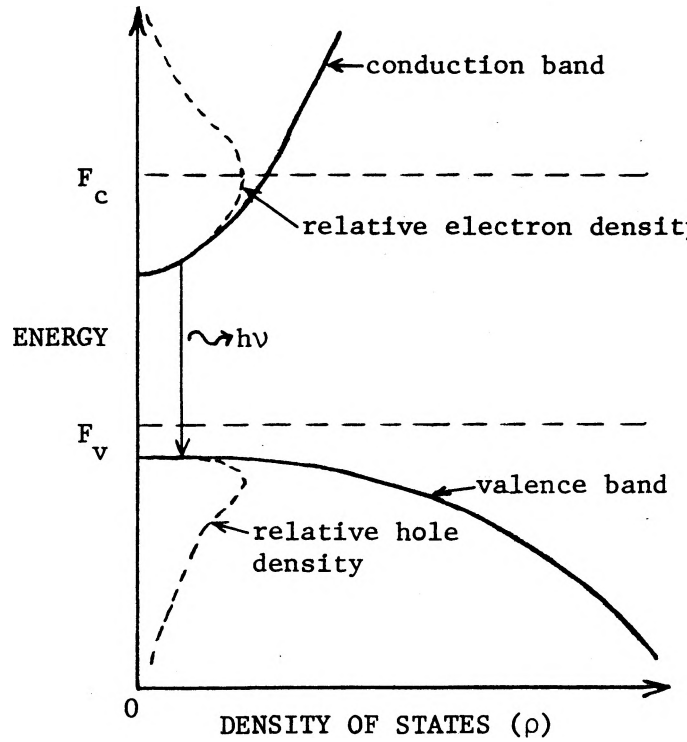

FIGURE 2.3 Relation between electron energy and density of states for an undoped semiconductor.

gives the small effective mass of electrons in the conduction band relative to the effective mass of holes in the valance band. The figure shows electron and hole density distributions for particular values of the conduction and valence band quasi-Fermi levels, F_c and F_v, which define the energy level where the states have an occupation probability of 1/2. For the undoped semiconductor in thermal equilibrium, the Fermi level is approximately in the middle of the energy gap since the states below it are nearly full while those above it are nearly empty. With injection of carriers into the bands, the fast thermalization of carriers brings each band into equilibrium, but not with the opposite band. For net stimulated emission to occur, the separation of the quasi-Fermi levels, F_c-F_v, must be greater than the incident photon energy, $h\nu$. Since no electrons are available to participate in stimulated emission at energies in the bandgap, F_c-F_v must be greater than the energy gap, E_g.

Doping of the semiconductor affects the density of states distribution. Introduction of p-type ionized impurity states causes band tails in the conduction and valence bands and introduces an acceptor band into the valence band tail. With high doping ($> 10^{18}$ cm^{-3}), the acceptor band moves into the valence band tail. The existence of these states makes transitions of energy less than the band gap possible since the effective separation between the valence and conduction band edges is reduced.

The relationship between gain and photon energy shown in Figure 2.4 can be directly related to the density of states diagram in Figure 2.3.

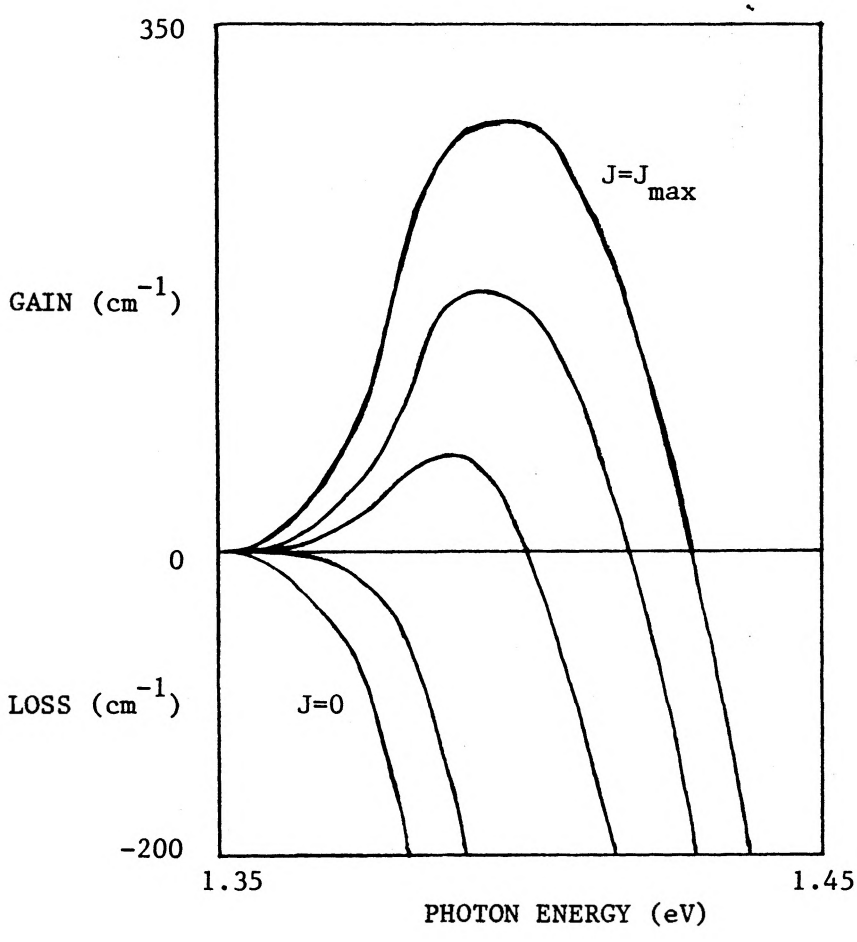

FIGURE 2.4 Gain versus photon energy for zero injection current density (J=0) to a maximum J_{max}.

For photons with energy less than the separation of the bands, no interaction occurs. As the photon energy increases, the increase in the density of states for electrons at higher energy causes more stimulated emission, and therefore more gain. The gain reaches a maximum and begins to fall off rapidly as the quasi-Fermi level is approached since photons with energy greater than $F_c - F_v$ are absorbed [7]. The quasi-Fermi level separation can be increased by increasing the rate of carrier injection. The peak of the gain shifts to higher energy and the gain spectrum broadens with higher injection current density.

2.5 Light-Current Characteristics

The threshold condition for a laser is the achievement of approximately unity net gain for a round trip in the optical cavity. A significant contribution of spontaneous emission is present as the threshold current density is approached. The Fabry-Perot (FP) modes define the peaks of the spontaneous emission in the cavity which experience amplification due to the gain in the semiconductor. Threshold current density is reached when the gain equals the sum of the absorption and mirror losses. The light output goes up rapidly at threshold, and the linewidth of the modes goes down drastically. Various parameters of the laser structure (which will not be discussed here) determine whether or not single longitudinal mode CW operation is possible.

Gain saturation is an important concept which contributes significantly to both the CW and dynamic response of semiconductor lasers. Increasing photon density in a particular mode induces a higher rate of

stimulated recombination into the mode, which reduces the effective injected carrier lifetime. When this lifetime becomes comparable to the time required to replenish the injected carrier concentration in the conduction band, the gain saturates. In the CW case, the gain saturates at its threshold value so all additional injected carriers, in principle, contribute directly to stimulated emission.

2.6 Transient Response

The interaction of the injected carriers and the photons present in the laser cavity is important to the dynamics of semiconductor lasers. Application of a current step which takes the current beyond threshold causes the injected carrier density to increase beyond its threshold value (Figure 2.5). The delay time for the carrier density to cross threshold depends on the initial dc current, the carrier recombination time, and the amount of current overdrive. When the carrier density goes through threshold, the lasing emission grows exponentially from the spontaneous level on a time scale very short compared to the rise time of the injected carrier density. The increase in photon density begins to saturate the gain, but the optical intensity continues to increase until the gain falls below the threshold value. When the inversion goes below threshold, the photons in the cavity experience a net loss and the photon density begins to drop rapidly. Since the gain is no longer saturated when the photon density is low, the inversion increases and again overshoots the steady state value. The entire process repeats in a damped oscillatory fashion. As the oscillations are damped, the lasing spectrum narrows until the

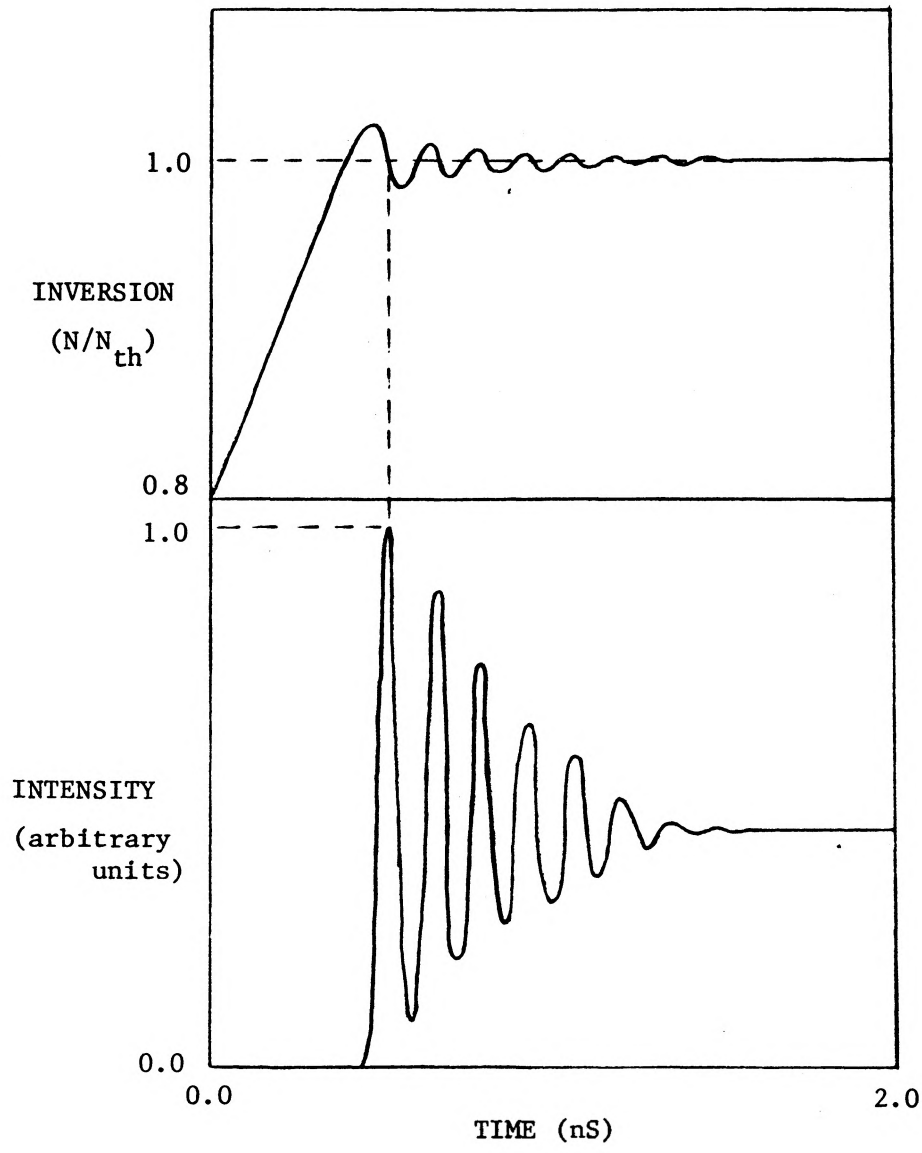

FIGURE 2.5 Illustration of damped relaxation oscillations for a step current input to the laser.

steady state spectrum appropriate to being biased to the same level above threshold is reached.

The following coupled rate equations describe the dynamic behaviour of the injected carrier density and the photon density [1].

$$\frac{dN}{dt} = \frac{J}{ed} - E(N) - \sum_i g(\lambda_i,N)\ S_i \tag{2.1}$$

$$\frac{dS_j}{dt} = C_j\ E(N) + g(\lambda_j,N)\ S_j - \Gamma_j\ S_j \tag{2.2}$$

J is the injected current density, d is the thickness of the active region, N is the injected carrier density, $g(\lambda_j,N)$ is the gain for the mode at λ_j, C_j is the spontaneous emission factor, and Γ_j is the confinement factor.

The spontaneous emission is represented by E(N). For a low level of injected carriers relative to the background doping, monomolecular recombination occurs with a time constant τ. The spontaneous emission rate is then $E(N) = N/\tau$. For a high level of injection, the carrier lifetime decreases with increasing injection. The bimolecular recombination gives a spontaneous emission rate $E(N) = bN^2$.

2.7 Rate Equation Model

A rate equation model developed in reference [1] and modified as described in reference [8] was used to simulate the dynamic response of lasers used in this work. The model uses measured device parameters,

such as the gain and stimulated emission spectra, the carrier lifetime, spontaneous emission factor, etc., to predict the dynamic behaviour. The original version made several assumptions to reduce calculation time. Symmetry of the gain spectrum about the peak (taken as fixed in wavelength) was assumed so that only half as many longitudinal modes were required, and variable time steps were used in the predictor-corrector solution to reduce the number of calculations.

A modified version of the original rate equation model proved essential to account for the spectral and temporal characteristics of very short gain switched optical pulses on the 10 to 50 ps time scale. Comparison of experiments and simulations on this time scale consistently leads to a significant underestimate of the observed optical pulse length and spectral width using the original version of the program. This was attributed to the chirp characteristics of semiconductor lasers. Chirping of the output refers to the change in wavelength of a particular lasing mode during an optical pulse due to an injected carrier induced refractive index change. The chirp from short to long wavelength can be as large as the mode spacing for cases of sufficiently high pumping.

Two significant parameters are introduced to the rate equation model to give better agreement between experimental and calculated results. The peak of the gain is allowed to shift with inversion, a change which does not allow any symmetry in longitudinal mode development to be assumed. A factor which reduces the gain, or effective stimulated cross section is included. This factor is intended to represent the

percentage of photons in the cavity which are no longer at an appropriate wavelength to cause stimulated emission since the wavelength of the Fabry-Perot cavity modes is changing. These modifications give simulated optical pulse length and spectral width in much better agreement with the experimental values.

2.8 Summary

This chapter was intended to present the background and basic theory relevant to a discussion of semiconductor lasers. The basic approach taken in modeling the dynamics of diode lasers in this work is also introduced.

CHAPTER 3

OPTOELECTRONIC FEEDBACK

3.1 Introduction

Optoelectronic feedback was first used by Paoli and Ripper [9] to frequency stabilize the optical pulses of CW GaAs injection lasers. The technique was developed to operate at pulse frequencies away from those characteristic of self-pulsations of the light intensity. The purpose of this work is to investigate some of the limitations on optical pulse length and intensity obtained from a diode laser operated in an optoelectronic feedback scheme. The results of previous workers' attempts using optoelectronic feedback are discussed, and suggestions are made on how to obtain shorter, more intense pulses. A fairly detailed description of the experimental setup used in this work is included since the limitations on pulse length are mainly imposed by the electronic loop parameters. The discussion includes various simulations to illustrate some of the experimental characteristics of the feedback loop.

3.2 Experiment

The optoelectronic regenerative pulser described by Damen and Duguay [10] was made up of a laser operated in a feedback loop made up of a photodiode, amplifier and delay line. In this type of arrangement,

the length of the optical pulses obtained is very dependent on the bandwidth and gain available from the photodiode-amplifier pair. The diode laser itself can have a modulation bandwidth of 2 to 4 GHz depending on the laser structure and its package. The circuit used by Damen and Duguay gave 40 mA peak current pulses (0.4 I_{th} where I_{th} = threshold current) with a FWHM of 400 ps to produce optical pulses with a FWHM of less than 100 ps at a repetition frequency of 130 MHz.

A modification to this feedback scheme was made by Park and Garside [11]. By using a step recovery diode (SRD) pulse shaping circuit at the input to the laser, the limitation on current pulse length imposed by the amplifier frequency response is reduced. Current pulses with $I_{pulse} = I_{th}$ and a FWHM of 500 ps produced optical pulses with a FWHM of 80 to 90 ps.

This work is based on further modifications of the feedback experiment described in reference [11]. It has been observed that shorter and more intense gain switched optical pulses can be produced by using higher peak current pulses. A lower threshold laser gives the advantage of obtaining a higher relative current pulse peak for the same feedback loop electrical gain. The maximum peak output from a commercially available dc to 0.5 GHz amplifier is about 10 V into 50 Ω. Since the maximum current pulses can be greater than 3 times the threshold current of the laser, the manner in which oscillations in the feedback loop are started becomes important. Because the laser is biased above threshold at startup, using maximum gain could produce current pulses large enough

to damage the diode. The likely damage mechanism would be the large optical intensity at the facets of the laser which ultimately destroys the end mirrors. To avoid this problem, a voltage controlled broadband attenuator was placed in the feedback loop. The attenuation range of 2 to 20 dB allows a low loop gain at start up while giving much larger gain when necessary.

The experimental setup is shown schematically in Figure 3.1(a). Part of the laser output goes to a photodiode with a pulse response FWHM of 210 ps. A second photodiode which has a pulse response of 90 ± 2 ps (including the 56 ps sampling oscilloscope response) was used to detect the output optical pulses. The slower photodetector output goes through an amplifier chain which has a total pulse response of 1.47 ns. The variable attenuator mentioned above is included in the amplifier chain. A standard two SRD pulse shaping circuit [12] (Figure 3.1(b) is used to give a current pulse at the laser output with rise and fall times of approximately 100 ps. The capacitor in the pulse shaper circuit functions as a high-pass filter to limit the low frequency response to 7 MHz. Without this capacitor, significant envelope modulation occurs on a microsecond time scale.

The step recovery diode is essentially a charge storage device. In Figure 3.6(b), the forward biased SRD1 stores charge because of the long minority carrier lifetime of the diode. A negative pulse which arrives at SRD1 must deplete the charge stored in the forward biased junction before the SRD switches to its reversed bias state. The

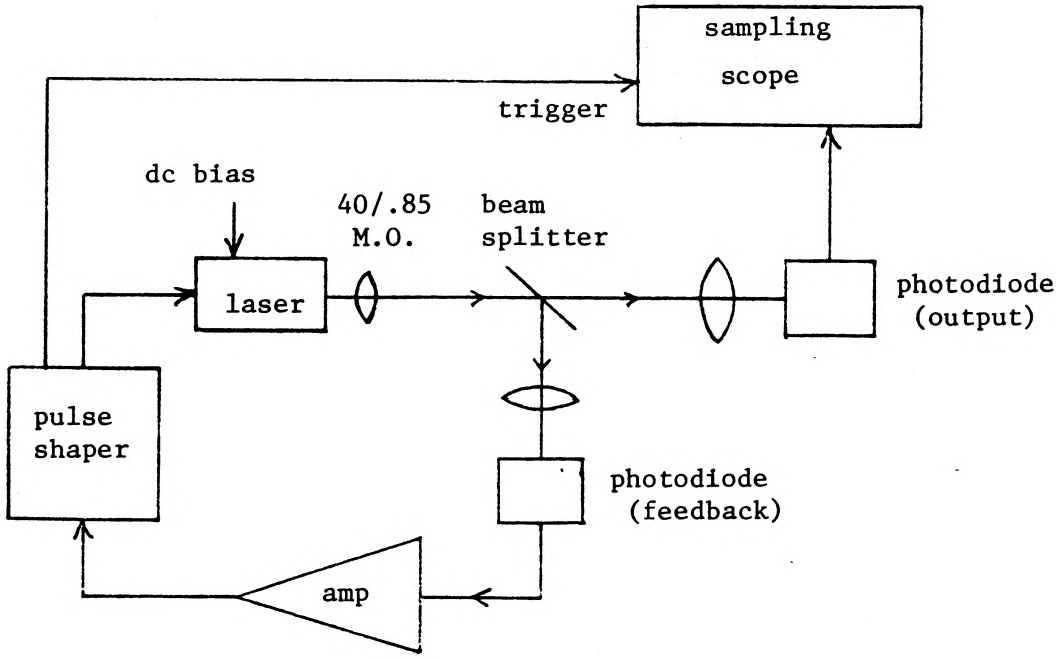

FIGURE 3.1(a) Schematic of experimental setup for opto-electronic feedback.

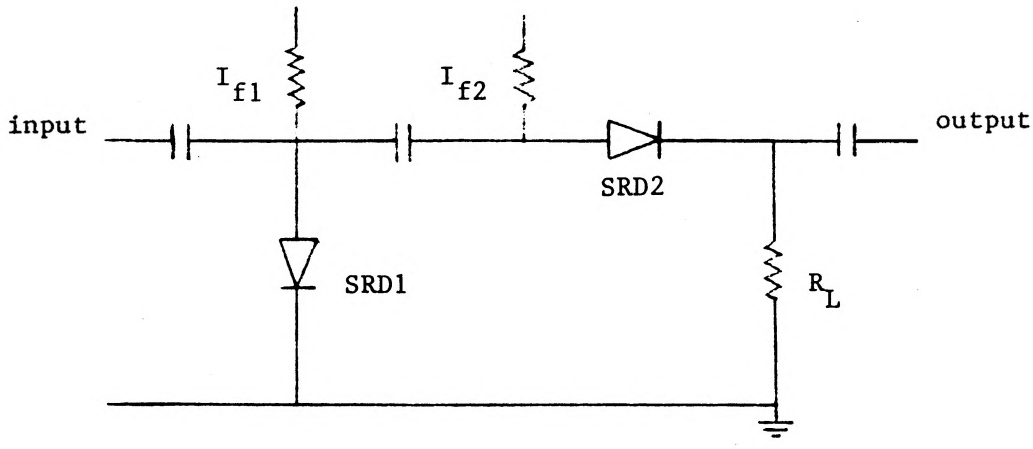

FIGURE 3.1(b) Standard two step recovery diode (SRD) pulse shaping cicuit.

switching time is limited by the circuit risetime (RC controlled) and the intrinsic diode transition time. After SRD1 switches, the current pulse begins to deplete SRD2. The switching of SRD2 to its reverse bias state blocks the remainder of the current pulse from the output of the pulse shaping circuit. SRD1 sharpens the rising edge of the pulse while the initial forward current through SRD2 determines the output current pulse length. The typical pulse shaping characteristics are illustrated in Figure 3.2 by placing a current monitor in the feedback loop before the pulse shaping circuit. The 1.47 ns FWHM current pulse from the output of the amplifier chain is shown early in the oscilloscope trace. Later in the trace (approximately 8 ns), the initial reflection from the forward biased SRD1 can be seen, followed by the reflection from the second SRD. The remainder of the pulse not reflected is the output current pulse.

The total energy gain of the amplifier chain is 57 dB but the actual multiplication of the peak photodiode output is much less than this for short optical pulses (approximately 33 dB) because of the long pulse response of the amplifiers. The peak of the current pulse is reduced by the pulse shaping circuit because of the switching characteristics of the SRD's. The roughly 100 ps risetime of the SRD's limits the current pulse FWHM to approximately 250 ps if no further loss of peak current is to occur. A fast rise time trigger signal is available from a current monitor placed in the feedback loop after the pulse shaping circuit.

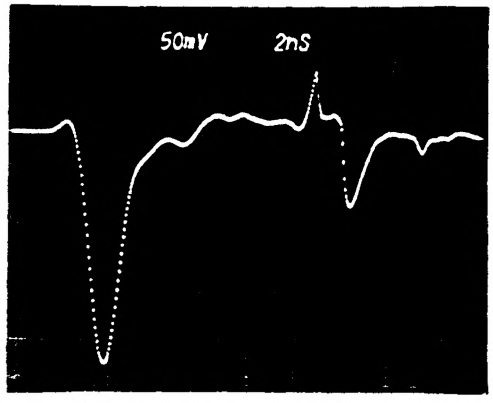

FIGURE 3.2 Oscilloscope trace of the current pulse seen by placing a current monitor ∿4 ns from the input of the pulse shaping circuit.

Care must be taken to avoid a significant reflection of the current pulse coupled to the laser. The fast rise time current pulse available from the pulse shaping circuit has significant frequency components which are beyond the design limitations of the standard 50 Ω coaxial LDL laser package. The reactive impedance of the standard package causes large reflections ($\geq$ 20%) which can be longer in duration than a short incident current pulse (less than 400 ps).

In the feedback loop, a negative current pulse which partially reflects from the laser package will return to the output of the pulse shaping circuit as a negative pulse. Since SRD2 appears as a reverse biased diode from the output side, multiple reflections of the current pulse will occur between the laser diode and SRD2 with a period corresponding to the length of coaxial cable between the two (approximately 2 ns). Since multiple reflections of current pulses in the feedback loop can be detrimental, a different method for introducing the pulse component of the current to the laser package was necessary.

Time domain reflectometry and network analyzer measurements confirmed that the technique shown in Figure 3.3 is an improvement over the standard coaxial package. The modified amount consists of a 50 Ω stripline on a low loss microwave pc board. The stripline is terminated with a 50 Ω chip resistor which is silver pasted to either the contact pad next to the laser chip, or directly to the gold wire leading to the laser chip. Even though reflection of the incident current pulse remains as high as 10 to 15 percent, the inductance of the mount is drastically

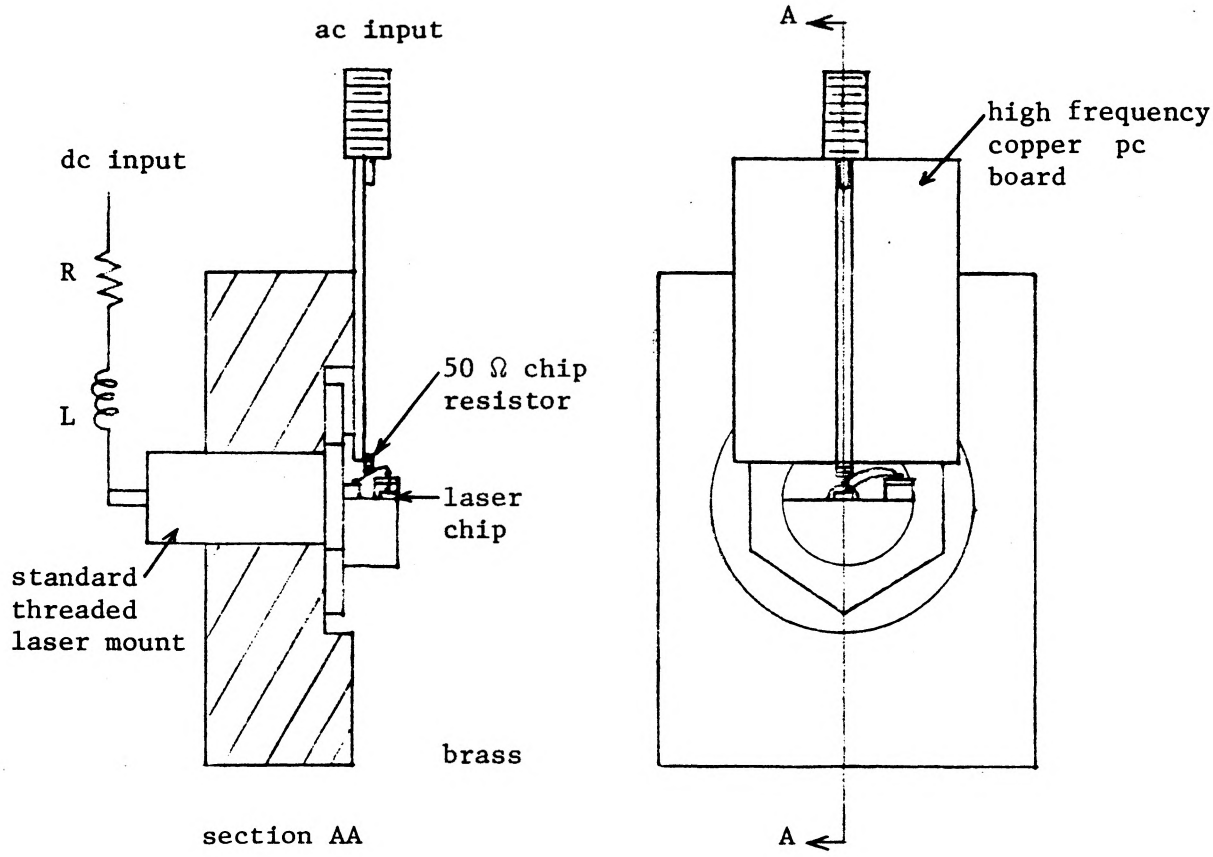

FIGURE 3.3 Custom high frequency laser mount.

reduced. The direct current bias of the laser is decoupled from the ac input by placing a small inductor at the dc input of the standard package, and a decoupling capacitor at the ac input. The mounting technique discussed above is equally important later in this thesis when short current pulses (FWHM = 85 ps) are used to modulate the laser at 500 MHz repetition rates.

3.3 Experimental Results

Oscillation is started in the feedback loop by turning the dc bias of the laser to slightly above threshold. When the output intensity of the laser is significant, a noise spike generated in the feedback loop builds into pulses at a repetition rate dependent on the sum of the optical and electrical loop delays. At startup, the typical optical pulse has several relaxation oscillations. As the dc bias is reduced below threshold, the amplifier gain is increased to maintain unity loop gain for the pulses in the optoelectronic feedback loop.

For the experimental setup used, the shortest optical pulses were obtained with the shortest available current pulses (FWHM = 260 ps) at a peak current $I_p = 3.24\ I_{th}$. The threshold current of the LDL SCW20 laser used in this experiment is 37 mA. Maintaining single pulse output (no second relaxation oscillation) required operation with $I_{dc} \leq 0.76\ I_{th}$. The loop gain was insufficient to sustain stable oscillation at I_{dc} much below $0.76\ I_{th}$ for a FWHM = 260 ps current pulse.

The optimum current pulse and corresponding optical pulse are shown in Figure 3.4 for a pulse repetition rate of 50 MHz. The repetition rate could be varied from 10 MHz to 100 MHz, where it is limited by the minimum optical and electrical loop delay time. The current pulse trace (Figure 3.4) is slightly distorted at the rising and falling edges due to the capacitance of the current monitor used. Assuming Gaussian pulses, the detected optical pulse of 105 ps can be deconvolved from the 90 ± 2 ps system response time to yield output pulses of 55 ± 5 ps FWHM. The peak power of these pulses is estimated to be 45 ± 5 mW.

Since the current pulse peak $I_p = 3.24\ I_{th}$ is the maximum available from the circuit components for the particular laser diode used, increasing the current pulse width is required to sustain oscillation at lower bias current. The available amplifier gain and the current pulse width (given by the pulse shaping circuit) determine the minimum bias current required for oscillation. The variation of the minimum dc bias with amplifier gain was found experimentally and is shown in Figure 3.5. The minimum bias current is roughly inversely proportional to the logarithm of the amplifier gain.

3.4 Simulations

A rate equation model developed in reference [1] and modified as described in reference [8] was used to simulate the dynamic response of the laser used in this work. The characteristics of the two versions of this model are discussed in the introductory chapter of this thesis. Although the original model significantly underestimates the optical

(a) Optical Pulse

FWHM (deconvolved)
=55±5 ps

Peak Power
=45±5 mW

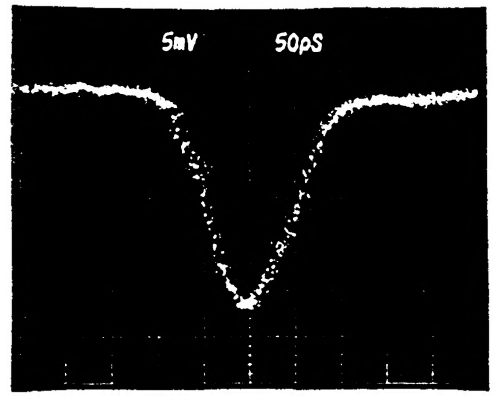

(b) Current Pulse

FWHM≃260 ps

Peak≃133 mA

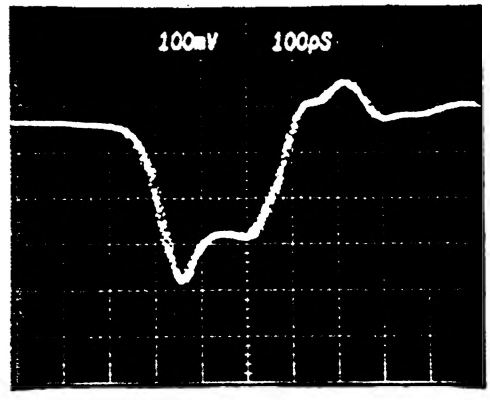

FIGURE 3.4 Current pulse and corresponding optical pulse for optimum feedback conditions.

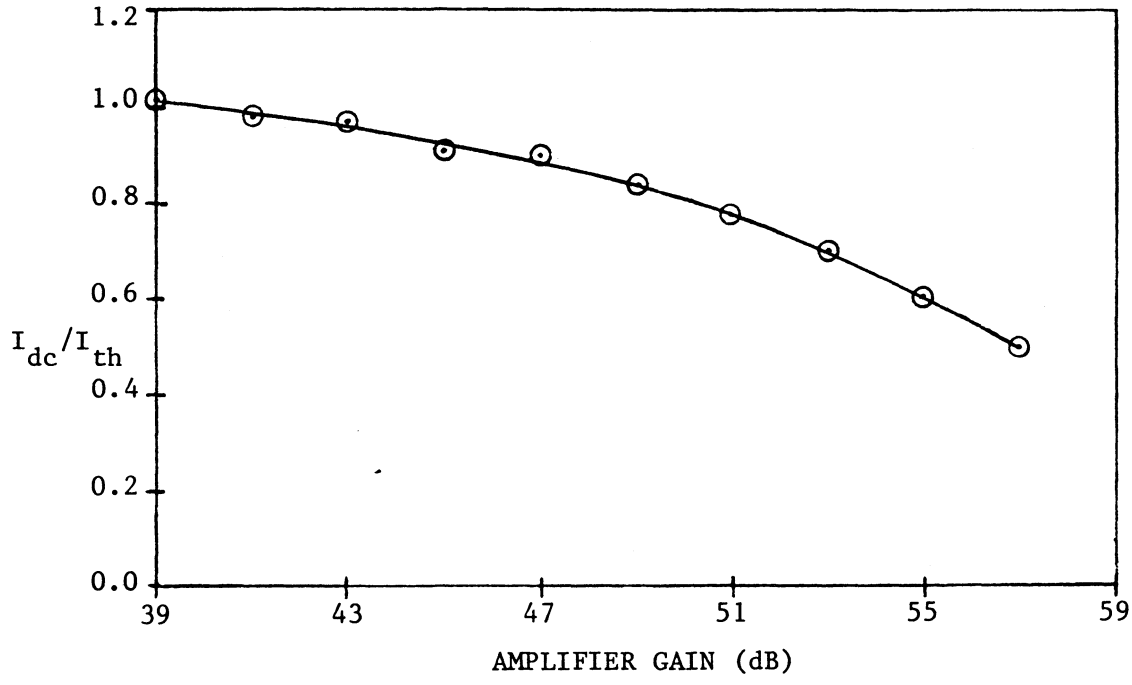

FIGURE 3.5 Minimum bias current (I_{dc}) versus amplifier gain in dB.

pulse length and spectral width for 20 ps to 50 ps optical pulses, it was used as one part of a new program which calculates self-consistent optical and current pulses for given optoelectronic feedback circuit parameters in order to minimize the overall program run time. The modified version of the rate equation model is significantly slower than the original, and is therefore inappropriate for use in an iterative program to simulate the optoelectronic feedback conditions. However, the modified version is useful for predicting optical pulse lengths given a particular input current pulse.

The program written to simulate the optoelectronic feedback conditions (FBACK) assumes a Gaussian optical pulse and Gaussian response from the photodiode/amplifier pair. The output optical pulse can be represented as

$$I(t) = I_0 \exp[-t^2/(2\sigma_0^2)] \tag{3.1}$$

where I_0 is the peak photon density calculated by the rate equation model. The response of the photodiode and amplifier can be written in a similar form (equations (3.2) and (3.3)), where G is the amplifier energy gain.

$$g_d(t) = \exp[-t^2/(2\sigma_d^2)] \tag{3.2}$$

$$g_c(t) = G \exp[-t^2/(2\sigma_c^2)] \tag{3.3}$$

The current pulse at the output of the amplifier is a convolution of $I(t)$, $g_d(t)$, $g_c(t)$ given by equation (3.4).

$$g_{out}(t) = \frac{I_o \, GM \, \sigma_o}{(\sigma_d^2 + \sigma_c^2 + \sigma_o^2)^{1/2}} \exp[-t^2/\{2(\sigma_d^2+\sigma_c^2+\sigma_o^2)\}] \qquad (3.4)$$

The factor M includes the conversion of the program output from photon density to power and the detector responsivity ($mAmW^{-1}$). Equation (3.4) illustrates expected behaviour such as the increased gain requirement G for a slower amplifier (larger σ_c).

The basic algorithm of the Fortran program FBACK is as follows. A current pulse is entered as a starting point. The rate equations are solved for the input current pulse, and the resulting output optical pulse is translated into an output current pulse using equation (3.4). The pulse shaping circuit is simulated by maintaining fixed current pulse width, and rise and fall times, while varying the peak according to the new value calculated using equation (3.4). The program repeats with the new current pulse until it obtains a self consistent value.

The result of FBACK simulations at $I_{dc} = .76\ I_{th}$ for a current pulse with 100 ps rise and fall times and a FWHM of 260 ps is a self-consistent current pulse peak of $3.12\ I_{th}$. This is in good agreement with the experimental value $I_p = 3.24\ I_{th}$ obtained under the same conditions. Since the program gives somewhat shorter pulse lengths than seen experimentally (as expected for this version), the variation in optical pulse intensity and FWHM with I_{dc} shown in Figure 3.6 is given as a percentage of the values obtained for $I_{dc} = 0.76\ I_{th}$. For I_{dc} much greater than $0.76\ I_{th}$, a second relaxation oscillation occurs. For lower dc bias current, the peak optical intensity begins to drop rapidly and the

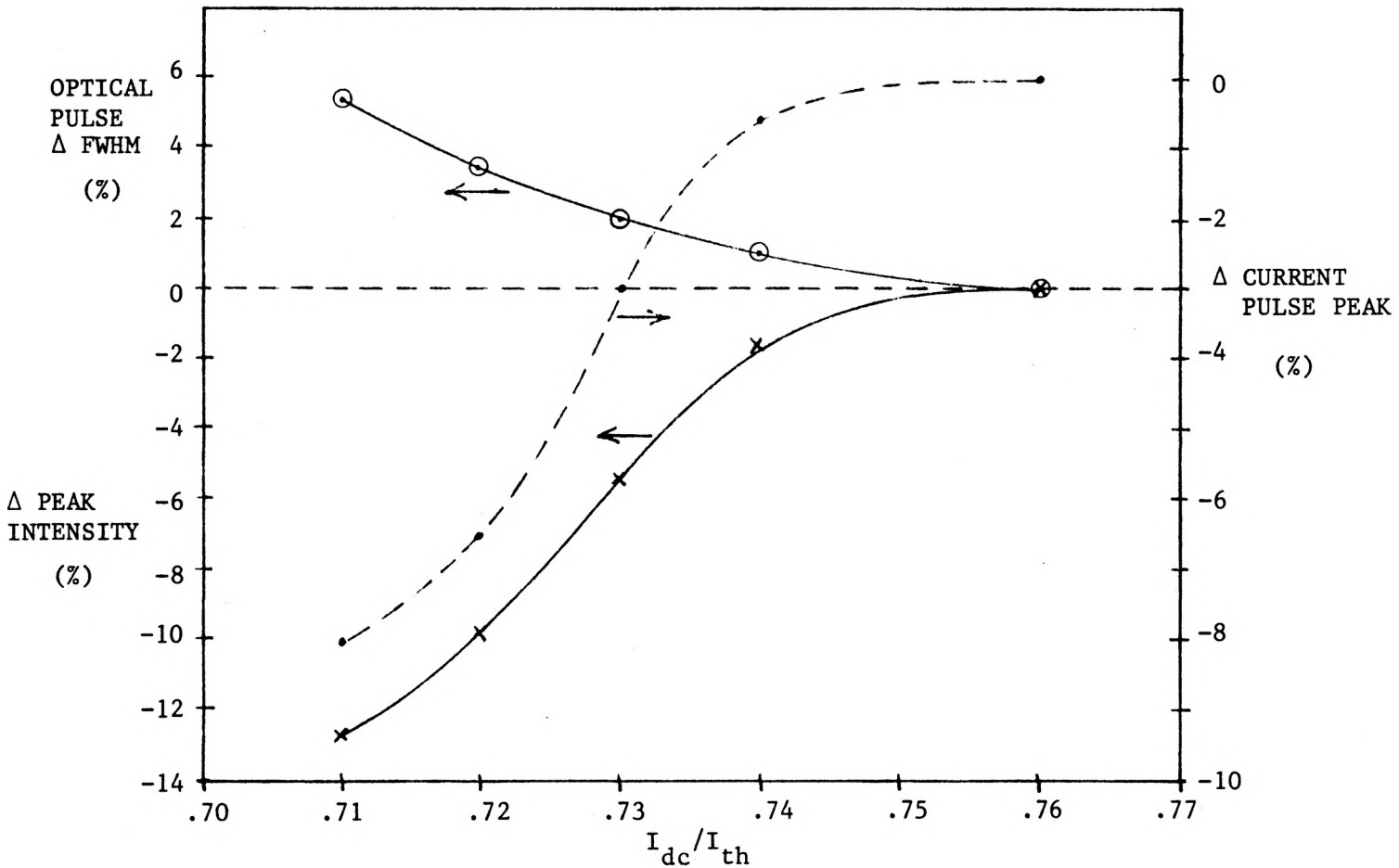

FIGURE 3.6 Simulation of opto-electronic feedback.

optical pulse width increases. The integrated energy of the optical pulse becomes too small to sustain oscillation in the feedback loop below $I_{dc} = 0.71\ I_{th}$ for the same current pulse width and amplifier gain.

Simulations can be done to illustrate the optical pulse dependence on current pulse width for fixed dc bias. Figure 3.7 shows the output optical pulses for current pulse widths from 200 to 450 ps for a peak pulse of $3.12\ I_{th}$ and $I_{dc} = 0.76\ I_{th}$. The 100 ps rise time, large amplitude pulse causes the inversion to rise rapidly at a rate determined by the current pulse peak, dc conditions, and the injected carrier lifetime. If the current pulse causes the inversion to overshoot its threshold value, relaxation oscillations will begin. The optical pulse intensity will increase and the FWHM will decrease for longer current pulses until the current pulse is long enough to provide enough inversion for a second relaxation oscillation. At this point, the initial relaxation oscillation no longer changes significantly with increased current pulse length. The simulation results in Figure 3.7 show that the optimum current pulse FWHM for $I_{dc} = 0.76\ I_{th}$, $I_p = 3.24\ I_{th}$ is in the region of 300 ps. This is in reasonably good agreement with the experimentally optimum value of FWHM = 260 ps.

The results of simulations using $I_{dc} = 0.76\ I_{th}$ and a current pulse FWHM of 260 ps with increasing pump amplitude are shown in Figure 3.8. The pump amplitude starts at $I_{po} = 3.12\ I_{th}$ and is increased in steps of $0.5\ I_{po}$ to $3.0\ I_{po}$. Significant pulse shortening occurs

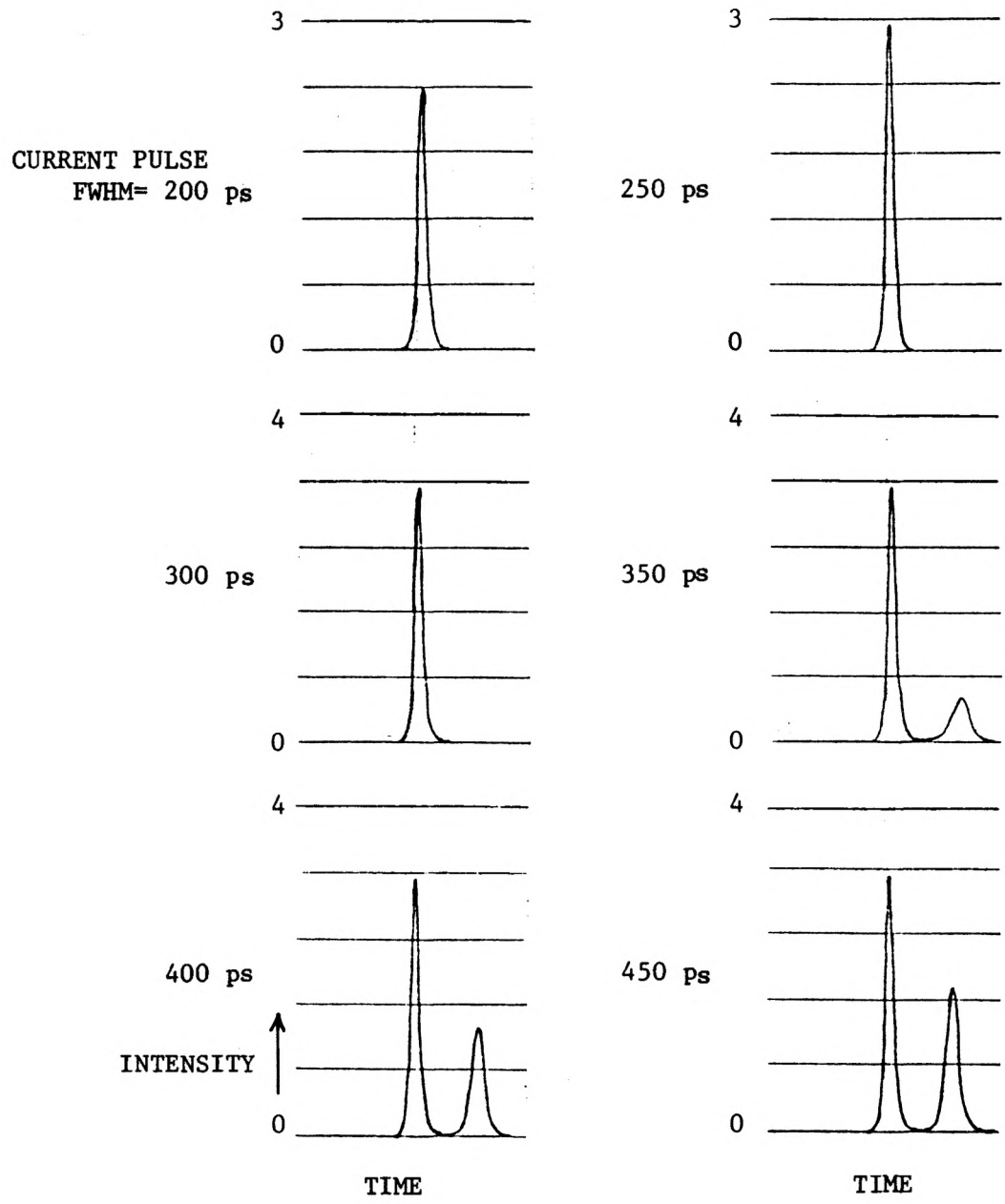

FIGURE 3.7 Simulation of the output optical pulse for $I_{dc}=0.76I_{th}$ and $I_p=3.24I_{th}$ with varying current pulse FWHM.

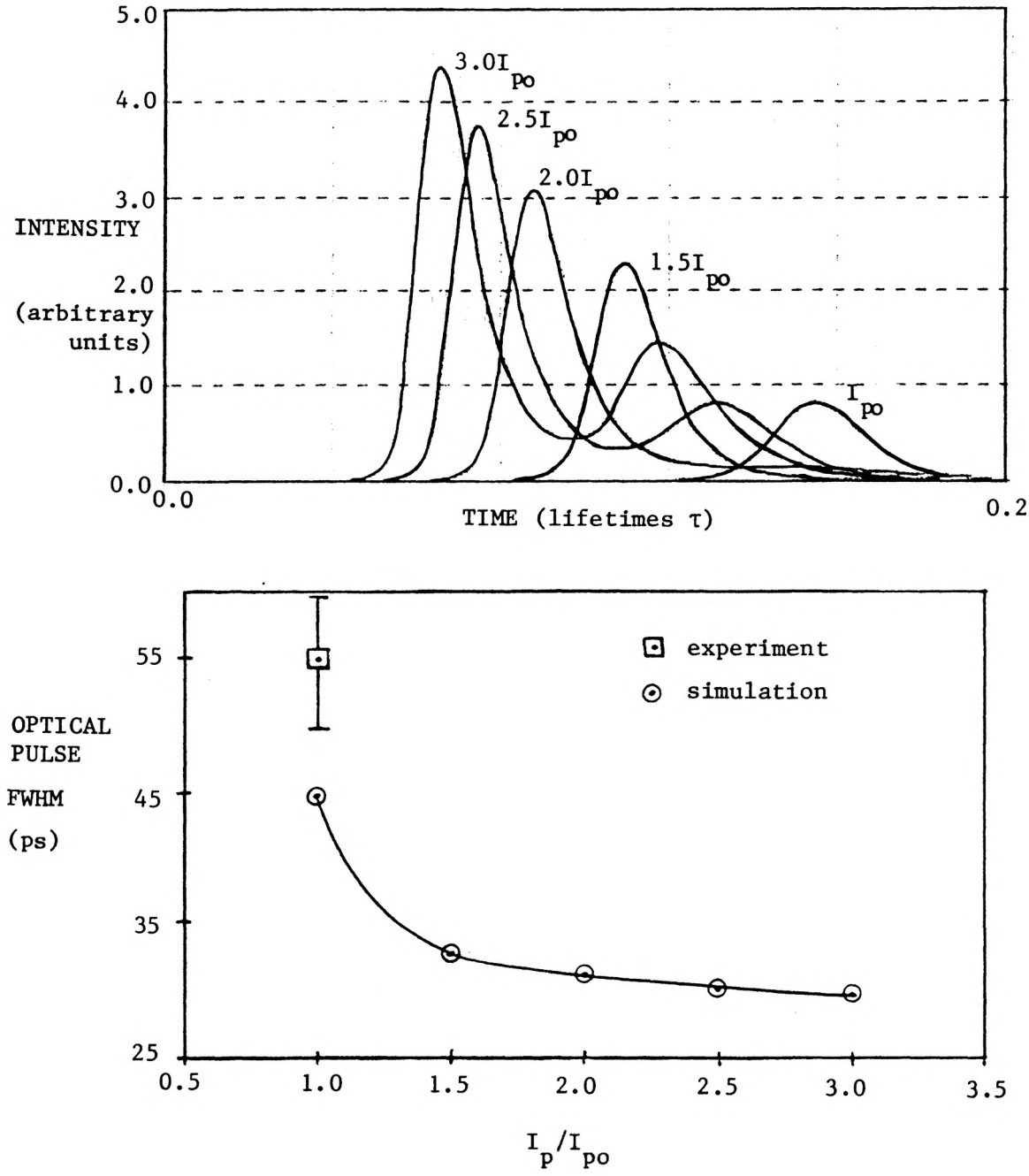

FIGURE 3.8 Simulation of the optical pulse versus peak current pulse relative to $I_{po}=3.12I_{th}$ for a fixed bias current.

up to 1.5 I_{po}, but a second relaxation oscillation begins with higher pump amplitude. The simulated optical pulse FWHM is in reasonable agreement with experiment at $I_p = I_{po}$ considering that the simulation is in a region of rapid change of pulse length relative to pump amplitude.

The simulations indicate that both a narrower and higher peak current pulse is necessary to obtain shorter optical pulses while suppressing a second relaxation oscillation. The optical pulse FWHM dependence on dc bias is shown for two pump amplitudes, 6.24 I_{th} and 9.36 I_{th}, in Figure 3.9. The current pulse has rise/fall times of 60 ps and FWHM = 140 ps. The shortest optical pulses obtained are in the 27 to 29 ps range. These are not a great deal shorter than the minimum pulses obtained using a longer current pulse (see Figure 3.8).

With the pulse shaping circuit used in this work, the current pulse FWHM is limited to approximately 260 ps. Higher peak input to the pulse shaping circuit would result in shorter optical pulses, however, the peak limit is given by the maximum amplifier output. Faster step recovery diodes have resulted in pulse shaping circuits which produce $\sim$ 160 ps FWHM current pulses [13]. The much higher relative pump amplitude required in conjunction with short current pulses to obtain slightly shorter optical pulses is again limited by the peak amplifier output. Since the amplifier used in this work is capable of giving as large a peak output as anything available commercially, the most likely combination of parameters which will yield shorter optical pulses than

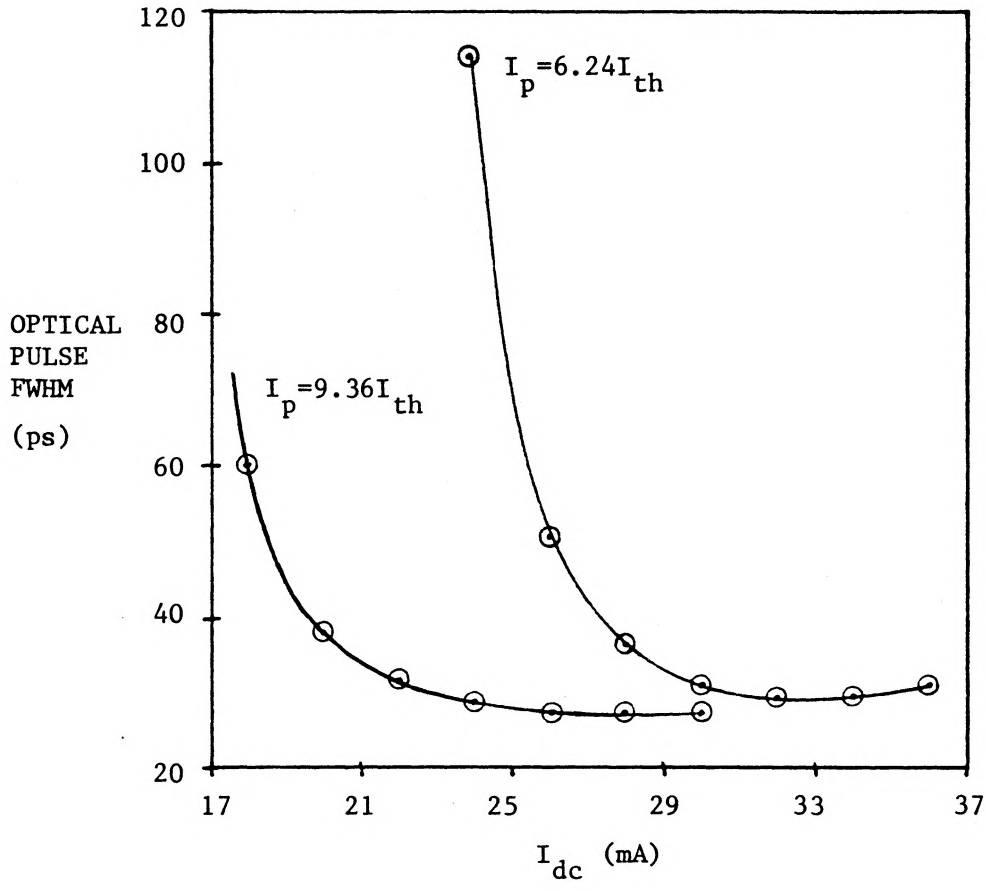

FIGURE 3.9 Simulation of optical pulse FWHM versus bias current for two different current pulse peaks. The current pulse FWHM= 140 ps with 60 ps rise and fall times.

those reported here is a laser threshold of less than 20 mA and a current pulse FWHM of about 140 ps. Lasers with threshold currents in the 10 mA range are available, but some types have proven to be extremely sensitive to small line transients or static discharge which often is enough to destroy them. Even with a lower threshold laser, the amplifier/pulse shaper limitations on the current pulse may restrict the minimum optical pulse length available using optoelectronic feedback to approximately 25 ps, as indicated by the simulations in Figure 3.9.

3.5 Summary

The aim of the work presented in this chapter is to investigate some of the limitations on optical pulse FWHM and intensity obtained from a diode laser operated in an optoelectronic feedback scheme. A reduction of the minimum optical pulse FWHM obtained has resulted from using a lower threshold laser and different pulse conditions than in previous work ([9] to [11]). The 45 ± 5 mw peak power, 55 ± 5 ps FWHM optical pulses obtained experimentally correspond well to the value found using a rate equation model of the laser dynamics. Modeling of the optoelectronic feedback loop using measured electronic and laser parameters resulted in oscillation characteristics similar to those seen experimentally. Simulations indicate that a minimum optical pulse length in the region of 25 ps may result by using a lower threshold laser and shorter current pulses in an optoelectronic feedback scheme.

Optoelectronic feedback is a promising scheme for obtaining short duration, high peak power optical pulses from laser diodes at stable repetition rates. However, the dynamic spectrum of the output pulses is as broad as in the case of a directly modulated laser with no feedback. A narrower dynamic spectrum may be obtainable by adding optical feedback to the optoelectronic feedback scheme, but the necessary synchronization of the optical pulses and current pulses returning to the laser is difficult to achieve because the delay in the optoelectronic feedback loop is at least an order of magnitude greater than the delay corresponding to a practical external cavity length.

An alternate approach to obtain short duration, spectrally narrow optical pulses is to directly modulate a laser diode at a repetition frequency synchronous with the optical feedback from an external reflector. The next two chapters discuss the effects of optical feedback on the CW operation of diode lasers to aid in the understanding of the modelocking characteristics examined in the final chapters of this thesis.

CHAPTER 4

OPTICAL FEEDBACK EFFECTS ON SEMICONDUCTOR LASERS

4.1 Introduction

The operation of CW GaAlAs lasers within an external resonator has been studied extensively in the past. There are several reasons for considering external cavity operation of laser diodes. Coupling light back into the laser chip from an external reflector provides a means of probing the properties of the diode. The optical feedback can also be used to alter output characteristics of the diode laser such as the emission bandwidth and frequency response. For practical engineering applications, the effect of optical feedback from the end of optical fibres in communication systems or from discs in optical storage units is of interest when evaluating the performance of such systems.

In this chapter, the effects of the external feedback on the spectrum of the laser output and the threshold current of the diode will be examined. It is necessary to examine these effects so that the coupling efficiency to an external cavity can be determined in order to use the optical feedback as a probe of the laser characteristics, and in order to do accurate simulations of the modelocking characteristics. Coherent optical interference due to multiple reflections in the compound cavity

are found to contribute significantly to the detected emission linewidth of the external cavity operated laser. An expression for the effective mirror reflectivity of the chip facet and the external reflector based on these effects is used to calculate the total loss reduction due to the external feedback. The measured effective mirror reflectivity includes the effects of the reduced mirror loss and the inseparable reduction in modal propagation loss which make up the total loss reduction due to the external feedback. The limiting bandwidth due to a dispersive element in the cavity is discussed in comparison with the emission linewidth of the same laser operated with a plane mirror as the feedback element.

4.2 Spectral Characteristics

Non-zero chip facet reflectivity in an external cavity operated laser diode will cause multiple reflections within the compound cavity. Most rate equation analyses of self-pulsing or modelocking in external resonators utilize a time delayed intensity term to represent the optical feedback. Reasonable agreement with some observed dynamic characteristics is achieved, but the multiple reflection interference effects due to feedback must be considered to explain the spectral and threshold characteristics.

With external cavities that are orders of magnitude longer than the laser chip, the longitudinal external cavity modes are much more narrowly spaced than the chip modes ($\lambda_{q+1} - \lambda_q = \frac{\lambda^2}{2n_{eff}L}$). The

longitudinal mode spacing for a 210 μm long chip is typically 4 Å while that of a compound cavity is 0.0115 Å for a 30 cm cavity length. The optical feedback results in more than just an intensity modulation of the compound cavity modes by the spectrum of the diode. To solve for the effects of the feedback, the boundary conditions on the coherent optical fields must be matched at the interfaces of the compound cavity.

The cavity is shown schematically in Figure 4.1 along with the fields at each interface. At the diode facet, the reflected and transmitted fields can be written as

$$R_1(t) = t_2\, T_2^*(t) + r_2\, E_1^* \tag{4.1}$$

$$T_1(t) = r_2'\, T_2^*(t) + t_2 E_1^* \tag{4.2}$$

where r_2, r_2', t_2 are the amplitude reflectivities and transmittivity, and the capitalized symbols are the fields shown in Figure 4.1. The single pass gain is given by

$$\sqrt{G} = e^{(g-\alpha)\ell} \tag{4.3}$$

where g and α are respectively the gain and loss coefficients per unit length. The loss coefficient, α, includes the free carrier absorption and the scattering loss in the laser cavity. The fields within the diode can be related as in (4.4), (4.5) and (4.6).

$$E_1^* = E_1 \sqrt{G}\, e^{-i\phi_\ell} \tag{4.4}$$

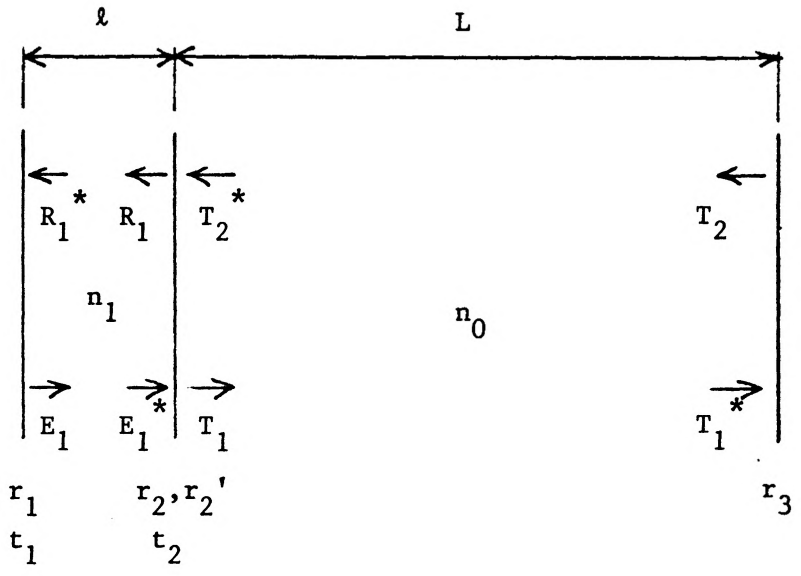

FIGURE 4.1 Schematic of one-dimensional compound cavity. The chip length ℓ is much less than the external cavity length L.

$$R_1^* = R_1 \sqrt{G}\, e^{-i\phi_\ell} \tag{4.5}$$

$$E_1 = r_1 R_1^* = r_1 R_1 \sqrt{G}\, e^{-i\phi_\ell} \tag{4.6}$$

The change in phase for a single pass in the diode is $\phi_\ell = 2\pi n_1 \ell/\lambda$. The spontaneous emission terms which should appear in (4.4) to (4.6) are ignored to obtain an approximate oscillation condition. Equations (4.1) and (4.2) can be rewritten using $\phi_L = 2\pi n_o L/\lambda$ as the phase change for a single pass in the external resonator.

$$R_1 = t_2 r_3 T_1 e^{-2i\phi_L} + r_2 E_1 \sqrt{G}\, e^{-i\phi_\ell} \tag{4.7}$$

$$T_1 = r_2' r_3 T_1 e^{-2i\phi_L} + t_2 E_1 \sqrt{G}\, e^{-i\phi_\ell} \tag{4.8}$$

Substitution of equation (4.6) into (4.7) and (4.8) results in the gain condition given in equation (4.9)

$$G = \frac{[1 + r_2 r_3 e^{-2i\phi_L}]}{r_1 e^{-2i\phi_\ell} [r_2 + r_3 e^{-2i\phi_L}]} \tag{4.9}$$

This is a confirmation of the result obtained in reference [14]. There are many discrete solutions to (4.9) which vary with the degree of optical feedback from the external cavity mirror. A numerical solution to (4.9) found in reference [14] for $r_1 = r_2 = .565$ and three values of r_3 is shown in Figure 4.2. Since the discrete solutions to (4.9) are much closer together in phase than the solitary diode modes, they are drawn as a continuum. The spectrum is made up of compound cavity modes

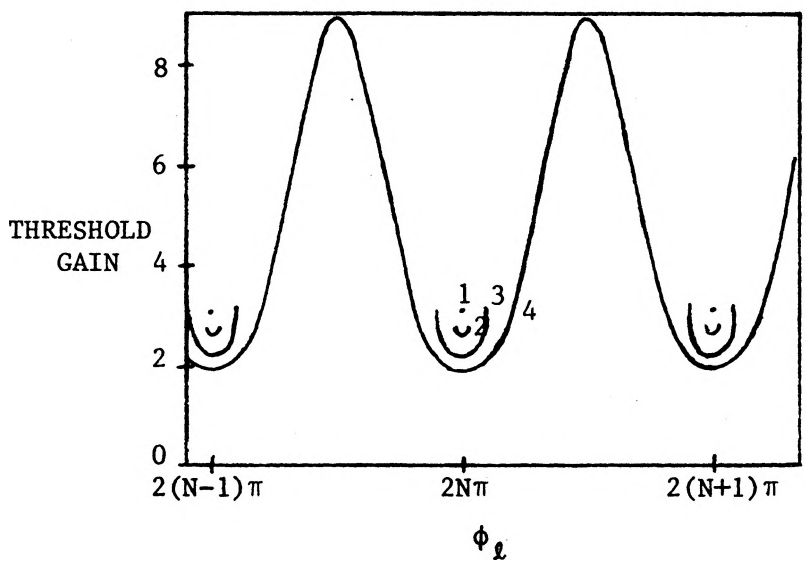

FIGURE 4.2 Numerical solution of equation 4.9 taken from reference [14]. For curve 1, r_3=0, curve 2, r_3=0.1, curve 3, r_3=0.4, and for curve 4, r_3=0.7. The threshold gain is given in arbitrary units.

clustered at the wavelengths of the original diode longitudinal modes. The peak mode of each cluster is the one nearest to the original chip mode. For fixed current, increased optical feedback will cause the threshold of more compound cavity modes to cross gain threshold, causing an increase in the apparent linewidth of the output. For fixed external feedback, increasing the current will result in an increase in linewidth until a maximum when the highest threshold of a compound cavity mode is surpassed. When the effective mirror reflectivity is larger than that of the chip facet, solutions to the phase condition result all over the frequency axis. It is shown in reference [15] that only modes near the free running laser modes have low threshold gains when $r_3 > r_2$.

To determine experimentally the effects of optical feedback on the spectral characteristics of a GaAlAs laser, a diode with facet reflectivity $r_2 = .33$ was coupled to an external resonator using a 40/0.85 microscope objective. The 30 cm long external cavity was formed with a 90 percent power reflectivity plane mirror. The output linewidth was measured using a 0.5 m grating spectrometer with resolution of less than 0.1 Å. The experimental results are shown in Figure 4.3. The current is given as a ratio in terms of the external cavity operated threshold current for the particular level of feedback. With increasing current, the linewidth levels off at 0.85 Å for full feedback. When an attenuator with an amplitude transmittance of 50 percent is placed in the cavity, the linewidth levels off at a lower value, as expected. These results agree qualitatively with those in [14] which are given for somewhat different laser diode characteristics. A decrease in the facet reflectivity,

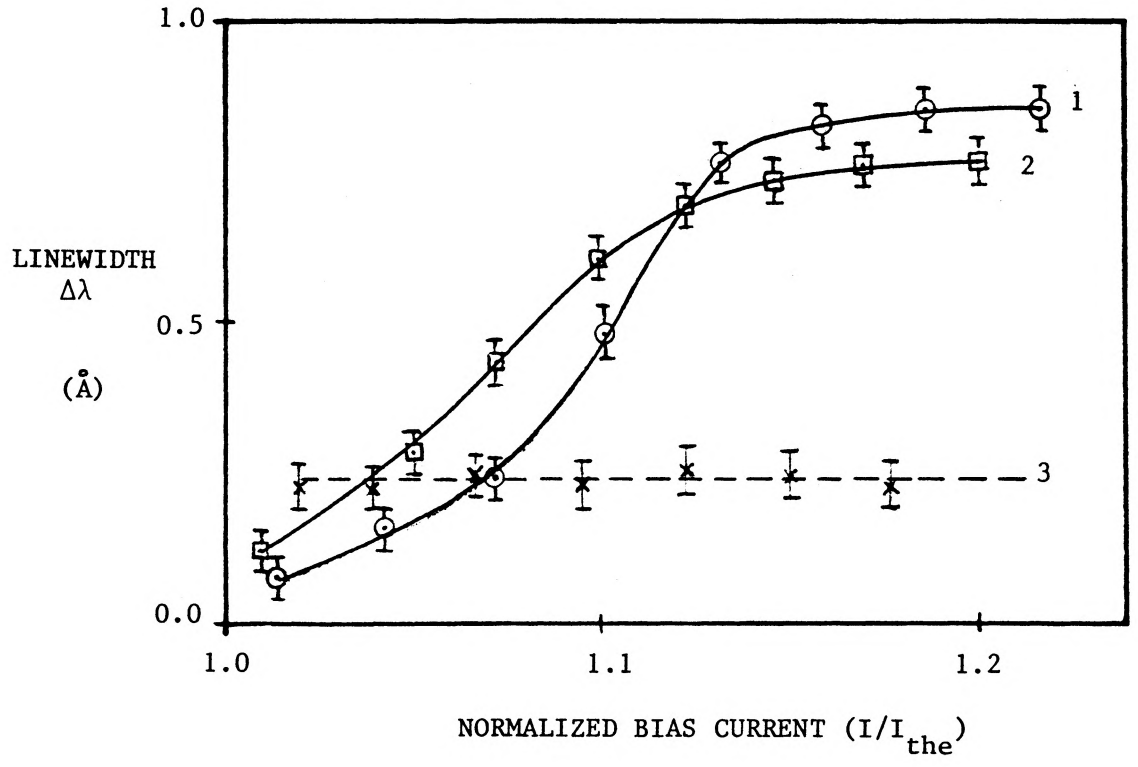

FIGURE 4.3 Dependence of mode linewidth on external feedback using a plane mirror cavity (1,2) and a grating cavity (3). Case 1 is for full feedback from the external mirror while case 2 is for 50% attenuation in the external cavity.

r_2, will increase the coupling and result in a broader linewidth until the limit of $r_2 = 0$ where the linewidth is limited only by the spectral width of the diode gain ($\sim$ 170 Å). Even small residual reflectivities ($r_2 \leq 0.01$) will result in significant deviation from the zero facet reflectivity spectrum. A shorter external cavity length, L, reduces the number of phase solutions to 4.9 and would result in a narrower linewidth.

Optical feedback effects on the full spectrum of a plane mirror coupled diode laser have been seen experimentally in this work. Figure 4.4 shows the development of the wavelength spectrum for the full feedback case for dc bias just above to 1.16 times the external cavity threshold current. The intensity scale is arbitrary, but the scale is consistent for I_{dc} = 36 to 40 mA. The total intensity versus current characteristics are fairly linear throughout the current range used. However, the peak intensity of each mode cluster tends to stop increasing when the number of lasing compound cavity modes broadens the linewidth. The increasing number of compound cavity modes whose threshold gain is surpassed use some of the recombining carriers which were previously available to increase the intensity of the peak modes. The peak intensity of the mode clusters is expected to increase again when the maximum linewidth is attained.

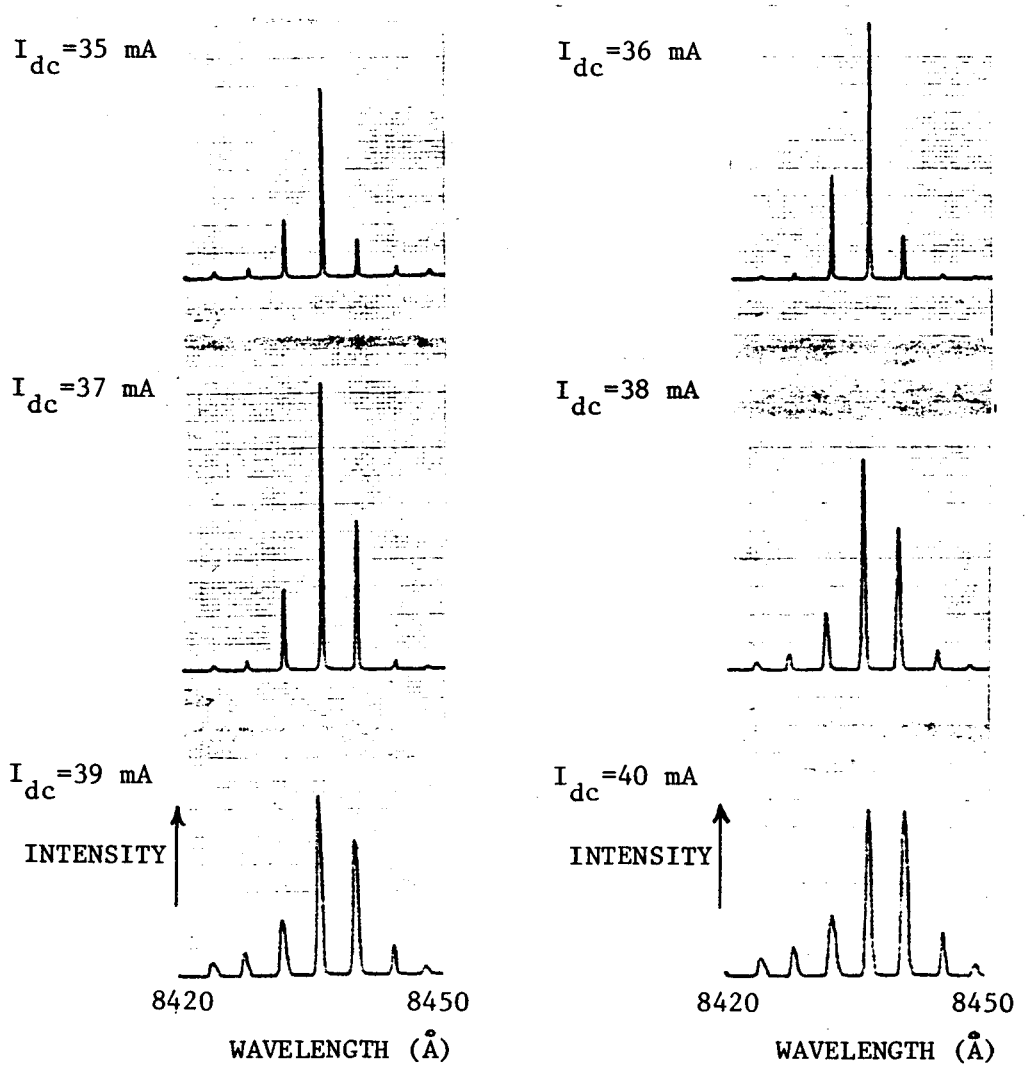

FIGURE 4.4 Development of the CW mode spectrum with increasing dc bias current for plane mirror feedback.

4.3 Threshold Current

The minimum threshold condition of a laser operated in an external cavity can be derived from the lowest loss solution (in phase feedback) of equation (4.9), given in (4.10).

$$g-\alpha = \frac{1}{\ell}\left[\ln\left(\frac{1}{r_1 r_2}\right) + \ln\left(\frac{r_2}{r_{eff}}\right)\right] \tag{4.10}$$

When the external feedback is zero, $r_{eff} = r_2$, and the expected threshold condition is retained. The final term in (4.10) gives the mirror loss reduction due to the external feedback. Using equations (4.4), (4.6) and (4.7), the effective reflectivity due to the facet and the external mirror can be written as in (4.11).

$$r_{eff} = \frac{R_1}{E_1^*} = \frac{r_2 + r_3\, t^2}{1 + r_2\, r_3\, t^2} \tag{4.11}$$

The amplitude transmittance, t, of an attenuator placed within the external resonator is included in (4.11) for completeness.

The threshold reductions corresponding to several levels of feedback were measured experimentally. Knowledge of the gain current relationship for the peak of the gain (see Chapter 5) allowed calculation of the effective mirror loss reduction (in cm^{-1}) for each level of feedback. The measured effective mirror loss reduction includes both the reduction in mirror loss and the reduction in modal propagation losses due to the external feedback. Such a reduction in modal propagation loss is thought to be due to an increase in the mode size, which reduces diffraction losses in the cavity, and possibly a spatial shift of the

lasing to a region with lower background loss. The effective reflectivity of the external mirror, r_3, calculated from the threshold current reduction therefore yields a higher coupling efficiency to the external mirror than is actually achieved. The effects of the separate contributions to the total loss reduction are inseparable in the CW case, but are important when considering the size of the external coupling term in the equations which represent the dynamics of an external cavity operated diode.

The measured effective mirror loss reduction for each level of feedback is shown in Figure 4.5 along with the loss reduction calculated using (4.10) and (4.11). The good agreement between calculated and experimental loss reductions illustrates that consideration of coherent optical interference effects gives a good description of the threshold characteristics of external cavity operated diodes.

4.4 Grating Feedback

When a dispersive element is used in the external cavity, the limiting bandwidth of the feedback changes the effect of optical feedback on the spectral linewidth of the output. In this work, the first order diffraction from a 1200 line/mm grating with a 90 percent efficient blaze at 7500 Å is used for wavelength selective optical feedback to the diode laser. The rulings of the grating are oriented parallel to the plane of the diode junction so that a maximum number of lines are filled by the collinated laser output. The threshold reduction of 10 mA due to the grating feedback is approximately the same as that achieved using a plane mirror.

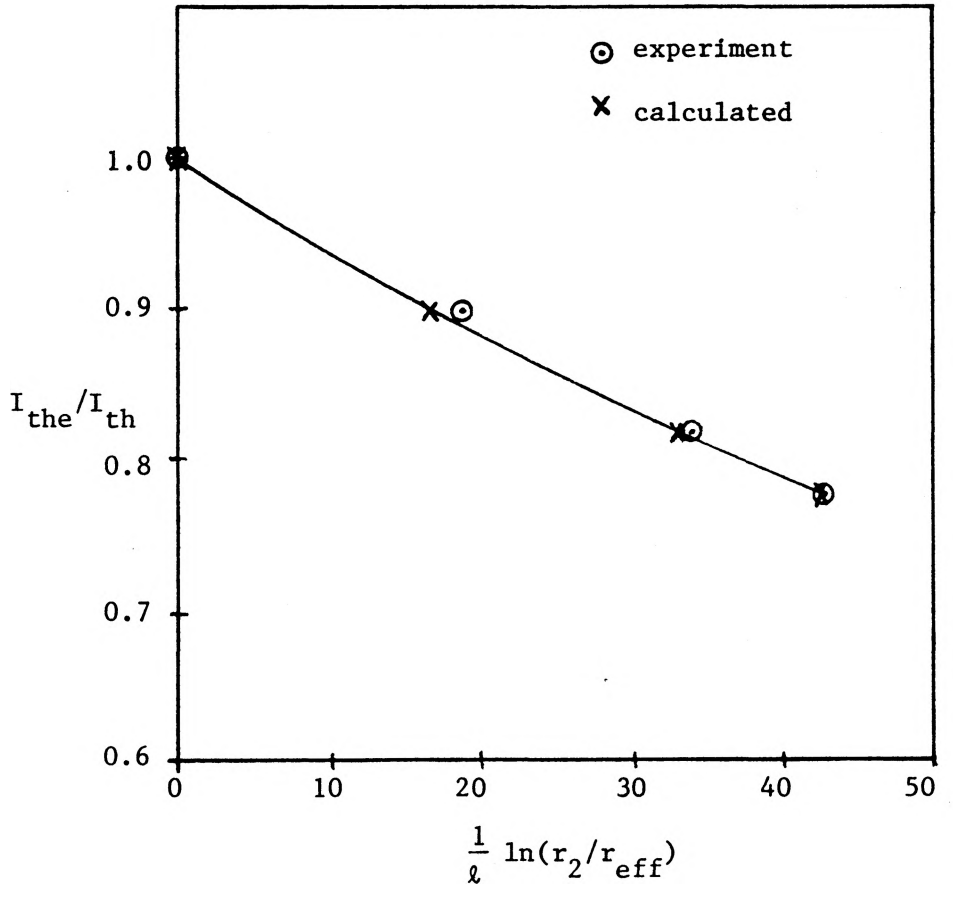

FIGURE 4.5 Experimental and calculated mirror loss reduction for several levels of feedback.

For an autocollimated grating orientation in the external cavity, the resolving power of the grating is given by (4.12),

$$R = \lambda/\Delta\lambda = (2Na \sin \theta)/\lambda \qquad (4.12)$$

where λ is the wavelength, $\Delta\lambda$ is the resolution, Na is the product of the number of lines illuminated and the line spacing, and θ is the autocollination angle ($\theta \simeq 29.90°$ in this case). Using (4.12), the calculated resolution is 1.0 ± 2 Å. A calculation of the resolution using the linear dispersion ($D_\ell = \frac{d\lambda}{dx}$) and the active region thickness ($d \simeq 0.2$ μm) yields a better resolution than is possible for the calculated resolving power ($\Delta\lambda \simeq 0.4$ Å). The exact value of the resolution due to the active region thickness is unknown due to the uncertainty in the effective thickness of the active region. The best available resolution is taken as the $1.0 \pm .2$ Å limit imposed by the resolving power of the grating.

Because of the finite resolution of both the spectrum of the feedback and the active region thickness, lasing will occur for a small range of wavelengths (i.e. grating positions) about an optimum wavelength which corresponds to a chip mode. The measured range is shown in Figure 4.6 to be about 1.3 Å, roughly 1/3 of the chip mode spacing. In Figure 4.6, the output intensity increases as the feedback approaches the longer wavelength end of the tuning. The linewidth changes very little through the tuning range, and is about 0.22 Å for the most intense output. The detected linewidth is limited by the monochromator resolution in this case. The spectral linewidth is not found to vary with increasing

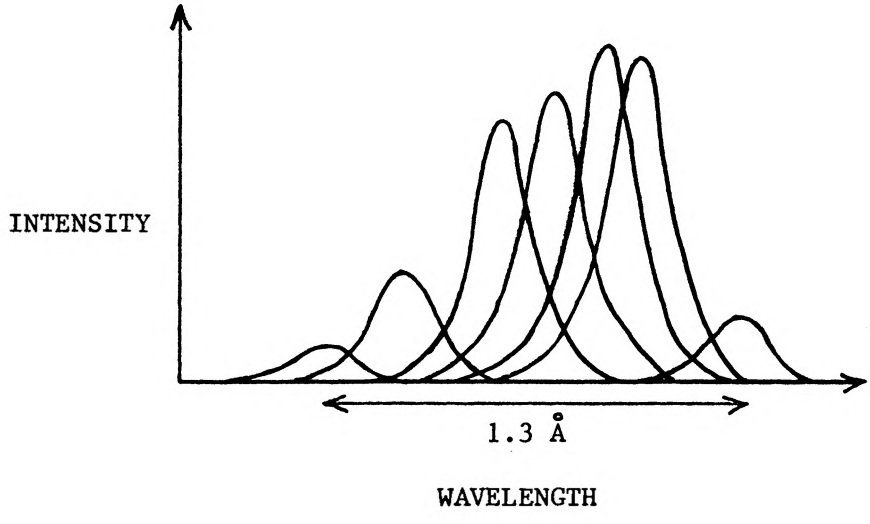

FIGURE 4.6 Wavelength tuning range over a single chip mode for grating feedback.

dc current as was shown for optical feedback with a plane mirror cavity (see comparison in Figure 4.3). Also, the measured linewidth for the grating cavity is significantly less than the calculated resolution of the optical feedback. If coherent optical interference effects were significant in determining the linewidth of a diode laser operated with grating feedback, the linewidth would be expected to increase with increasing dc current until the bandwidth limit of the grating was reached. Experimental results indicate that the linewidth of a diode operated with grating feedback is essentially the same as that of an isolated diode. Whether or not it is exactly the same as for the isolated device cannot be determined here because the detected linewidth is commensurate with the monochromator resolution.

An important characteristic of the output of a diode coupled to a grating external cavity is that higher power can be obtained over a smaller wavelength range than with non-dispersive feedback. Diodes with low facet reflectivity ($r_2 < 0.01$) have broad chip modes whose linewidth can be limited by the bandwidth of the gating feedback [16]. For the diode used in this work ($r_2 = 0.33$), the resolution of the grating feedback obtained has no detected effect on the CW spectral linewidth. The resolution of the gating feedback does however effect the dynamic spectrum obtained by active modelocking of the diode laser in a grating external cavity, which is discussed later in this thesis.

4.5 Summary

The effect of multiple reflections in a compound cavity made up of a diode laser and an external reflector have been evaluated. Experimental measurements of the mode linewidth dependence on optical feedback from a plane mirror give good qualitative agreement with a theory based on optical interference effects in the external resonator. The threshold current dependence on optical feedback is found to be in good agreement with the theory discussed. The spectral linewidth of a diode coupled to a grating external cavity is found to be indistinguishable from that of the isolated diode, and is not dependent on optical interference effects. These results are relevant to the discussion of CW and dynamic optical feedback effects in the remainder of this thesis.

CHAPTER 5

GRATING EXTERNAL CAVITY MEASUREMENTS

5.1 Introduction

A representation of the gain spectrum of a single mode double heterostructure GaAlAs laser is given which includes a significant wavelength dependent background loss term. The net gain curves obtained by using standard Hakki and Paoli type gain measurements are considered as having two parts; the total gain minus the linearly decreasing absorption loss gives the measured net gain. Optical feedback from a grating is used as a wavelength selective probe to do the gain measurements which determine the background loss.

Some of the parameters measured in the determination of the wavelength dependent absorption loss are applied to calculations of the threshold current of a laser coupled to a grating external cavity. An equation developed by Gade et al. in reference [17] which describes the wavelength dependence of the threshold current is verified using only one fitting parameter. A comparison made between the gain calculations and curves obtained by direct gain measurement gives better agreement than in the original work.

5.2 Wavelength Dependence of Absorption Loss

Using a grating for optical feedback reduces the effective mirror loss over a narrow wavelength range. This makes it possible for grating feedback selected individual modes to lase at a reduced threshold current. The external cavity arrangement used for this work is shown in Figure 5.1. The output of the LDL SCW20 laser is collimated by a 40/.85 microscope objective. The 1200 line/mm grating along with the 30 cm external cavity length gives a wavelength selectivity of much less than the chip mode spacing. The length of the external cavity is much greater than the length of the laser diode to ensure that the chip modes must only slightly detune to match the very narrowly spaced (in frequency) external cavity modes. The zeroth order reflection from the grating is monitored by a photometer to measure the intensity and a monochromator to identify the wavelength of the lasing mode. A variable attenuator is placed in the external cavity to change the level of feedback, and therefore the threshold current, for particular chip modes. This arrangement is suitable for finding the gain versus current relationship for selected modes if the effective change in mirror loss due to the full range of attenuation is known. The manner in which the optical feedback probes the gain is shown in Figure 5.2(a).

To scale the range of the mirror loss reduction induced by the optical feedback, gain data was acquired using the standard Fabry Perot (FP) technique originated by Hakki and Paoli [18]. In this method, the emission of the laser is imaged onto the entrance slit of a monochromator.

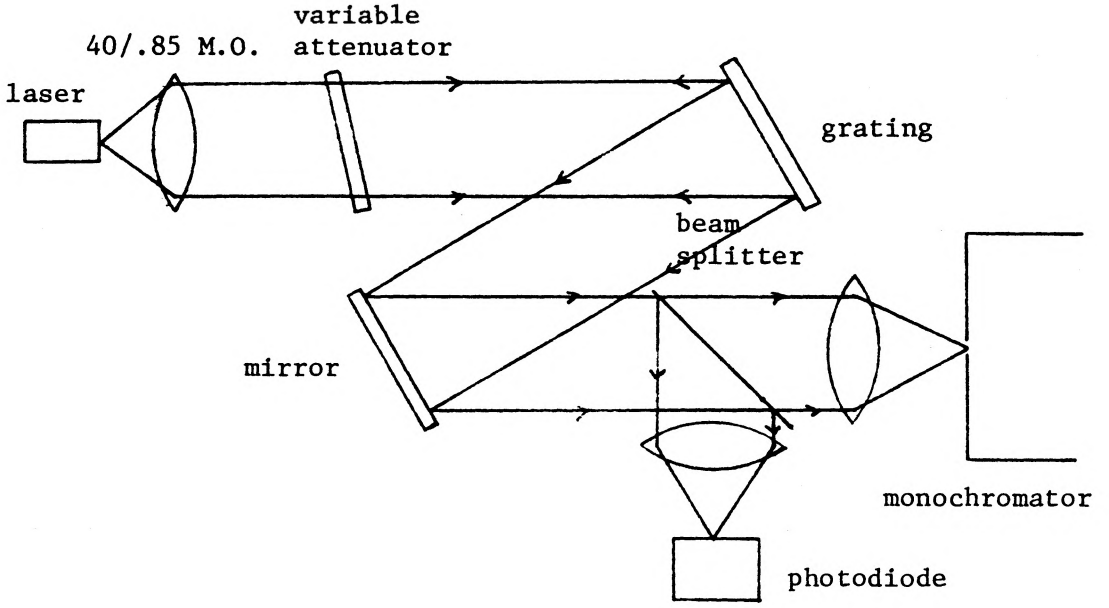

FIGURE 5.1 Grating external cavity arrangement.

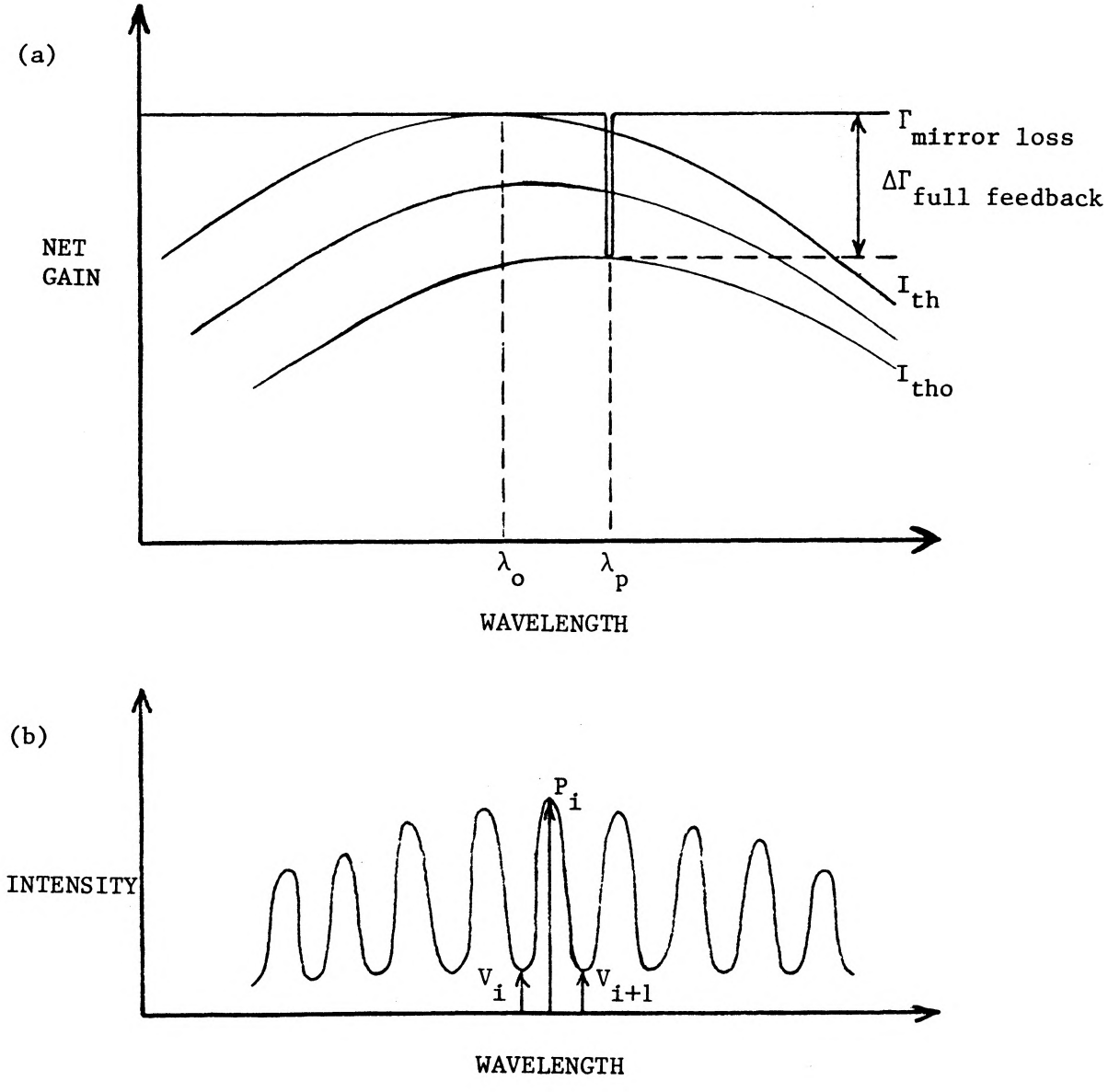

FIGURE 5.2 In (a), the optical feedback from the grating acts as a wavelength selective probe of the gain.
In (b), the typical mode spectrum below lasing threshold is shown. P_i indicates the peak heights, V_i the valleys.

The Fabry-Perot modulated spectrum of the laser operated below threshold is used to calculate the net gain from the peak and valley heights (Figure 5.2(b)). Care must be taken to eliminate excess spontaneous emission from outside the lasing region when doing gain measurements of this type. Excess spontaneous light will decrease the peak to valley ratio, and therefore decrease the measured gain. Convolution of the monochromator spectral resolution (less than 0.2 Å) with the laser mode also reduces the measured peak to valley ratio. These effects are most noticeable in the wavelength region near the peak of the gain since the peak to valley ratio is greatest there. An effective method for eliminating the excess spontaneous light is to orient the junction plane perpendicular to the monochromator slits. The depth of modulation is given by dividing each peak value by the average of its adjacent valleys,

$$\gamma_i = \frac{2\,P_i}{V_i + V_{i+1}} \tag{5.1}$$

The net gain is given by

$$G_{net} = \frac{1}{\ell} \ln \left(\frac{\gamma^{1/2} + 1}{\gamma^{1/2} - 1}\right) + \frac{1}{\ell} \ln r_1 r_2 \tag{5.2}$$

where ℓ is the diode length and r_1, r_2 are the facet amplitude reflectivities. By doing these measurements at various bias levels, gain versus current relationships can be calculated at selected wavelengths.

Two options can be chosen to determine the wavelength dependence of the absorption loss using data obtained from grating external cavity

measurements. Each level of attenuation can be scaled using the gain slopes from the FP gain calculation and the change in threshold current relative to the minimum threshold at a particular wavelength. Another method is to calculate the effective reflectivity of the facet, attenuator, grating combination at each level of attenuation. A variable mirror loss term can then be calculated. The former technique will be used as a consistency check of the latter.

The effective reflectivity on the cavity side of the diode is given by

$$r_{eff} = \frac{r_2 + r_3 t^2}{1 + r_2 r_3 t^2} \tag{5.3}$$

where r_2 = facet amplitude reflectivity

r_3 = effective grating reflectivity

t = attenuator amplitude transmittance

For the LDL diode used, the rear facet has a high reflectivity coating ($r_1 = .975$). The front facet is passively coated ($r_2 = 0.52$). The measured length of the diode is $\ell = 210$ μm. Mirror loss can be calculated by adding the feedback term

$$\Delta\Gamma = \frac{1}{\ell} \ln (r_2/r_{eff}) \tag{5.4a}$$

to the expression for mirror loss to give

$$\Gamma = \frac{1}{\ell} [\ln (\frac{1}{r_1 r_2}) + \ln (\frac{r_2}{r_{eff}})] \tag{5.4b}$$

The effective reflectivity of the grating, r_3, can be found by fitting the change in mirror loss for the full range of attenuation (using equations (5.3) and (5.4)) to the value found using the gain slopes from the FP type calculations ($\Delta\Gamma$ 20 = cm^{-1}). Using this method, r_3 = .72 and r_{eff} = .902. The mirror loss (or gain) versus current relationships for particular modes can be extrapolated to zero current to yield a relative difference in absorption loss on the gain axis. The resulting loss versus wavelength is -0.90 ± .14 cm^{-1} $Å^{-1}$ for this method (Figure 5.3).

A loss calibration of each level of attenuation in the external cavity using gain slopes from the FP gain calculation and the change in threshold current relative to full feedback requires no knowledge of r_{eff}. A sample of the scaled data is shown in Figure 5.4. The result of extrapolating the gain current relationships to zero current is a wavelength dependent loss of -0.91 ± .14 cm^{-1} $Å^{-1}$ (Figure 5.5). This is consistent with the result of the calculation using r_{eff}. The values used in the r_{eff} calculation therefore have additional verification.

Gain versus current data for various wavelengths can be taken directly from the FP gain spectra calculations. The calculated gain spectra are shown in Figure 5.6 for several bias current levels. To confirm the repeatability of the FP measurements, the experiment was done twice. The resulting sets of data have gain slopes at various wavelengths which are in good agreement with each other. The shapes of the gain curves are different for low bias current and far below the peak of the gain

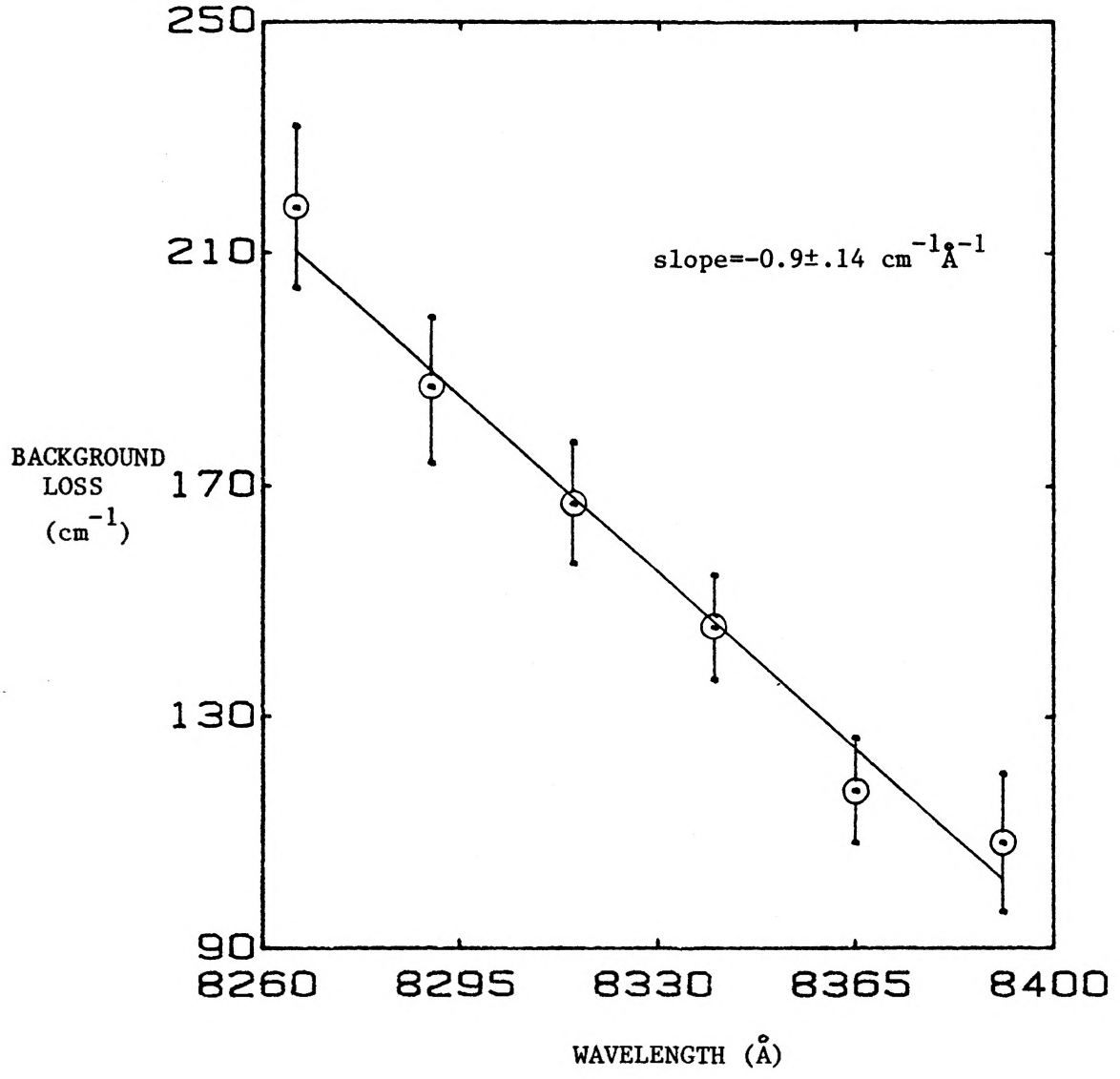

FIGURE 5.3 Variation of background loss with wavelength determined from the r_{eff} calculations. Zero on the loss axis corresponds to no mirror loss.

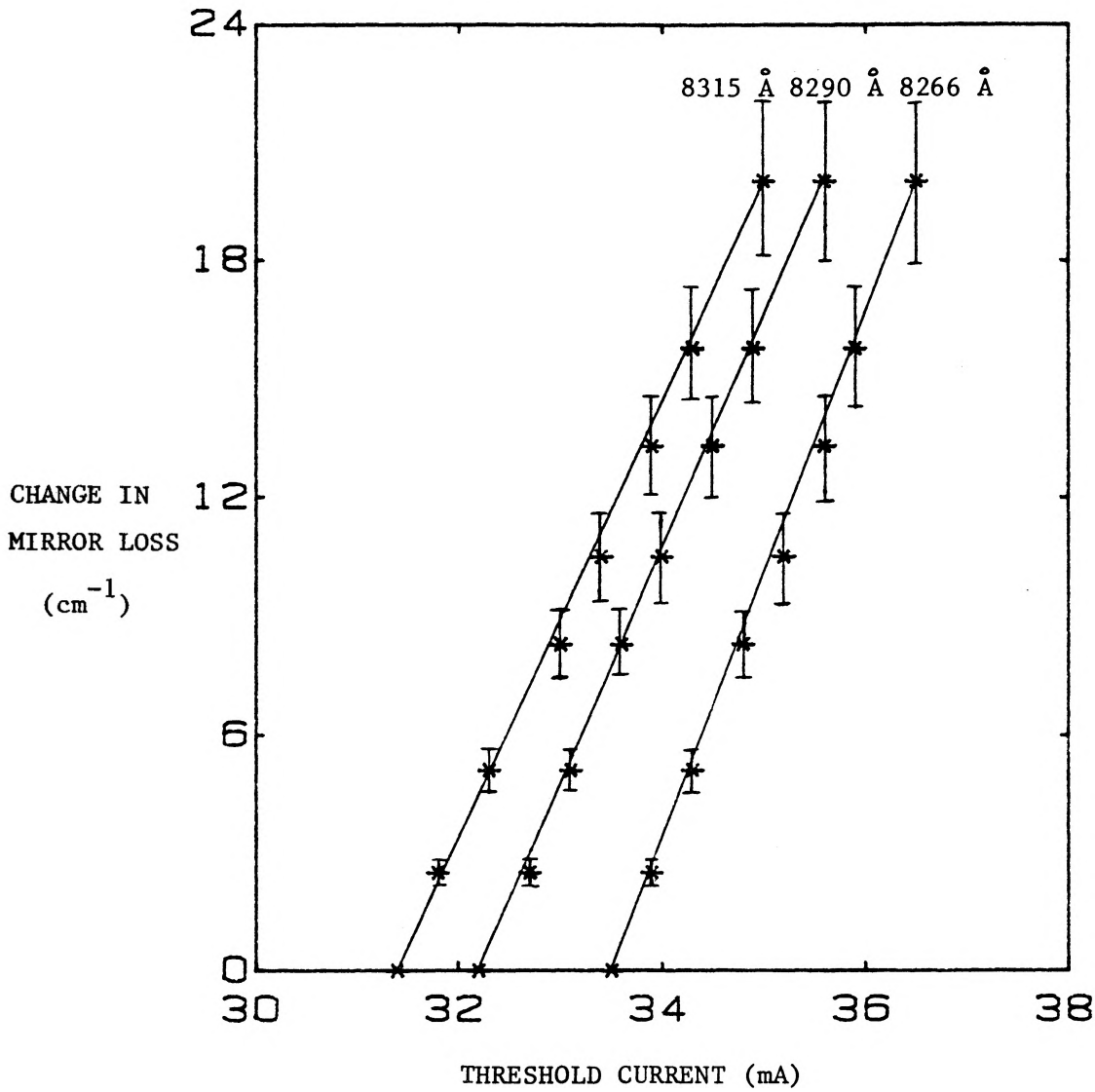

FIGURE 5.4 A sample of the data for the change in mirror loss versus threshold current for three grating selected wavelengths.

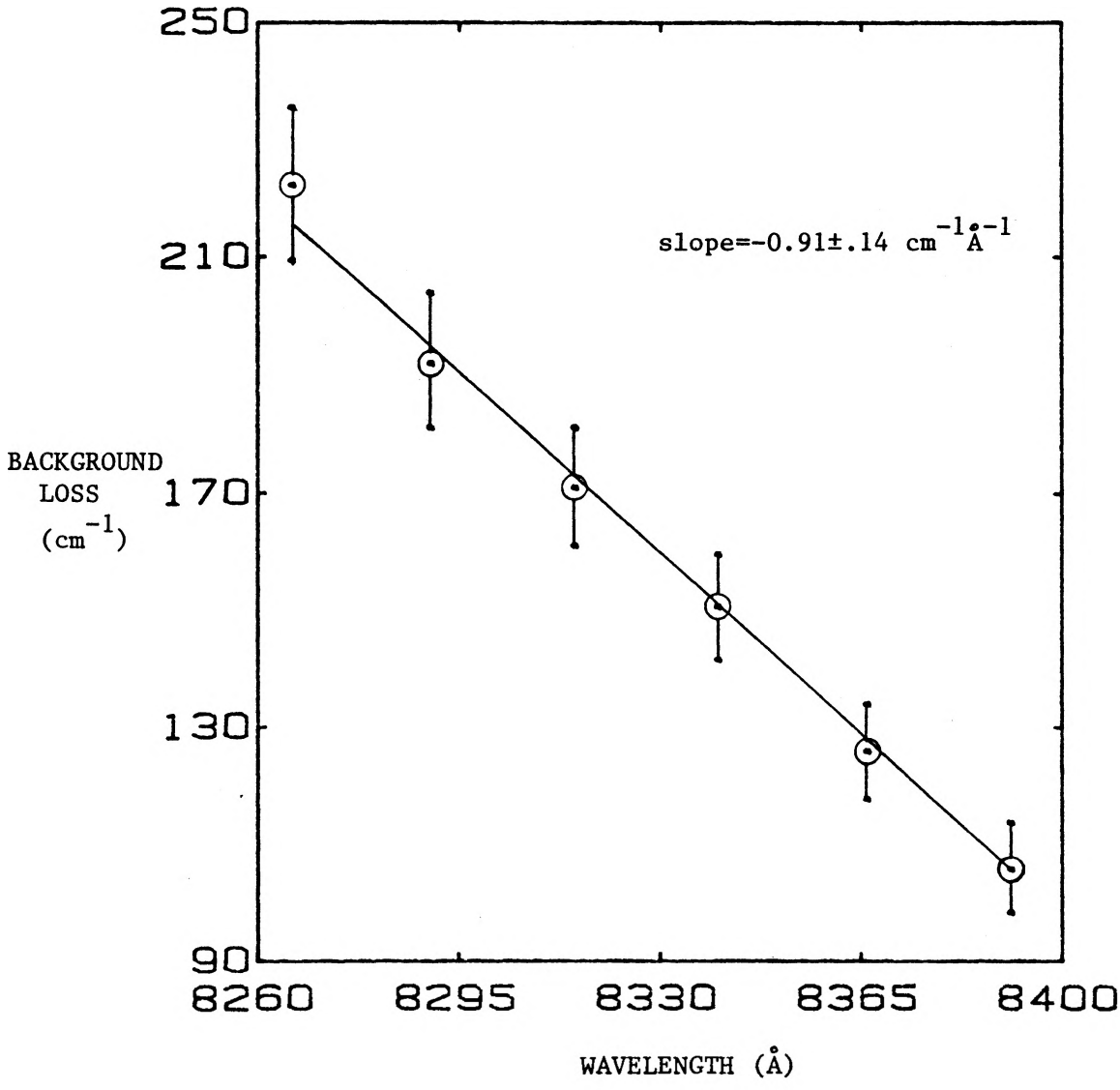

FIGURE 5.5 Variation of background loss with wavelength determined without the r_{eff} calculations.

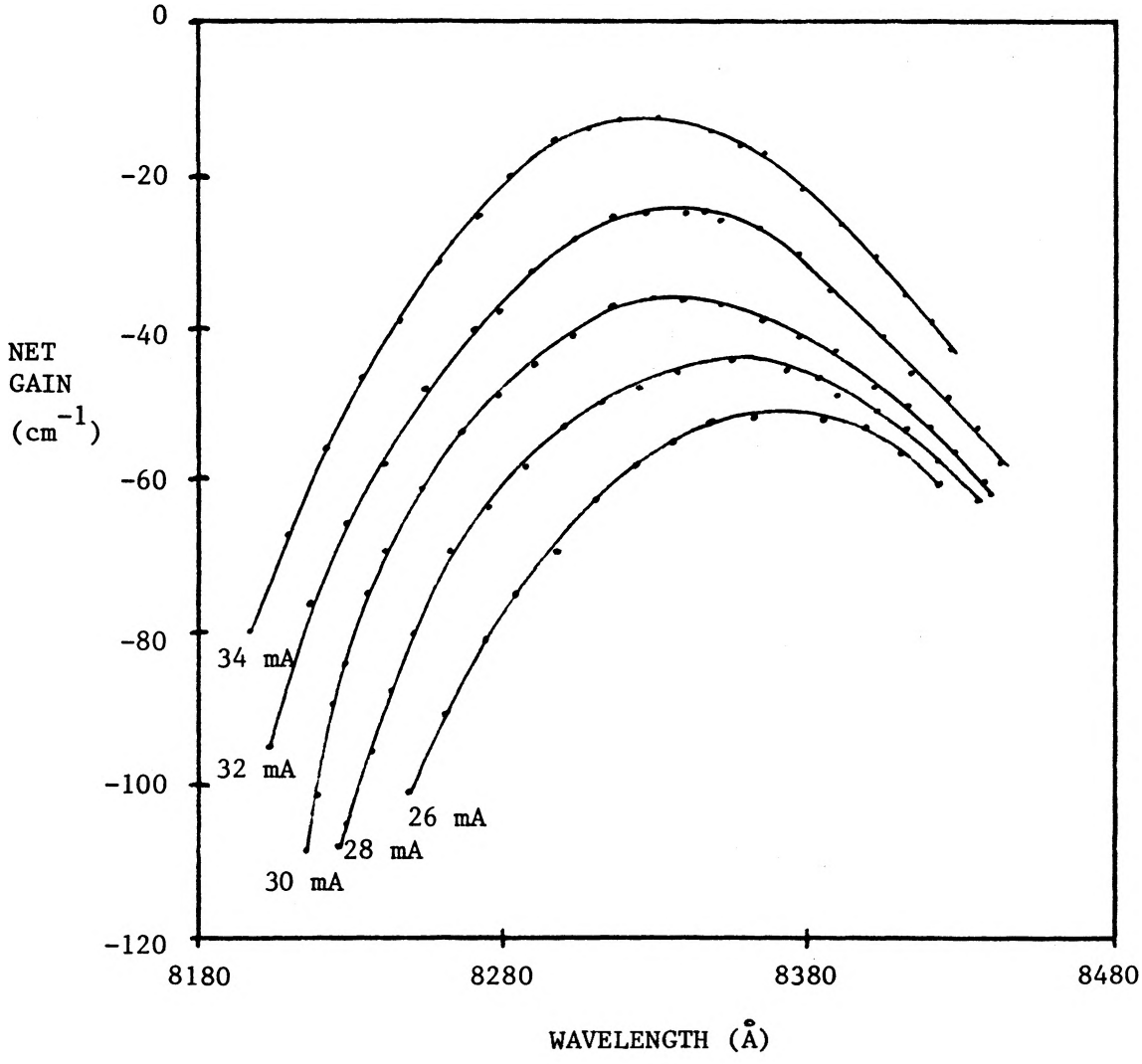

FIGURE 5.6 Mode gain versus wavelength measured using the standard FP technique.

($-30\ cm^{-1}$) for bias currents close to threshold. These are both measurement regimes in which the data is less accurate because the signal is small. These differences do not effect any of the calculations since only the gain slopes from the FP gain measurements are used. The result of extrapolating the gain-current relationships for various wavelengths to zero current is shown in Figure 5.7 to be a wavelength dependent background loss of $-1.0 \pm .2\ cm^{-1}\ \text{Å}^{-1}$. This value is in agreement with the value obtained using the other two methods.

5.3 Gain Measurements Using A Grating External Cavity

The optical feedback from a grating external cavity gives an increase in net gain for a single mode because of the reduction in the mirror loss term over a narrow wavelength range. The unsaturated net gain is given by

$$G_{net}(I,\lambda) = g(I,\lambda) - \alpha - \frac{1}{\ell}\left(\ln\frac{1}{r_1 r_2} + \ln\frac{r_2}{r_{eff}}\right) \tag{5.5}$$

where $g(I,\lambda)$ = unsaturated mode gain per unit length

α = internal loss per unit length

ℓ = diode length

r_1, r_2, r_{eff} = amplitude reflectivities as defined earlier

To second order in wavelength, the mode gain can be written as

$$g(I,\lambda) = \frac{1}{\ell}\left(g_o(I) - \left(\frac{\lambda-\lambda_o(I)}{\Delta\lambda}\right)^2\right) \tag{5.6}$$

Since the range of threshold reduction is small relative to I_{th}, $g_o(I,\lambda)$

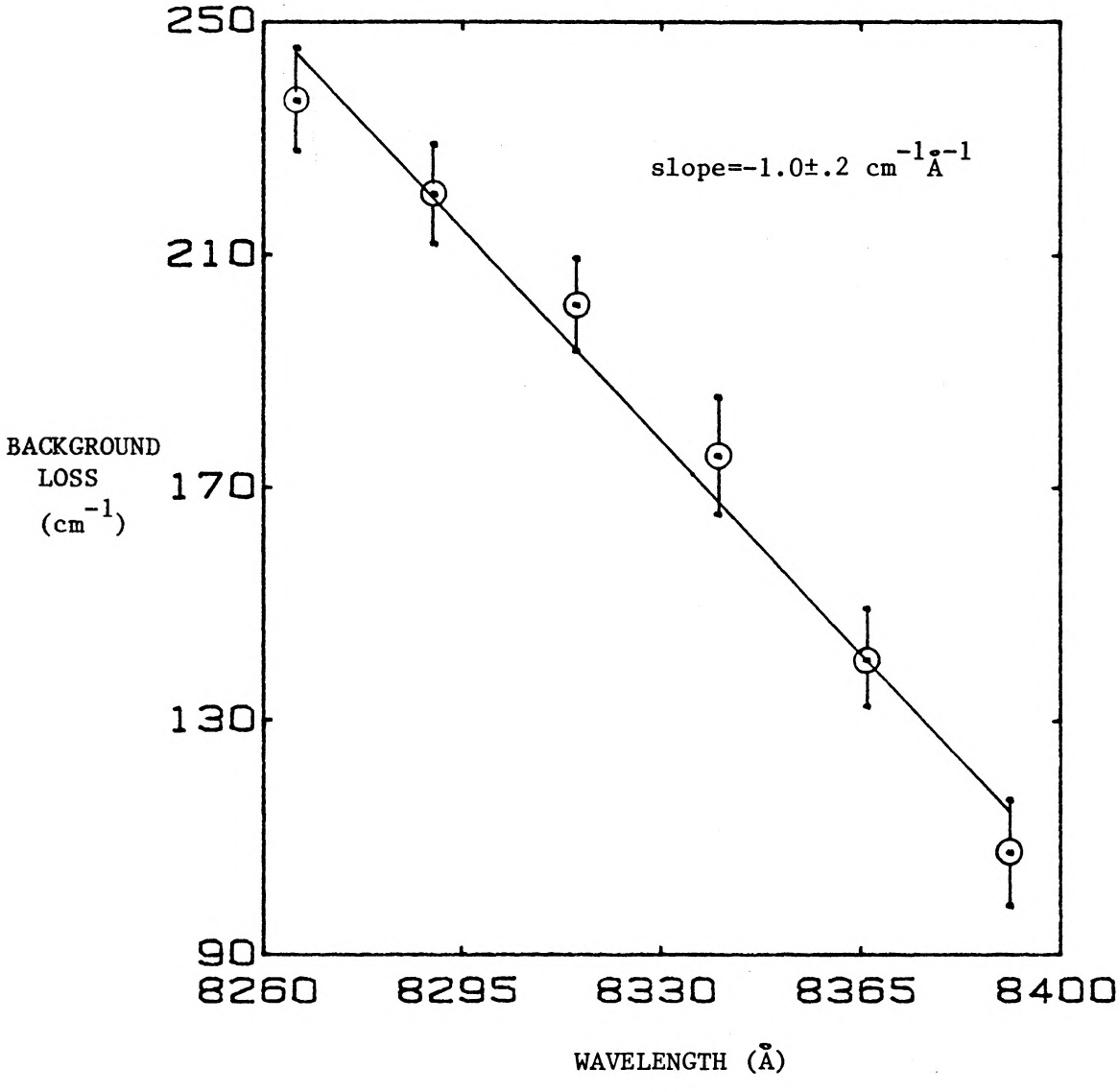

FIGURE 5.7 Variation of background loss with wavelength determined from the FP type gain measurements.

and $\lambda_o(I)$ can be written as

$$g_o(I) = k(I-I_o) \tag{5.7}$$

$$\lambda_o(I) = \lambda_{oo}-\delta\lambda\ (I-I_{tho}) \tag{5.8}$$

The above parameters are defined as:

k/ℓ = gain slope following the peak of the gain

$I_o(\lambda)$ = current required to achieve zero bulk gain

$\lambda_o(I)$ = mode with minimum I_{th} in grating cavity

$\delta\lambda$ = wavelength shift of peak of gain with current

I_{tho} = minimum threshold current

In equation (5.6), the wavelength dependence of the gain slope is effectively included in the shift of the peak of the gain with current (equation (5.8)). Substituting (5.7) and (5.8) into (5.5), and using the threshold condition $G_{net}(I,\lambda) = 0$ the threshold current can be written as

$$I_{th}(\lambda) = I_{tho} + \frac{1}{k}\left(\frac{\lambda-\lambda_{oo}+\delta\lambda\,(I_{th}(\lambda) - I_{tho})}{\Delta\lambda}\right)^2 \tag{5.9}$$

$$= I_{tho} + \frac{1}{k}\left(\frac{\lambda-\lambda_{oo}+\delta\lambda\,((\lambda-\lambda_{oo})/(\sqrt{k}\,\Delta\lambda))}{\sqrt{k}\,\Delta\lambda}\right)^2$$

From the FP gain measurements, the gain slope for the peak of the gain is k/ℓ=4.5 cm^{-1} mA^{-1}. The value for $\delta\lambda$, the wavelength shift of the peak of the gain per mA, is taken from the difference in wavelength between the peak mode without feedback and the mode with minimum I_{th} at

full feedback. This gives $\delta\lambda = 3.6$ $\mathring{A}mA^{-1}$ from a total wavelength shift of about 20 $\mathring{A}$.

Fitting equation (5.9) to threshold versus wavelength data will give all the necessary parameters to calculate the gain curves using equation (5.6). The only fitting parameter used in equation (5.9) is $\Delta\lambda$ which gives the width of the pseudo parabola. The theoretical curve is quite sensitive to the value for $\Delta\lambda$ but is fairly insensitive to the $\delta\lambda$ value. Threshold current versus wavelength data is shown in Figure 5.8 along with a theoretical fit. The gain curves which can now be calculated using equation (5.6) will be compared to those obtained using a direct gain measurement technique.

Measuring the gain directly using a grating external cavity involves varying the attenuation in the feedback and looking for the modes which have a particular threshold current. The gain width is effectively measured at each level of attenuation, as shown in Figure 5.9. The full depth of the gain measured is dependent on the maximum depth of the feedback probe. Since the data is in the form of attenuation versus wavelength for selected currents, the attenuation is scaled in terms of change in mirror loss using equations (5.3) and (5.4) (as in section 5.2). A comparison of a gain curve measured using the grating cavity technique and a theoretical gain curve using equation (5.6) is shown in Figure 5.10. The measured and calculated gain curves are in very good agreement.

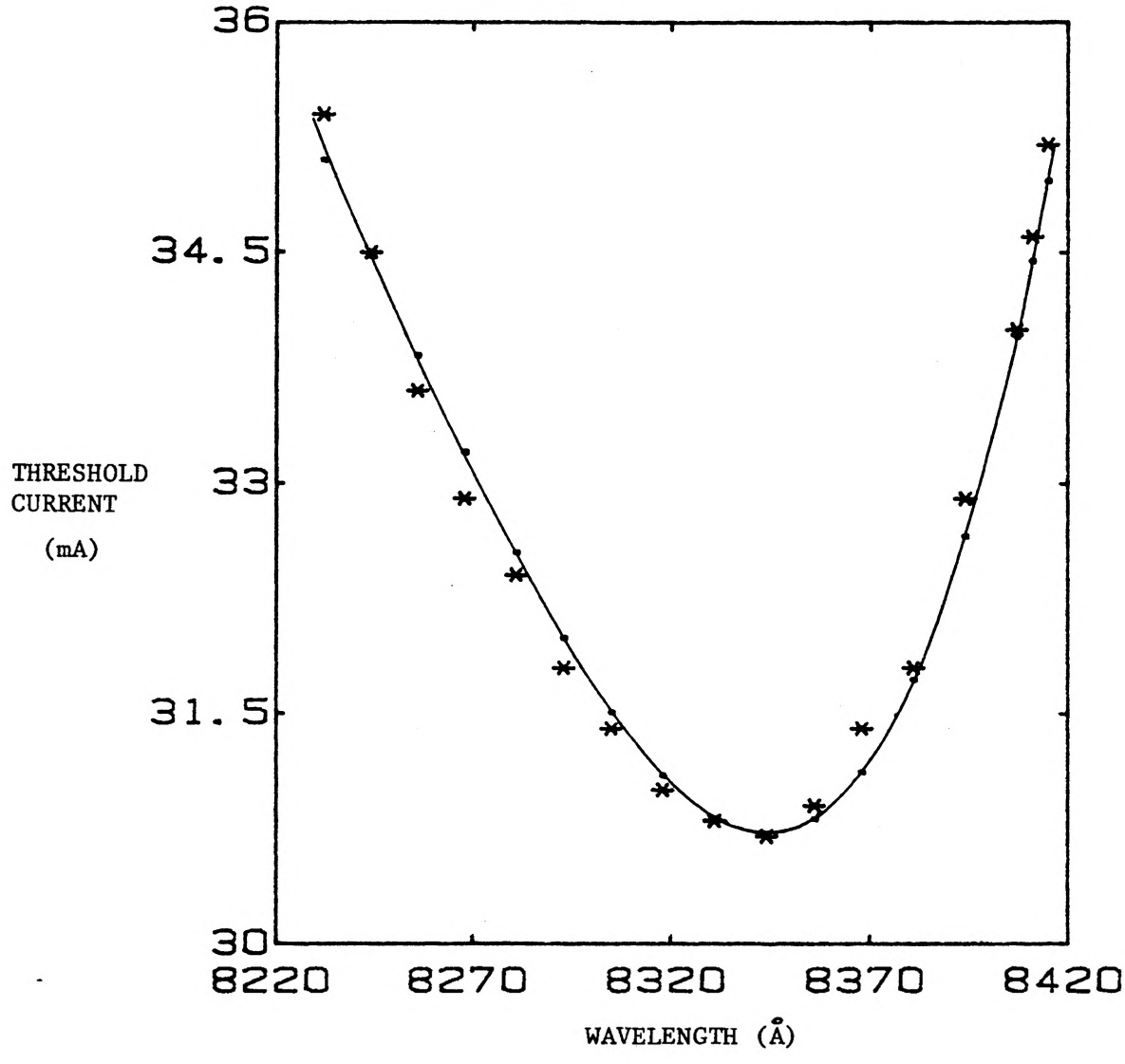

FIGURE 5.8 Threshold current versus wavelength data (points) and theoretical fit (solid line).

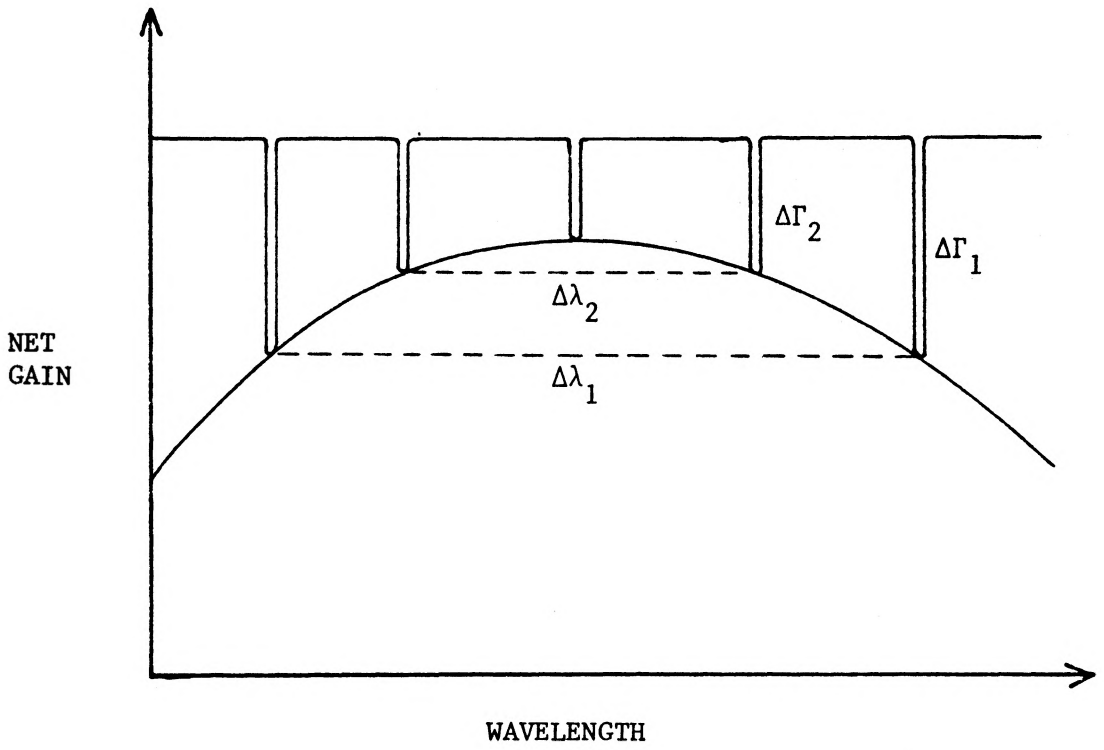

FIGURE 5.9 Grating external feedback probes the gain width when the coupling is varied.

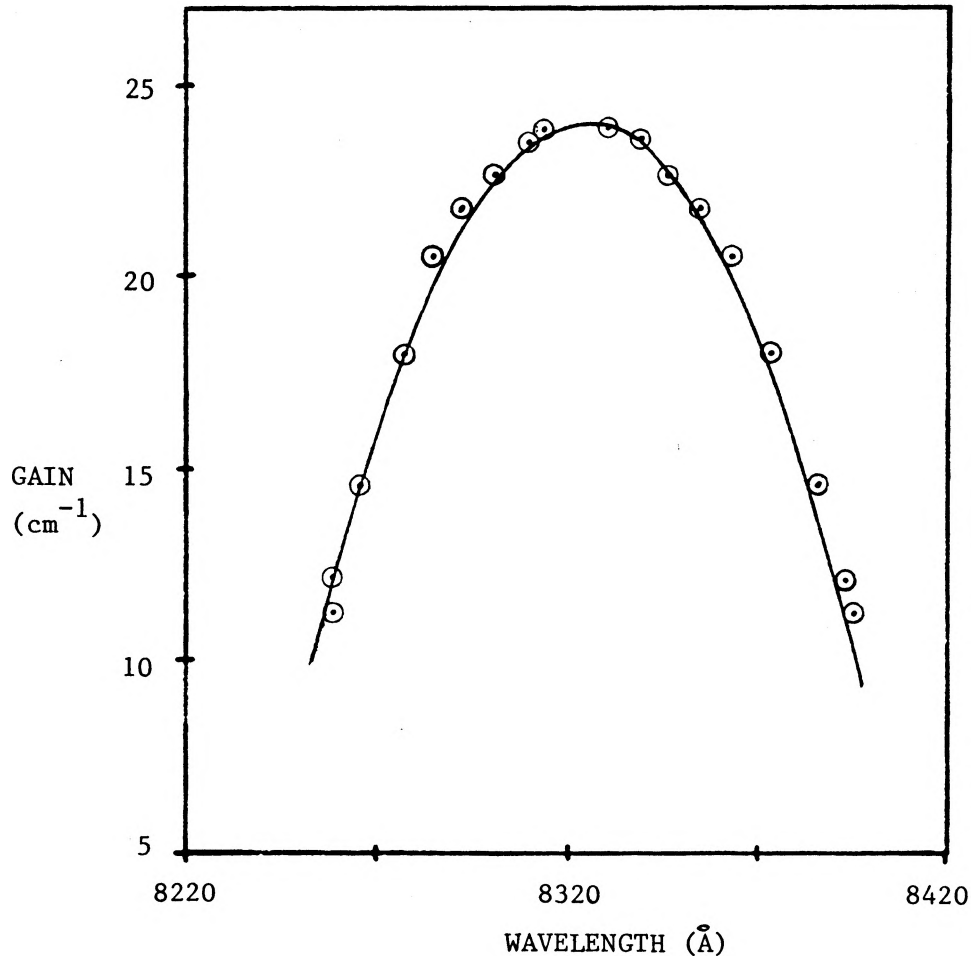

FIGURE 5.10 A comparison of the theoretical gain versus wavelength curve to the directly measured data (using the GEC technique) at a bias current of 34 mA. The solid line is the theoretical curve and the points represent the data.

Since the theoretical gain curves can be calculated for various currents using equation (5.7) (Figure 5.11(a)), these curves can be treated just as the gain curves derived from the FP type data to determine the wavelength dependence of the absorption loss. The gain current relationships are fairly linear over the range of bias currents from 28 to 38 mA (I_{th} = 37 mA), but are non-linear over the full range. Only the range close to threshold is meaningful since equations (5.7) and (5.8) were written only to first order in I (assuming a small range of currents). By extrapolating the gain versus current relationships to zero bias, the wavelength dependence of the loss is found to be $d\alpha/d\lambda = -0.86$ cm^{-1} mA^{-1} (Figure 5.11(b)). This is in extremely good agreement with the other values obtained.

5.4 Discussion 1

The gain curve of a diode laser can be represented by a wavelength dependent background loss term which is subtracted from a curve representing total gain. It has been shown that this type of representation can be applied to the mode gain in a range of bias currents below threshold. The reduction in background loss at longer wavelengths can be attributed to a lower absorption loss near the band edge. The wavelength dependent background loss term was found to be -0.90 ± 0.10 cm^{-1} $Å^{-1}$. Using several approaches to obtain a consistent value for $d\alpha/d\lambda$ gives verification of the measured parameters used in the determination of $d\alpha/d\lambda$.

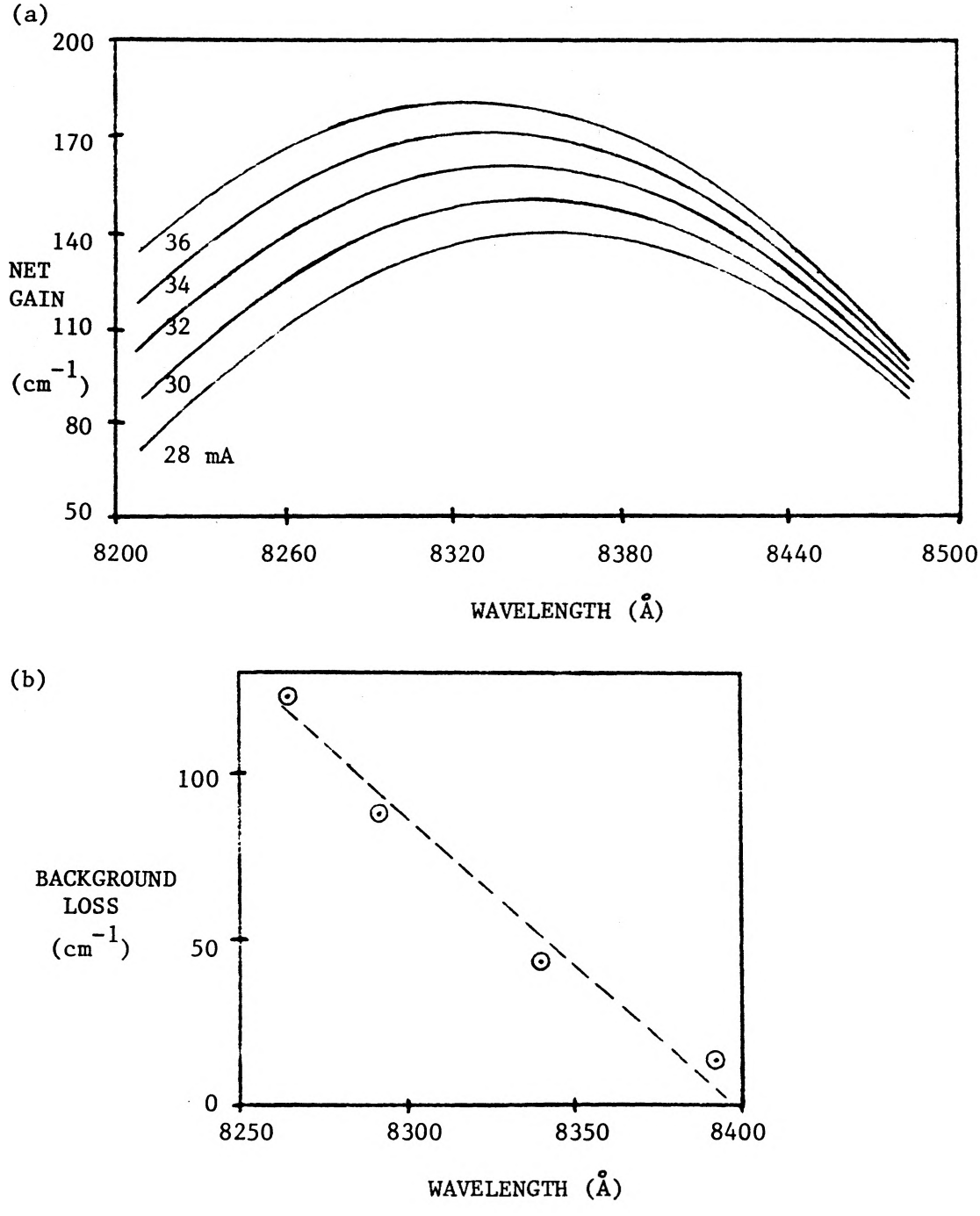

FIGURE 5.11 The calculated variation in background loss in (b) is determined from the theoretical gain curves of equation 5.7 for several bias currents (shown in (a)).

A similar value for $d\alpha/d\lambda$ was found in reference [6] where it was applied to a discussion of the loss reduction for a diode laser operated in an external resonator. The threshold reduction of a laser operated in a plane mirror external cavity gives the full loss reduction due to the optical feedback if the net gain curves are known. In reference [6], half of the total threshold reduction was attributed to a reduction in $\alpha(\lambda)$ due to a shift in the peak of the gain to a longer operating wavelength. The change in $\alpha(\lambda)$ was subtracted from the difference in net gain between the external cavity coupled and uncoupled cases. Since the net gain includes any variation in background loss, such a procedure is inappropriate. Curves which give the total gain must be used in this calculation if the effect of the varying background loss is to be included separately.

The total change in net gain corresponding to the full reduction in threshold current gives the sum of the loss reductions due to the changes in mirror loss and modal propagation loss. The measured effective reflectivity of the external grating ($r_3 = .72$) indicates a higher coupling efficiency than the actual mirror loss reduction would give alone. The relative size of the separate terms which contribute to the total loss reduction can be measured by doing FP type gain measurements of the diode laser spontaneous spectrum operated with and without an external cavity. These type of FP measurements, which were done in reference [6] using similar lasers to those used in this work, yield a mirror loss reduction term which is approximately half of the total measured loss reduction.

The mirror loss reduction term is important in determining the appropriate size of the delayed photon feedback term in the equations which describe the laser dynamics with an external resonator.

5.5 Discussion 2

A fourth order equation was developed in [17] to describe the wavelength dependence of the threshold current in the case of optical feedback induced single mode operation. The fitting of this equation to experimental measurements of threshold current versus wavelength provided the parameters necessary to describe the curvature of the gain in a small wavelength range below threshold. Since FP type gain measurements were done in this work, no fitting procedure was necessary to find the change in the peak of the gain with current. The wavelength shift of the peak of the gain with current was also measured. Therefore, a single parameter fit of the calculated to the measured wavelength dependence of the threshold current was possible. The resulting calculated wavelength dependence agrees with the experimental measurements.

The shape of the gain curve can be found using the parameters which result from fitting the measured wavelength dependence of the threshold current. A comparison of the calculated gain curve to the direct gain measurements, which were made using a grating external cavity, yields better results in this work than in the original [17]. In the work by Gade and Osmundsen, the directly measured gain curve is up to 4 cm^{-1} below the calculated gain curve on the long wavelength side. This is a large discrepancy given that the gain curve is measured to

only 9 cm^{-1} below the peak of the gain. The discrepancy in [17] was attributed mainly to a large 4°C difference in the temperature of the laser during measurements of the gain on the short versus the long wavelength side of the peak. The laser used in this work was not temperature controlled, but the direct gain measurements were made by scanning both wings of the gain at fixed bias current. The effects of extremely different temperatures for opposite sides of the peak of the gain are therefore eliminated. Another factor in the improved results of this work is that fewer parameters were unmeasured than in [17]. Most of the parameters which were fitted in [17] were directly measured in this work to show the validity of the discussed theoretical representation of the gain. In the present work, the difference between the measured and calculated gain curve is no more than 1 cm^{-1} in a gain region which is 14 cm^{-1} below the gain peak.

A set of calculated gain curves for various bias currents was used to calculate a wavelength dependent background loss term which agrees with the other values obtained. This aids in demonstrating the equivalence of the theoretical representation and the measured gain curves.

CHAPTER 6

OSCILLATOR STABILITY CONSIDERATIONS FOR ACTIVE MODELOCKING

6.1 Introduction

The characteristics of actively modelocked diode laser operation in an external cavity have been investigated in other work ([1], [19]-[23]). The use of sinusoidal modulation in the region of 1 GHz to 3 GHz has resulted in modelocked pulse lengths of less than 5 psec for lasers with an anti-reflection coated facet on the resonator side. In work using standard uncoated devices [1], a rapid change of optical pulse position with respect to the peak of the modulation has been seen in the tuning region of the shortest, most intense modelocked pulses. A computer model was developed in reference [1] which gives good simulation of the behaviour of devices with non-zero facet reflectivity, but the model was not tested for a reflectivity of less than 37 percent. This work uses a laser with an intermediate facet power reflectivity of 11 percent to illustrate the frequency tuning characteristics for several levels of feedback. Simulations are done to show that the model developed in [1] is capable of predicting the tuning behaviour for various degrees of coupling to the external cavity. The modelocking model is then used to predict the tuning characteristics of a laser with a low residual facet reflectivity of 1 percent, a change which increases the coupling to the

external resonator. The simulated rate of change of phase of the optical pulse with respect to the current modulation is rapid enough in the region of the most intense modelocked pulses to account for the previously unexplained extreme sensitivity of the modelocking process to oscillator stability.

6.2 Theory

Active modelocking of diode lasers offers several advantages over direct modulation schemes. Short optical pulses can be obtained using small current modulation, which in turn yields a narrow dynamic spectrum. Even for large modulation, the spectral content is lower than in the no-feedback case. The pulse need not build up from noise after each round trip since a fraction of the previous pulse is stored in the external resonator, narrowing the spectrum.

Since residual facet reflectivity results in temporal substructure on the modelocked pulses [23], zero diode facet reflectivity is desirable for achieving structure free Gaussian pulses. A perfect anti-reflection coated facet on the resonator side of the diode will result in the diode acting as a gain medium within a longer cavity. The spectrum of the diode output is as broad as its gain since the zero reflectivity facet provides no Fabry-Perot cavity within the chip. When the modulation is resonant with the cavity round trip time, the pulse will sit stably at the peak of the gain. This occurs since the optical pulse fed back to the laser will experience more gain on the leading than on the trailing edge, and will therefore move forward in time over a number of round trips

until it is at the peak of the gain. At a modulation frequency slightly below the cavity round trip frequency, the trailing edge of the pulse will always experience more gain than the leading edge. The pulse is shortened and undergoes a shift to later in time to compensate for the difference between the modulation and resonant frequencies. The pulses continue to shorten at lower modulation frequency until the gain can no longer support short pulses together with a large phase shift [19]. At frequencies above resonance, the leading edge of the pulse always experiences more gain than the trailing edge. The pulse must become wider with increasing frequency so that it can shift forward in time toward the peak of the gain. The width and phase of the mode-locked pulse with respect to the current modulation will change as the modulation frequency is varied to ensure that there is unity gain and no net shift for the pulse after each round trip in the cavity.

A laser with significant facet reflectivity changes the mode-locking characteristics somewhat. The spectrum of the diode output is largely determined by the amplitude modulation of the closely spaced external cavity modes ($\Delta\lambda \simeq .022$ Å) by the Fabry Perot cavity formed by the diode chip ($\Delta\lambda \simeq 4$ Å). Coherent optical interference effects in the cavity cause an increase in linewidth (the number of external cavity modes per chip mode) with increasing feedback to the laser. In the pulsed case, multiple chip reflections occur because of the finite facet reflectivity. This causes the modelocked pulse to go through a convolution of the amplification of the diode with the exponentially decaying chip response on each round trip. The decaying chip response

delays the pulse, and therefore introduces an offset between the round trip frequency and the modulation frequency required for the pulse to sit at the peak of the gain. The offset is on the order of 1 percent below the resonant frequency for a facet power reflectivity of 37 percent and a resonator length of 15 cm [1].

A modelocking model which includes the effects of finite facet reflectivity was developed in reference [1]. A time domain representation was found to be inappropriate due to the computer time and cumulative numerical errors associated with the larger number of iterations required to obtain a self-consistent solution. Use of a frequency domain representation of the rate equations was found to be more appropriate since it allows for all of the harmonics of the modulation of the photon density and carrier density. In the frequency domain, the harmonics evolve until a self-consistent solution is reached. A further advantage of the frequency domain representation is that the harmonics can represent a perturbed gain waveform. In a time domain representation, the gain is usually assumed to remain sinusoidal in the presence of optical pulses. Such a representation does not allow for the significant gain saturation which occurs for even moderately intense pulses (see Figure 6.1). The perturbation of the sinusoidal gain will cause changes in the tuning characteristics which are predicted by the frequency domain model.

The model developed in [1] is useful for conditions where the dc bias of the laser is above the external cavity threshold. Since no intra-cavity bandwidth limitation was used, such as a Fabry Perot etalon

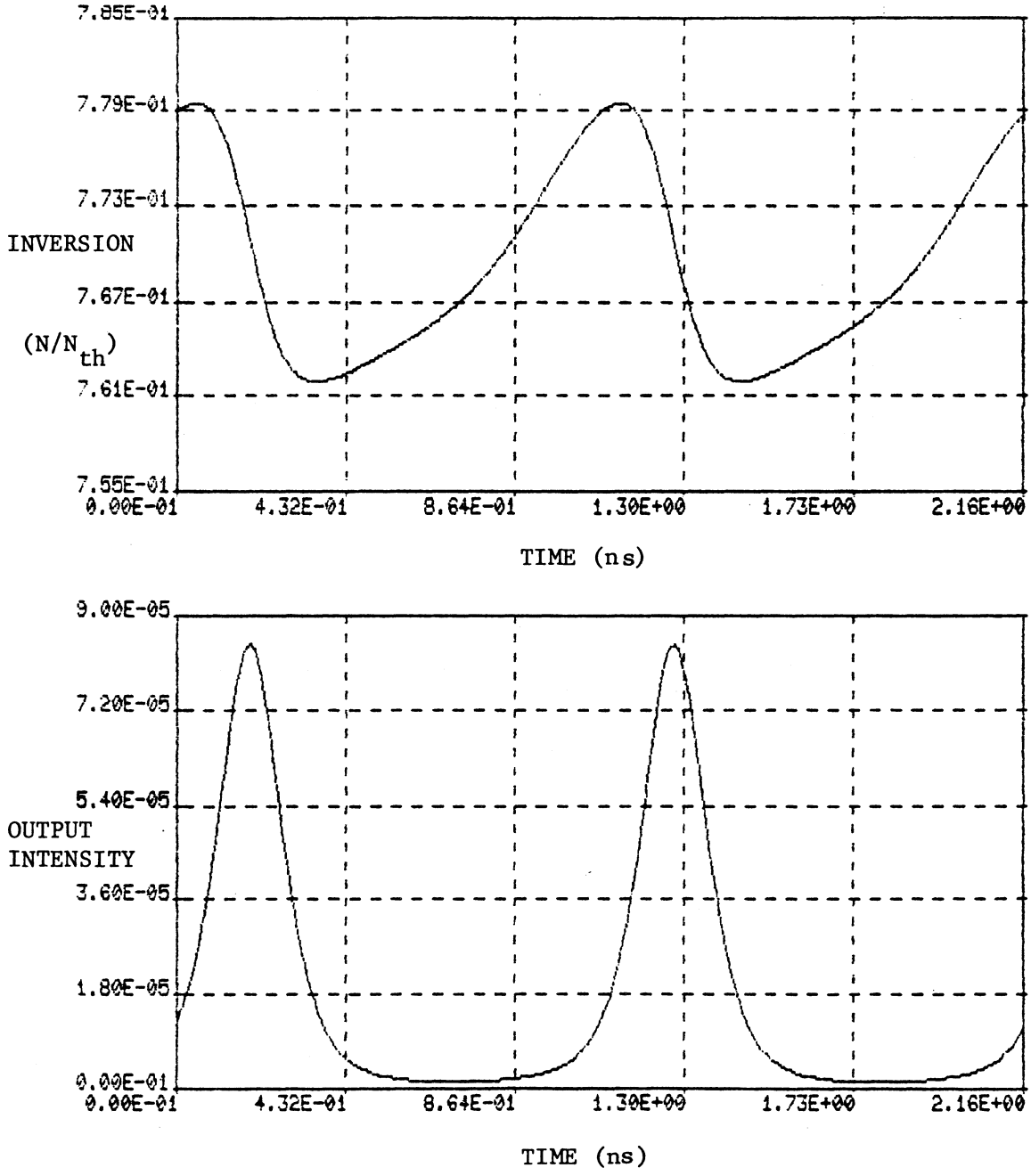

FIGURE 6.1 Illustration of the significant perturbation of the sinusoidal gain (inversion) due to gain saturation.

or a diffraction grating, small current modulation ($\simeq$ 4 percent) was employed to retain a narrow dynamic spectrum. The above threshold regime can be more easily modelled since the coupling efficiency remains constant there. Gain guiding effects in the plane parallel to the p-n junction which aid in coupling light back into the laser are fixed when the gain is clamped at threshold.

6.3 Experiment

The external cavity arrangement used in this work is shown schematically in Figure 6.2. The laser output is collected by a 40/0.85 microscope objective and focussed onto a 90 percent power reflectivity mirror. The cavity length is approximately 15 cm to correspond to the round trip frequency in the region of 1 GHz. Focussing on the mirror or using a collimated beam in the external cavity give the same threshold reduction. However, the feedback is much less sensitive to the mirror angle when the light is focussed on the external cavity mirror. Since the width of the diode active region is about 0.2 μm, piezoelectric control is required along the optical axis for the position of the diode with respect to the microscope objective. Such fine control is not necessary on the mirror mounts. At the output of the resonator, the light is focussed onto an avalanche silicon photodiode with a pulse response FWHM of less than 130 ps. A gain of approximately 10x was sufficient to detect the output pulses. The signal from the photodiode is displayed by a sampling oscilloscope used in conjunction with a signal averager. The signal averaging system is used to eliminate the

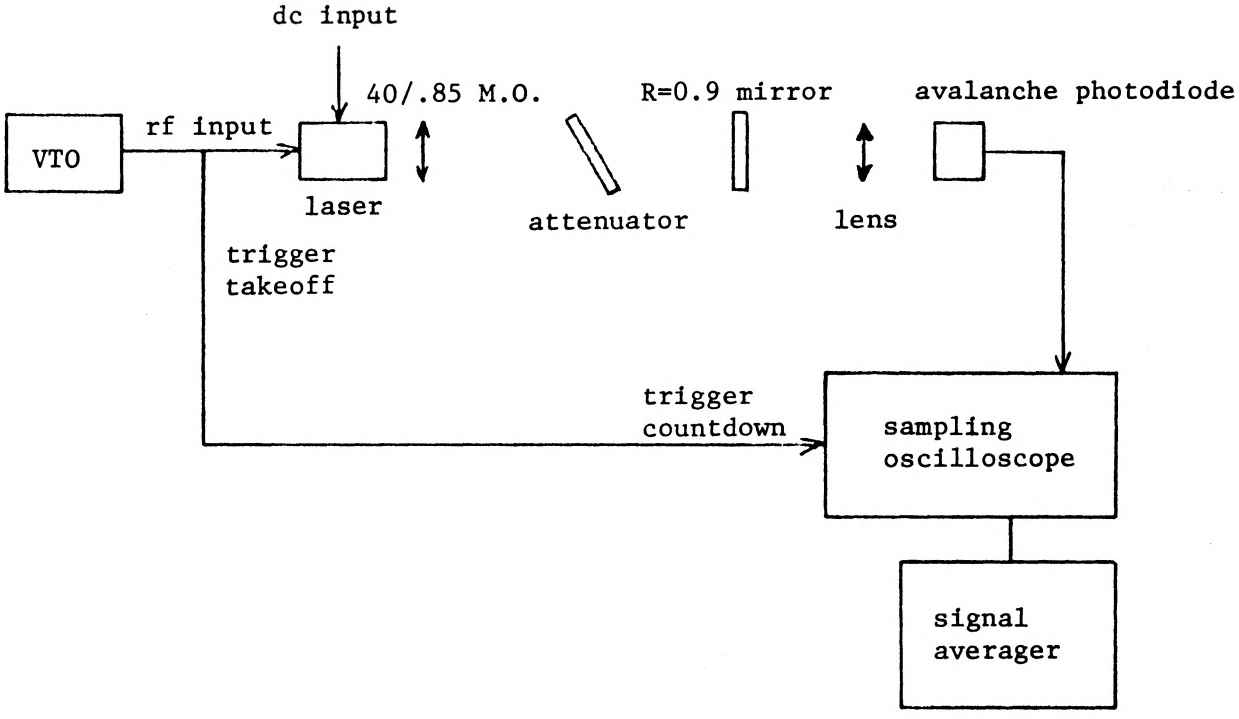

FIGURE 6.2 Schematic of experimental setup.

effects of random fluctuations in the detected pulse, to subtract background noise from the signal, and to display the detected pulse FWHM. Part of the output of the voltage tunable oscillator is used as an input to the high frequency trigger countdown which is built into the oscilloscope. The position of the optical pulse with respect to the current modulation is measured using a dual sampling head. The RF current goes through one channel of the sampling head to the laser, while the output of the photodiode goes into the other channel. The LDL SCW20 is mounted in such a way that a 50 Ω chip resistor which terminates a microstripline is adjacent to the laser chip, as described earlier in this thesis. Network analyzer measurements showed that this is an effective mount to avoid significant reflections of the sinusoidal modulation in the 1 GHz range. To make measurements of the tuning characteristics for reduced feedback, fixed attenuators were placed in the external resonator at an angle which avoided coupling any reflection from the attenuator back into the cavity.

The threshold current of the LDL SCW20 laser selected for detailed study is 44.5 mA. The general characteristics of the selected laser are the same as those of other lasers used in this thesis. The minimum threshold current obtained using the full feedback from the external mirror is 34.3 mA. The 10.2 mA threshold reduction corresponds to an effective mirror loss reduction of 42.8 cm^{-1} for this laser. This value is calculated from the gain spectrum measured using the standard Hakki and Paoli [18] technique discussed in Chapter 5 of this thesis. The light intensity versus dc current relationships for full

feedback and two reduced feedback cases are shown in Figure 6.3. The two reduced feedback cases are obtained using 20 percent and 50 percent amplitude attenuation values.

The frequency tuning characteristics are shown in Figures 6.4, 6.5 and 6.6 for each level of feedback. Measurements were made biased approximately 7.6 percent above the external cavity threshold with 4 percent current modulation. The frequency units shown in the figures are multiplied by the injected carrier lifetime (τ = 1.8 ns) to give a more direct comparison with the normalized frequency units used in the modelocking simulations. In normalized units, $f\tau$ = 0.01 corresponds to 5.55 MHz. As the feedback is reduced, the tuning range increases significantly. With no feedback, the output would vary with frequency according to the response of the isolated diode. The rate of change of the optical pulse position with respect to the current modulation in the region of the most intense pulses decreases as the feedback is reduced.

6.4 Simulations

The rate equation model developed in reference [1] to simulate the modelocking characteristics uses measured diode parameters as the input. Good prediction of the tuning behaviour is found when the total loss reduction due to the external feedback is divided equally between the feedback coupling term and the gain zero term included in the rate equations. The feedback coupling term corresponds to the actual mirror loss reduction, while the reduction in the gain zero term is indicative of a reduction in mode propagation losses (as discussed in Chapters 4 and

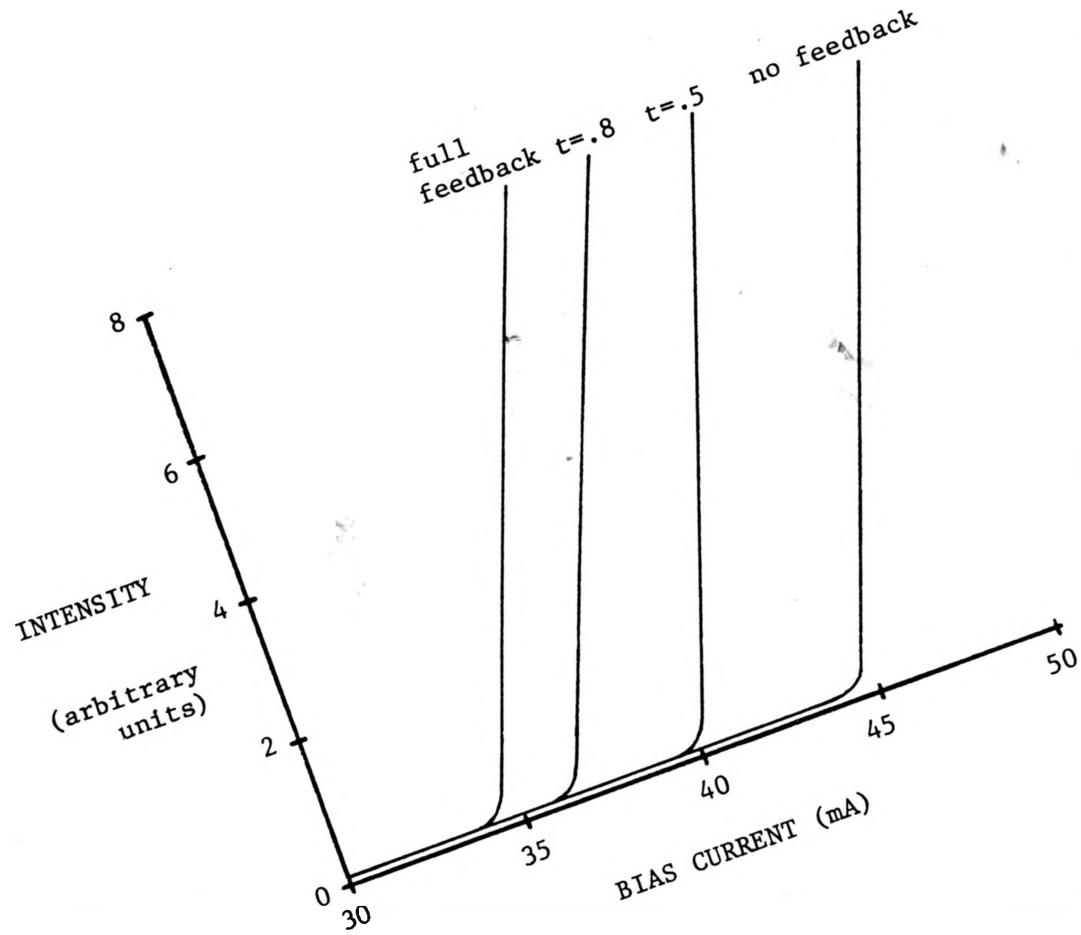

FIGURE 6.3 The threshold characteristics for various levels of feedback.

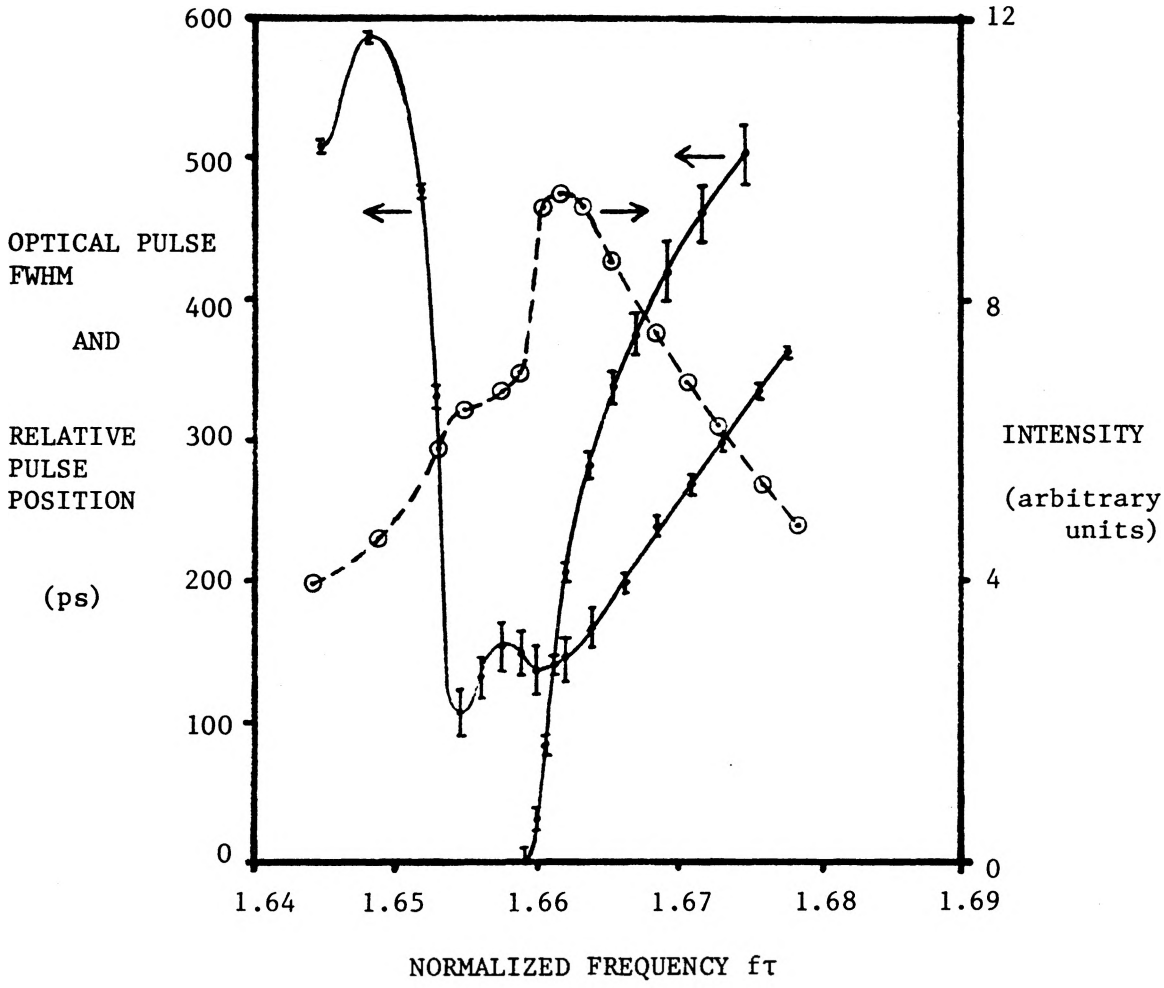

FIGURE 6.4 Experimental tuning characteristics for full feedback. (I_{dc}=1.076I_{th}, i_{mod}=4.0%)

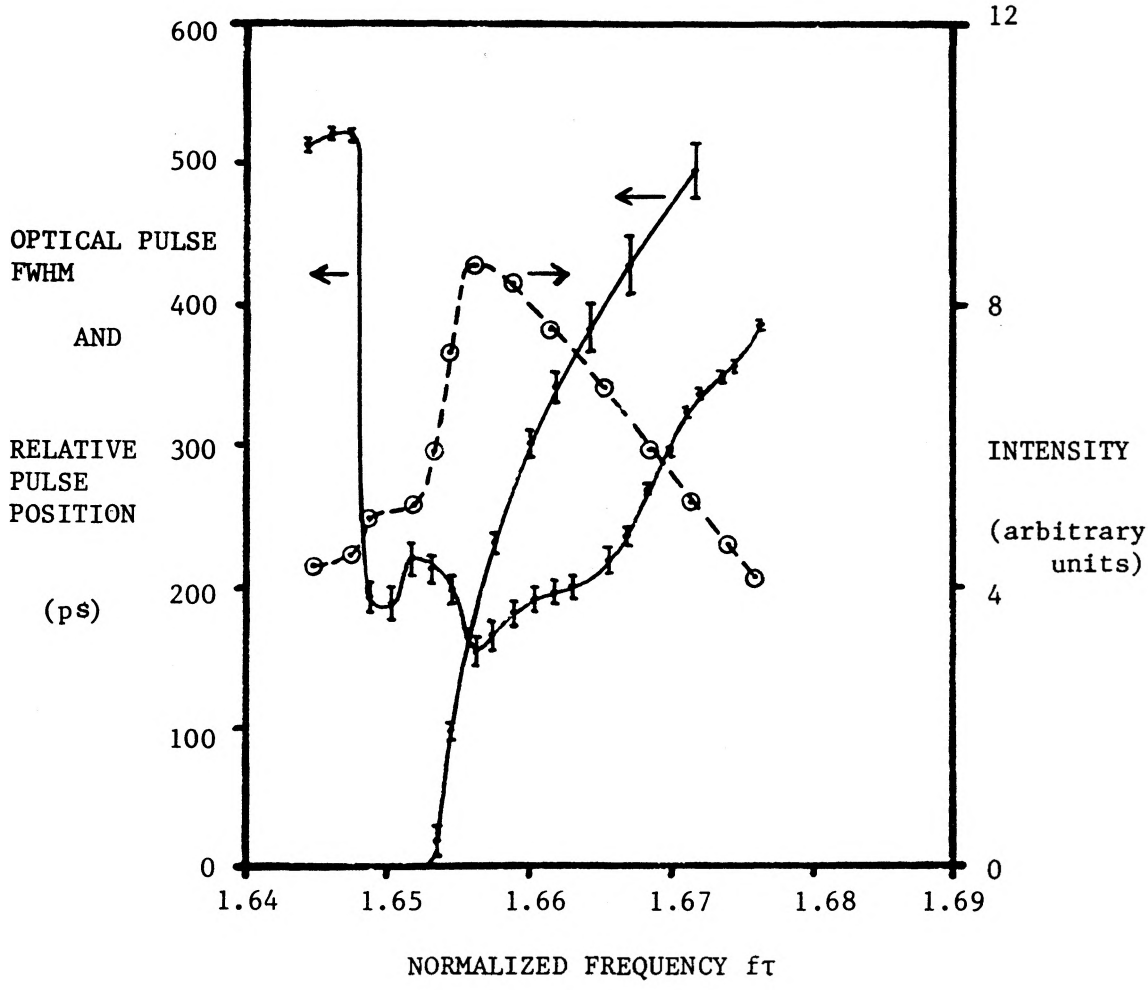

FIGURE 6.5 Experimental tuning characteristics for 20% attenuation in the external cavity. (I_{dc}=1.076I_{the}, i_{mod}=4.0%)

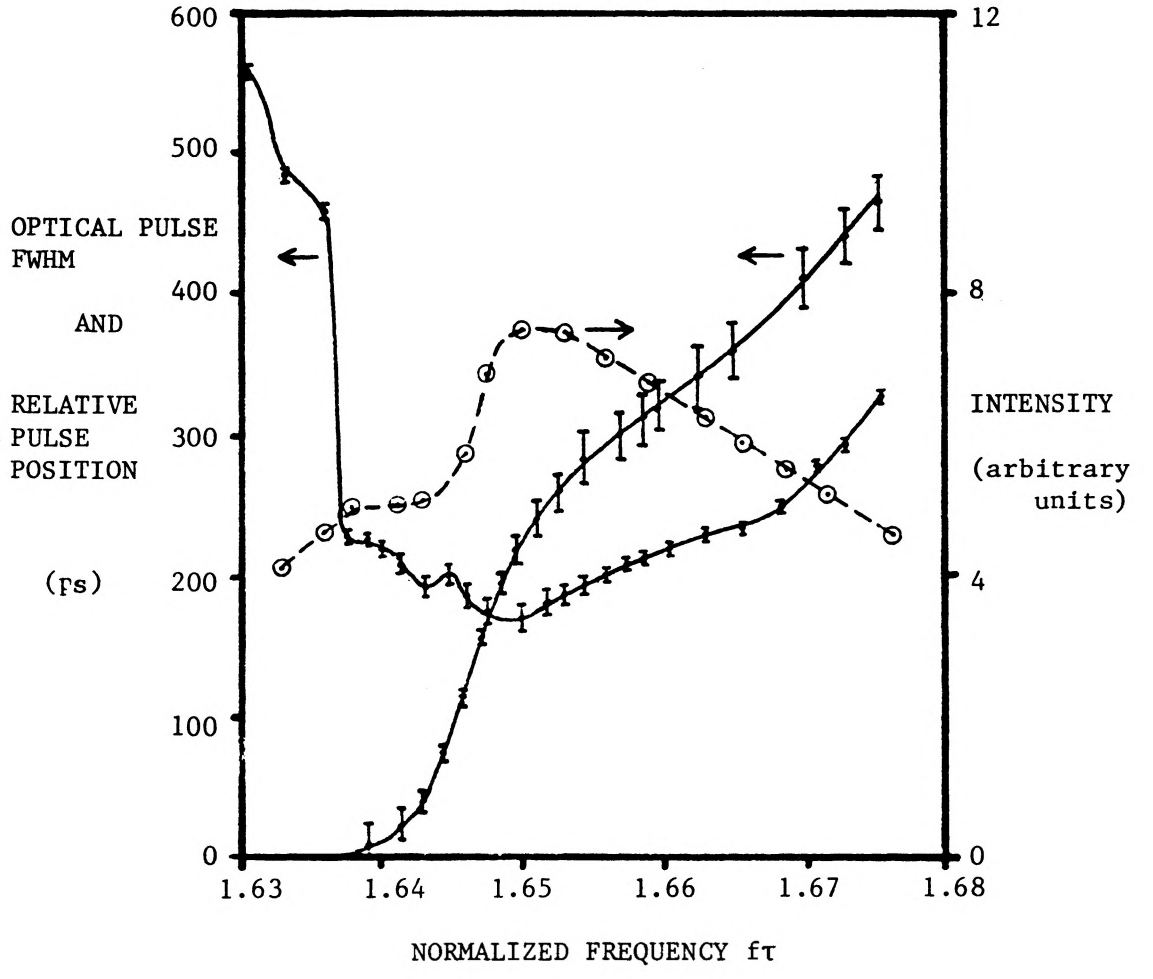

FIGURE 6.6 Experimental tuning characteristics for 50% attenuation in the external cavity. (I_{dc}=1.076I_{the}, i_{mod}=4.0%)

5). The relative magnitude of the mirror loss and mode propagation loss reductions induced by external feedback is the only fitting parameter used in the simulations. The relative magnitude of the losses found by fitting the simulations to the experimental data is the same as that measured experimentally in reference [6] for similar devices.

The simulations of the modelocking behaviour for the experimental conditions used are shown in Figures 6.7, 6.8 and 6.9. Comparison with experiment shows that the simulations give a good representation of the tuning width and rate of change of pulse position for various levels of optical feedback. A comparison of the rates of change of phase found experimentally with those found using simulations is shown in Figure 6.10. The very good agreement shown in Figure 6.10 lends weight to the use of the model for making predictions of the tuning behaviour for different levels of feedback corresponding to different facet reflectivities.

Simulation of the phase relationship from two very different facet reflectivities has been carrier out. A passively coated facet can have a power reflectivity of 37 percent while an anti-reflection coated laser can have a residual reflectivity in the region of 1 percent. Since the diode gain parameters and the effective reflectivity of the external cavity mirror are known, the equivalent full feedback conditions can be calculated for a change in facet reflectivity (see previous chapter for formulation of effective reflectivity). A 37 percent facet will reduce the effective coupling to the external cavity by more than

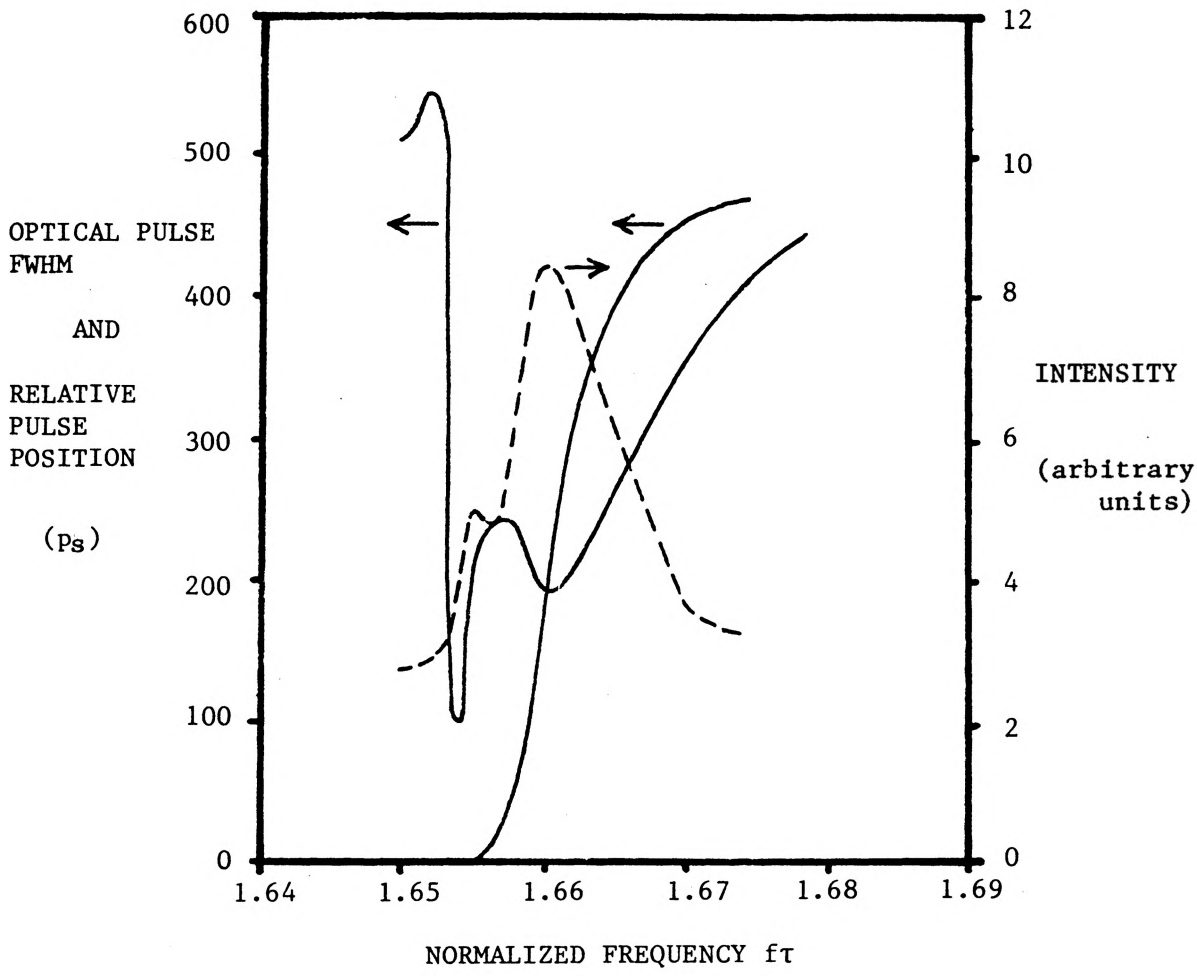

FIGURE 6.7 Simulated tuning characteristics for full feedback. (I_{dc}=1.076I_{the}, i_{mod}=4.0%)

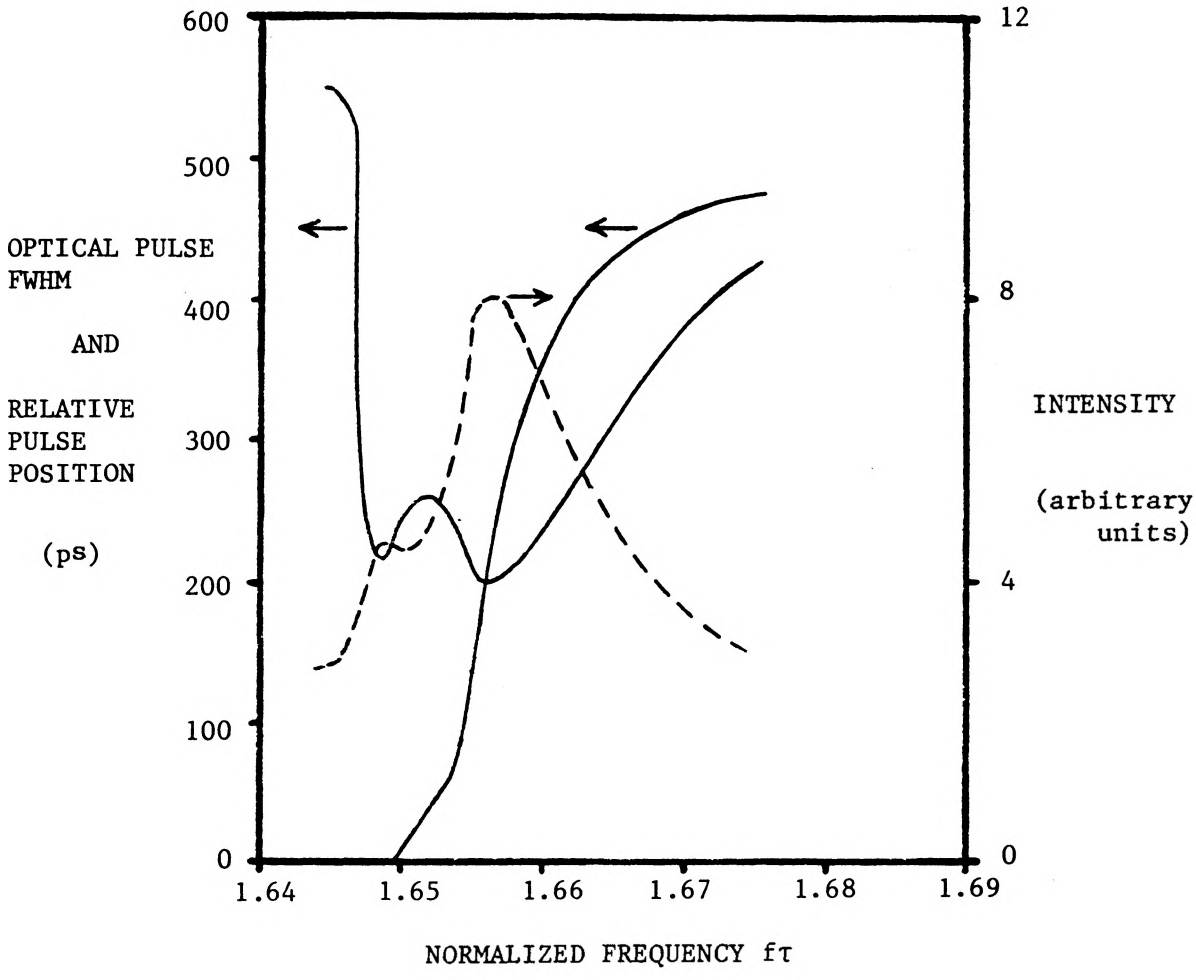

FIGURE 6.8 Simulated tuning characteristics for 20% attenuation in the external cavity. ($I_{dc}=1.076I_{the}$, $i_{mod}=4.0\%$)

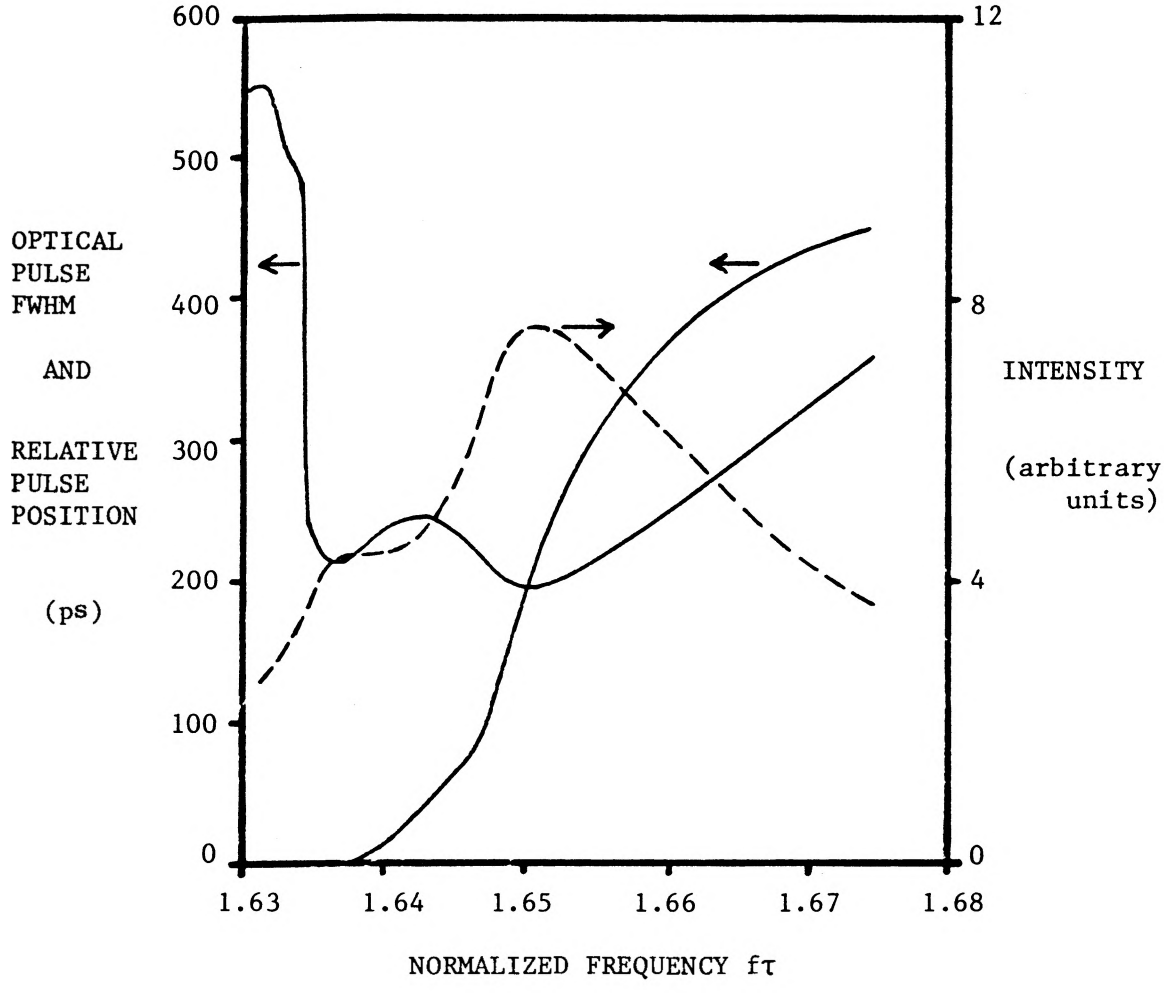

FIGURE 6.9 Simulated tuning characteristics for 50% attenuation in the external cavity. (I_{dc}=1.076I_{th}, i_{mod}=4.0%)

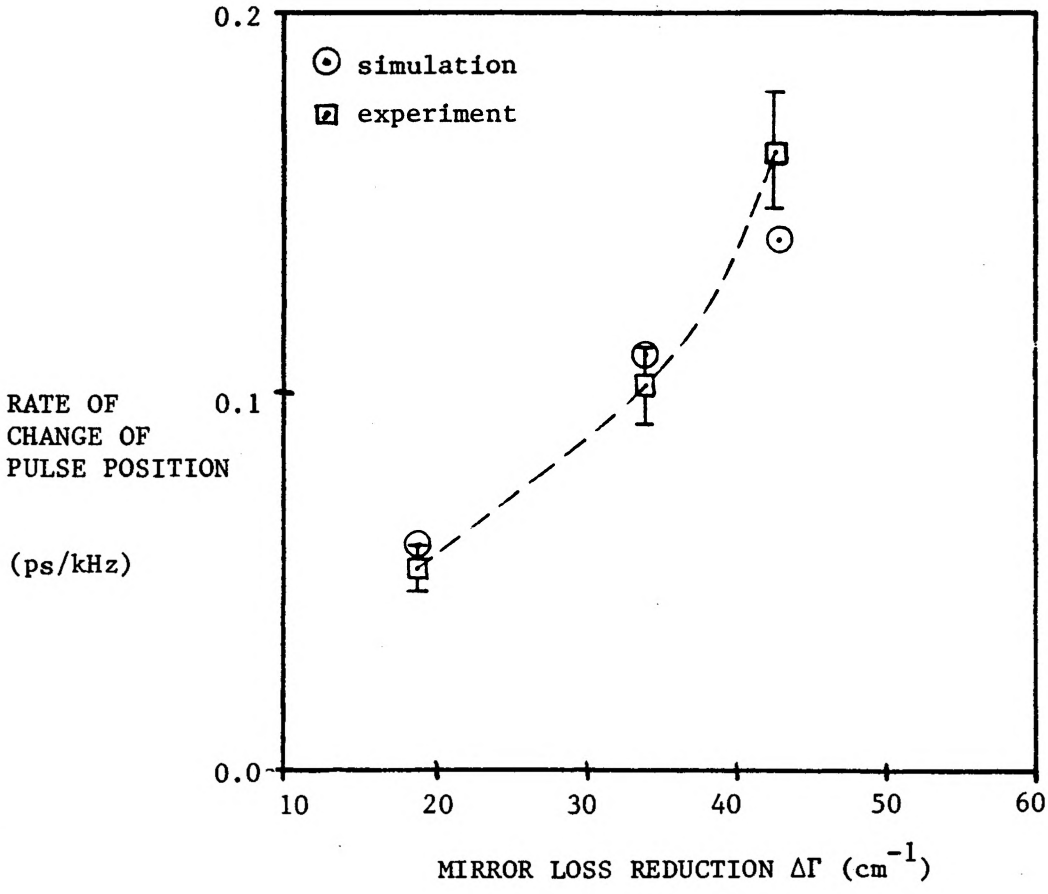

FIGURE 6.10 The rate of change of phase is shown for full feedback ($\Delta\Gamma$=42.8 cm^{-1}), 20% attenuation ($\Delta\Gamma$=34 cm^{-1}), and 50% attenuation ($\Delta\Gamma$=18.9 cm^{-1}).

half compared to the case of the 11 percent facet which was used experimentally. The resulting tuning characteristics for a 37 percent facet are shown in Figure 6.11 for dc bias 7.6 percent above the external cavity threshold and 4 percent modulation. The corresponding rate of change of pulse position is approximately 0.1 ps/kHz. The frequency tuning therefore becomes broader for higher facet reflectivity. Since the tuning range narrows for lower bias current (above the external cavity threshold), the rate of change of pulse position was experimentally found to be 0.2 ps/kHz for a similar laser with a 37 percent facet biased 2 percent above threshold with a 4 percent modulation index in [1]. The bias sensitivity of the rate of change of pulse position indicates that the values measured here are not necessarily the greatest rate of change of phase which could be encountered experimentally.

A 1 percent facet reflectivity gives greater than 4 times the coupling to the external cavity achieved with a 37 percent facet. To simulate the characteristics of a laser with a 1 percent facet, the relative magnitude of the mirror loss and mode propagation loss reductions due to the external feedback must be reconsidered. The maximum possible mode propagation loss reduction is not known, but it is probably limited to less than the large mirror loss reduction obtainable with a very low reflectivity facet. The extreme limits on the rate of change of pulse position can be obtained by simulating the case with equal reductions in the two loss-terms, and the case where the total loss reduction is attributed to the mirror loss term. The

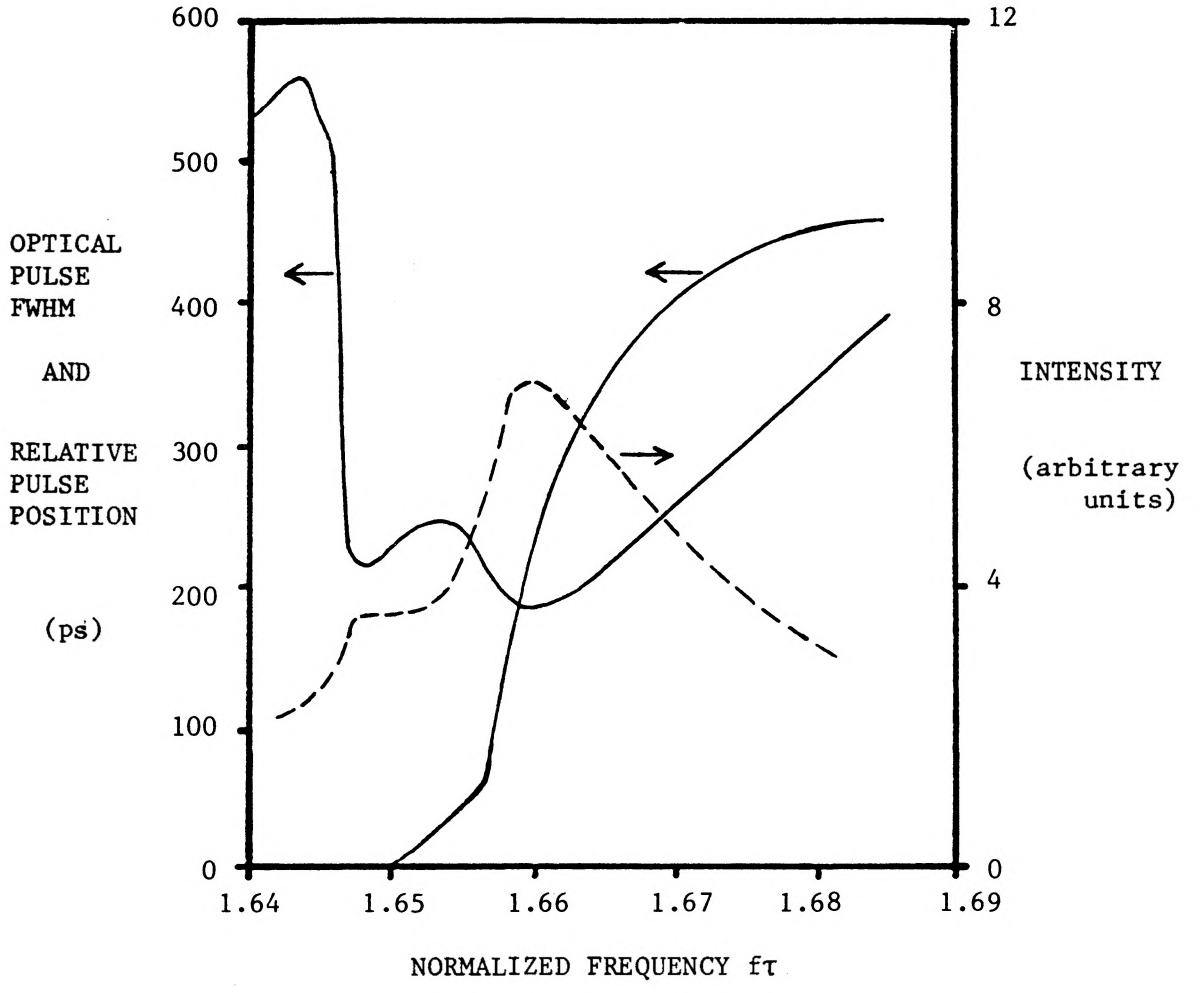

FIGURE 6.11 Simulated tuning characteristics for a diode with a 37% power reflectivity facet. (I_{dc}=1.076I_{the}, i_{mod}=4.0%)

calculated tuning characteristics for equal loss reduction terms using the same bias and modulation conditions as earlier is shown in Figure 6.12. The maximum rate of change of pulse position is 0.235 ps/kHz in this case. A simulation which attributes the entire loss reduction to a change in mirror loss results in a maximum rate of change of pulse position of 0.45 ps/kHz. A plot which gives the rate of change of pulse position relative to the current modulation for the range of reflectivities used in the simulations is shown in Figure 6.13.

The significant increase in the rate of change of phase of the optical pulse for low facet reflectivity indicates that consideration of the oscillator stability is essential when attempting to obtain short modelocked optical pulses. An oscillator frequency variation of ± 25 kHz at 1 GHz would broaden the apparent pulse width by about 12 ps when the diode facet reflectivity is 1 percent. A further increase in the pulse width would occur because of the drift from the frequency which produces the shortest pulses. The oscillator used in this work has a stability of approximately 50 kHz, which in the case of full feedback gives a pulse broadening of about 7 psec. This is a small effect relative to the 100 psec pulse widths obtained for the mode-locking regime used in this work.

However, active modelocking regimes which produce optical pulse widths in the region of 10 ps would give detected pulses which are severely broadened due to a 50 kHz oscillator stability. For example, proton bombarded lasers with less than 1 percent facet reflectivity

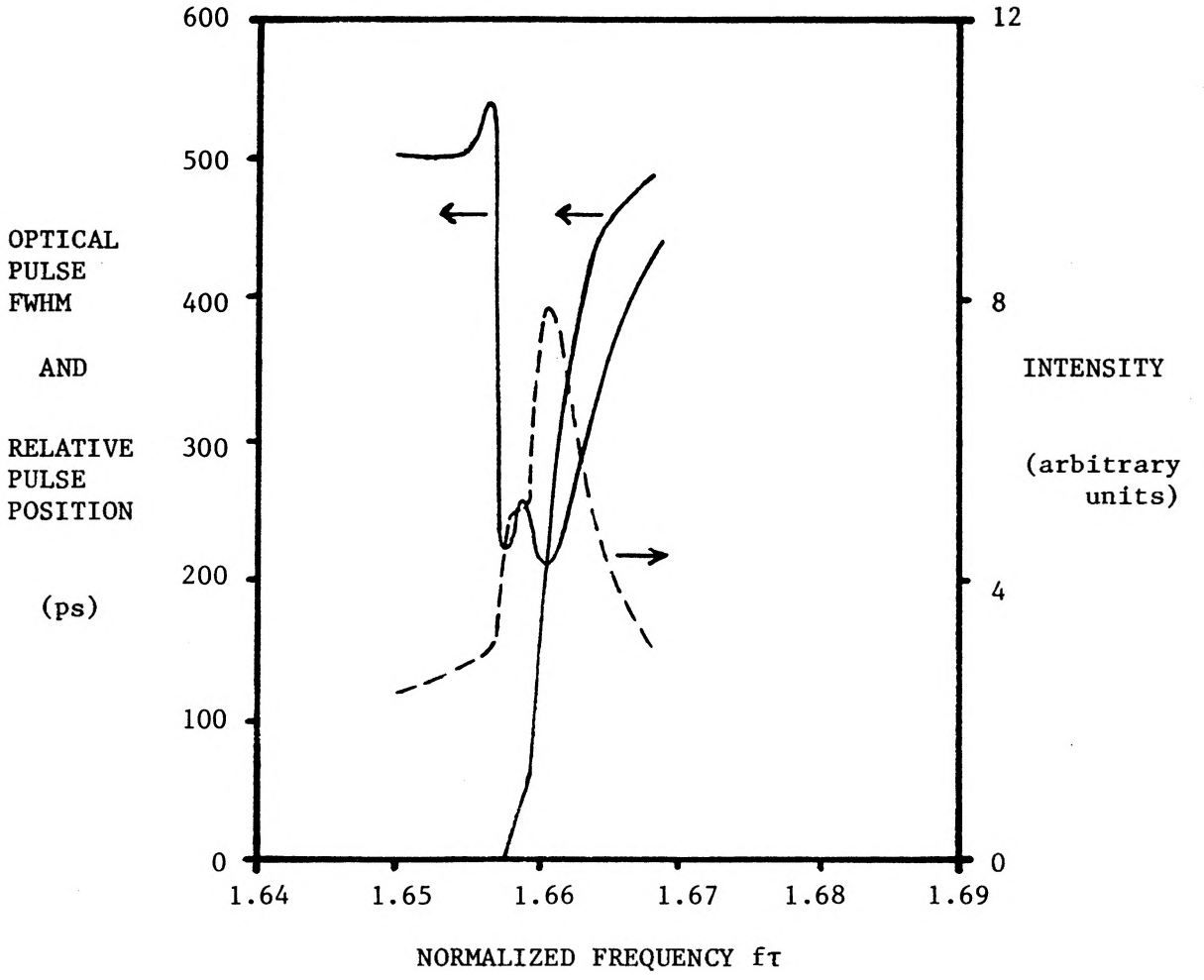

FIGURE 6.12 Simulated tuning characteristics for a diode with a 1% power reflectivity facet. (I_{dc}=1.076I_{the}, i_{mod}=4.0%)

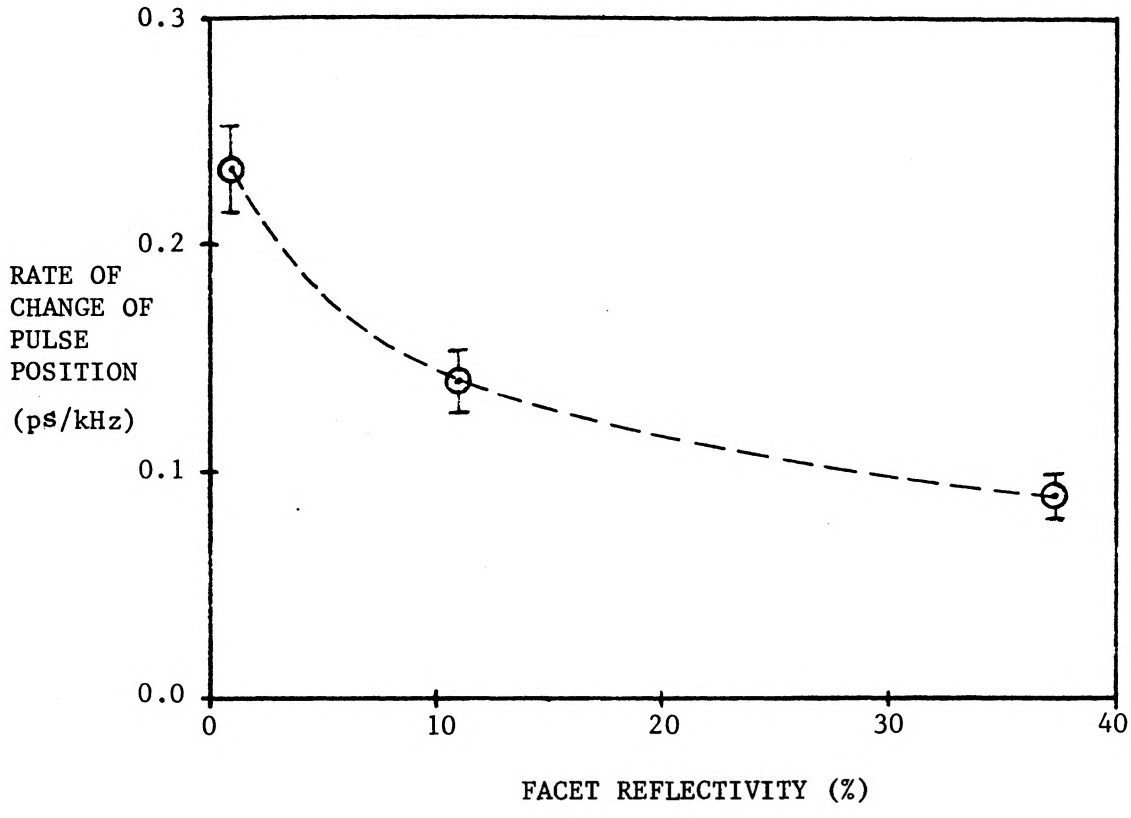

FIGURE 6.13 Simulated rate of change of pulse position relative to the current modulation for several values of chip facet reflectivity.

were actively modelocked in [19] to produce 5.3 ps FWHM optical pulses at a frequency of approximately 1 GHz under optimum bias and tuning conditions. The detected pulses in [19], which were produced using a Fabry-Perot etalon within a mirror external cavity to restrict the bandwidth of the feedback, were not time-bandwidth limited. The pulse broadening due to the oscillator stability can be large enough to account for the detected pulse's FWHM deviation from the bandwidth limit in this case. Production of actively modelocked pulses of less than 5 ps duration in the region of 1 GHz therefore requires an oscillator stability of less than 10 kHz for the detected pulse broadening to be less than 20 percent of the actual pulse FWHM.

6.5 Summary

An experiment was done to determine the effect of reduced external cavity feedback on the frequency tuning characteristics of an actively modelocked diode laser. The dc bias and depth of current modulation were set in a regime where a computer model of the mode-locking characteristics converged satisfactorily. The excellent agreement between model predictions and the measured characteristics for varying feedback strongly supported calculations of the effect of different facet reflectivity on the tuning behaviour. It was found that the increased feedback coupling associated with reduced facet reflectivity causes a significant increase in the rate of change of the optical pulse position relative to the peak of the current modulation, thereby accounting for the previously unexplained extreme sensitivity of the modelocking process to oscillator stability.

CHAPTER 7

GRATING EXTERNAL CAVITY INJECTION LOCKING

7.1 Introduction

The development of picosecond optical pulse sources is of interest to the study of ultrafast processes, high speed optoelectronics, and optical communications. Picosecond optical pulses (< 30 ps) with relatively low peak power ($\leq$ 25 mW) have been generated at gigahertz rates by direct modulation of semiconductor lasers [24] at the expense of a very broad dynamic spectrum. For high data rate optical communications applications, the dynamic spectrum must be narrow to minimize the pulse spreading caused by fibre dispersion.

In this work, a diode laser coupled to an external resonator and modulated with short current pulses ($\simeq$ 80 ps FWHM) which are synchronous with the round trip frequency of the optical feedback ($\simeq$ 500 MHz) is shown to significantly decrease the optical pulse FWHM, increase the peak power, and decrease the dynamic spectrum relative to the case of a directly modulated diode. Two external resonator injection locking schemes are used. The first, which is made up of a diode laser whose output is focussed onto a plane mirror to form a 30 cm resonator length, illustrates the basic improvement in the aforementioned output characteristics

achievable for the same current modulation relative to the isolated diode case. Replacing the plane mirror with a diffraction grating in the external resonator results in short ($\simeq$ 20 ps), high peak power ($\simeq$ 180 mW) optical pulses whose dynamic spectrum is basically limited by the wavelength resolution of the grating feedback ($\simeq$ 1.0 Å). The novel use of a grating as the feedback element in injection locking with short current pulses allows bandwidth limitation to be introduced into a compound cavity which includes a diode laser with a high reflectivity back facet ($R \simeq 0.95$). Using another type of bandwidth limiting element in the cavity, such as a FP etalon [25], would put a bandwidth restriction on the detected output as well as the optical feedback if the output is measured on the resonator side of the diode. In contrast, the detected fraction of the diode output in grating cavity operation undergoes a specular reflection from the grating. The monitored zeroth order reflection therefore includes all of the wavelength content of the diode output pulse.

Simulations of the frequency tuning characteristics of a diode injection locked in a grating external cavity are carried out using a non-iterative approach which employs a rate equation model that allows for the effects of external optical pulse injection into the active region. The comparison of the simulations to the experimental tuning characteristics again illustrates the importance of using an external coupling term whose magnitude corresponds to the <u>actual</u> mirror loss reduction rather than the total loss reduction induced by the external feedback.

7.2 Direct Modulation

Direct modulation of diode lasers is the simplest way to produce intense optical pulses of short duration. A narrow large amplitude current pulse can be superimposed on a below threshold dc bias to produce gain switched optical pulses of less than 40 ps FWHM. For low repetition rates ($\sim$ 1 kHz), optical pulses with FWHM in the 10 to 20 ps range have been obtained using gain switching [13], while 30 to 40 ps FWHM pulses have been obtained at 0.5 to 2.5 GHz repetition rates [24].

In this work, a commercially available step recovery diode pulse generator [26] which is capable of producing greater than 10 V peak current pules into 50 Ω with FWHM of $\sim$ 80 ps is used to modulate a diode laser directly. The pulse generator operates for a range of frequencies (450 to 550 MHz) controlled by the frequency of an amplified tunable oscillator at the input. The output optical pulses are detected directly using a photodiode and sampling oscilloscope with combined pulse response of 76 ps FWHM. A current monitor at the output of the comb generator provides a stable trigger source for the sampling scope. A signal averager [27] is used to reduce the effects of random fluctuations, to subtract the background noise level, and to calculate the detected pulse FWHM. The current pulses are coupled to the laser using a custom high frequency microstripline mount which is necessary because of the reactance of the standard coaxial laser package (see Chapter 3 for further discussion). The pulses from the comb generator have significant frequency components which are beyond the 1 to 2 GHz design limitation of the standard

laser mount. The LDL SCW20 laser selected for detailed study has a 44.5 mA threshold current and operates approximately in a single mode fashion above 50 mA. The CW output power increases linearly with current above threshold to 7 mW at 59 mA. The narrowing of the CW spectrum with increasing dc current above threshold is shown in Figure 7.1. This narrowing is due to the gain saturation by the dominant mode in the case of nearly homogeneous broadening of the gain, a condition which is approached for high CW pumping levels.

The variation in optical pulse FWHM with dc current for the maximum current pulse peak available ($I_p \approx 228$ mA) is shown in Figure 7.2. The optical pulse FWHM is deconvolved from the 76 ps detection system response assuming Gaussian shaped pulses. The measured pulse widths rapidly decrease with increasing dc current to a limiting value of approximately 50 ps. The detected peak pulse power increases for shorter optical pulses to 46 mW at $I_{dc} = 38$ mA. The measured variation in output FWHM with dc current is due to the increase in the gain (inversion) overshoot made possible by the higher initial inversion associated with higher dc bias. The fixed amplitude of the current pulse determines the constant rate of increase of the inversion. The peak inversion attainable is therefore limited by the saturation of the gain by the stimulated emission which begins when the inversion exceeds its threshold value. Since the output FWHM is related to the magnitude of the gain overshoot, the optical pulse width no longer decreases significantly for dc current above the value for which the current pulse gives a maximum inversion.

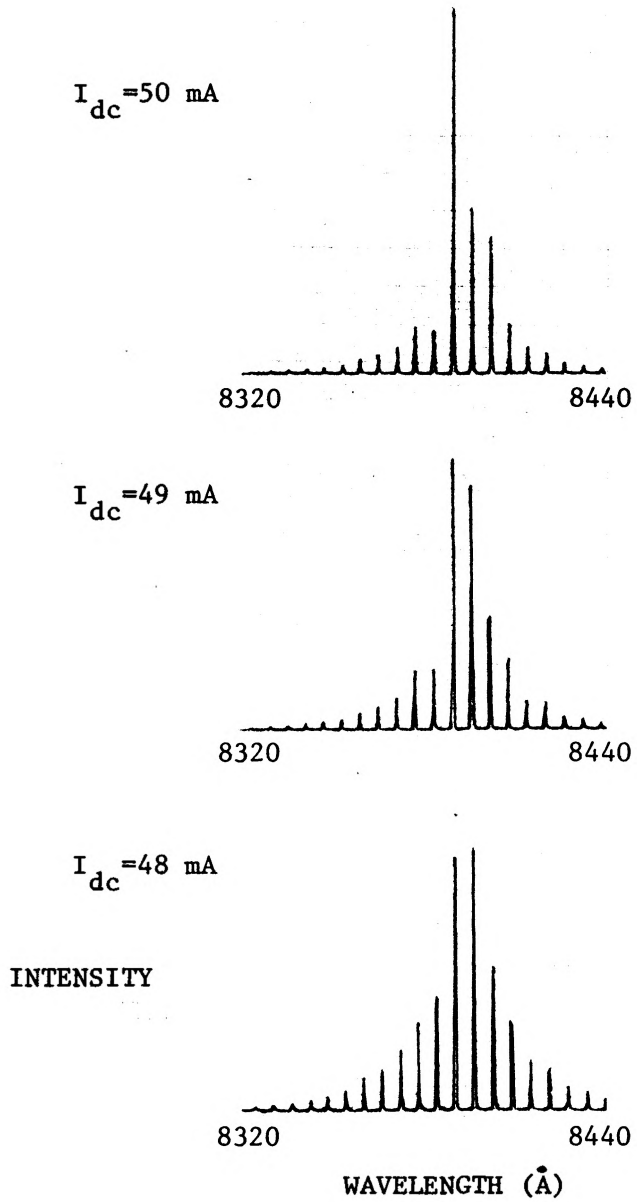

FIGURE 7.1 Evolution of the CW mode spectrum above threshold (I_{th}=44.5mA).

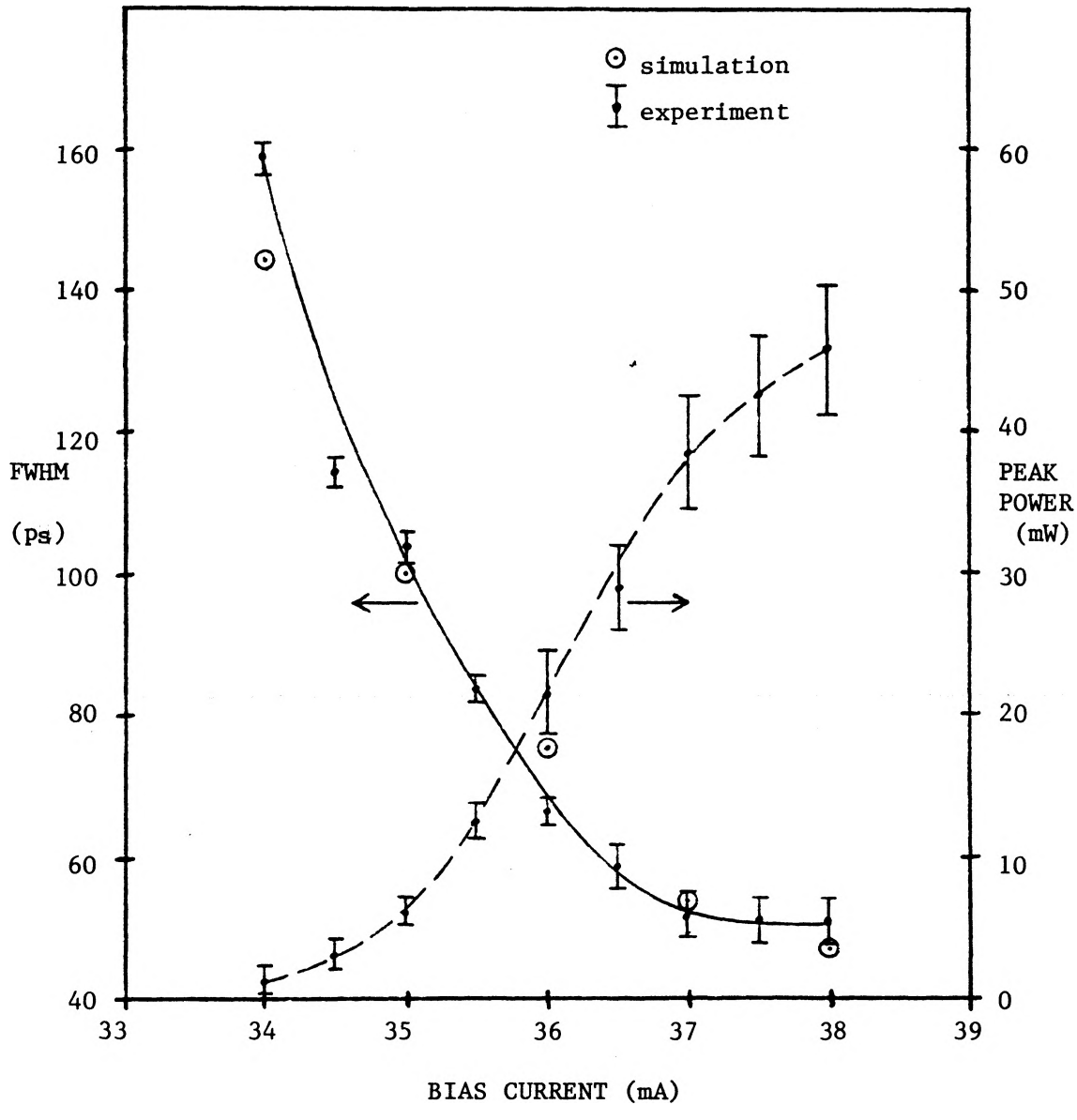

FIGURE 7.2 Optical pulse FWHM and peak power versus dc current at 465 MHz repetition rate. The simulated FWHM is compared to the measured.

The dynamic spectrum of the shortest, most intense optical pulses obtained using direct modulation was measured using a 0.5 m grating monochromator and an avalanche detector with a pulse response of 130 ps at moderate gain (~ 30 x). The monochromator resolution is 0.4 Å for the time averaged spectrum shown in Figure 7.3. Both the total spectrum and the individual Fabry Perot modes are broadened relative to the CW case when an intense output pulse is obtained. An optical pulse begins approximately when the inversion overshoot is at its peak, and ends when the inversion decreases to below its threshold value. The rapidly decreasing inversion during the optical pulse causes a decrease in the free carrier density and an associated increase in the refractive index of the active region. The individual Fabry Perot modes of the chip shift to longer wavelength during the optical pulse due to the increase in the refractive index. The envelope of the modes also shifts to longer wavelength during the pulse because of the shift of the peak of the gain to longer wavelength for reduced inversion. This causes the asymmetry about the central mode in the dynamic spectrum shown in Figure 7.3. The wavelength chirp of 3 Å for the individual modes is of the same magnitude as that seen by other workers ([28], [29]). The magnitude of the chirp is reduced when lower peak inversion is attained.

A computer program which solves the coupled rate equations that describe the diode laser dynamics was discussed earlier in this thesis. The modified version of the program which includes the effects of wavelength chirping during the output pulse was used to calculate the optical pulse FWHM for the experimental bias and pulse conditions used

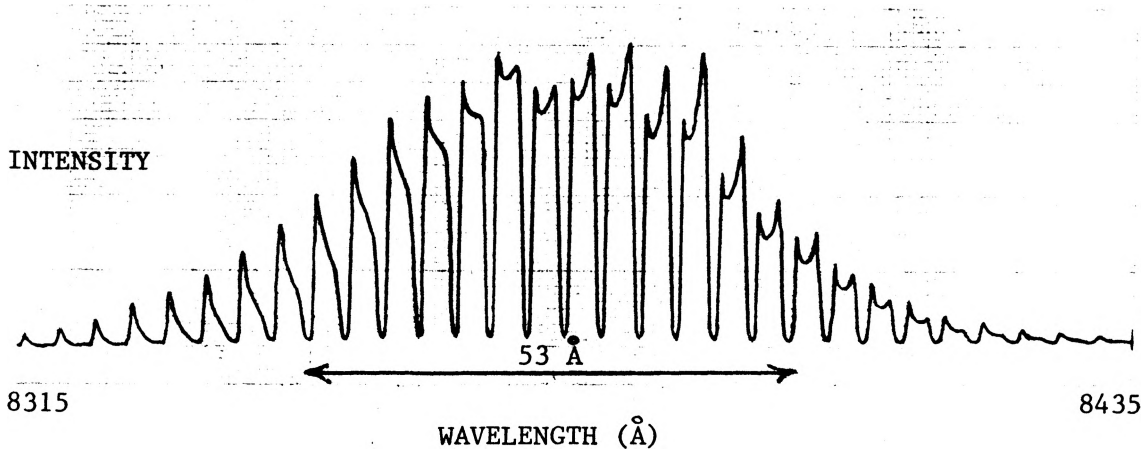

FIGURE 7.3 Dynamic spectrum of a diode laser under direct comb generator modulation for I_{dc}=38 mA, I_p=228 mA (I_{th}=44.5 mA).

to directly modulate the diode. The simulated pulse train was allowed to reach steady state since the period of the 500 MHz modulation is of the same order as the 1.8 ns injected carrier lifetime. The long carrier lifetime makes it impossible for the inversion to return to its initial value between pulses. The steady state minimum inversion value is therefore higher than the inversion given by the dc bias level. The simulation in Figure 7.4 illustrates the evolution of the inversion and intensity with time for modulation at 465 MHz. Good agreement between the simulated and measured dependence of pulse FWHM on bias current for a fixed pulse peak is shown in Figure 7.2. The applicability of the rate equation model to the prediction the laser output for direct comb generator modulation was essential in order that simulations of the injected locking characteristics of a comb generator modulated diode coupled to an external resonator could be attempted. Such simulations are discussed in the section of this chapter concerning grating external cavity injection locking.

7.3 Mirror External Cavity Injection Locking

When a diode laser is coupled to an external resonator which is much longer than the laser chip, current modulation at frequencies close to the round trip time of the cavity will result in injection locking. Modelocking was achieved in the experiments of the previous chapter by using a small sinusoidal modulation superimposed on an above threshold dc bias level. This results in a narrow dynamic spectrum since the gain variation is small. Shorter and more intense optical pulses can be

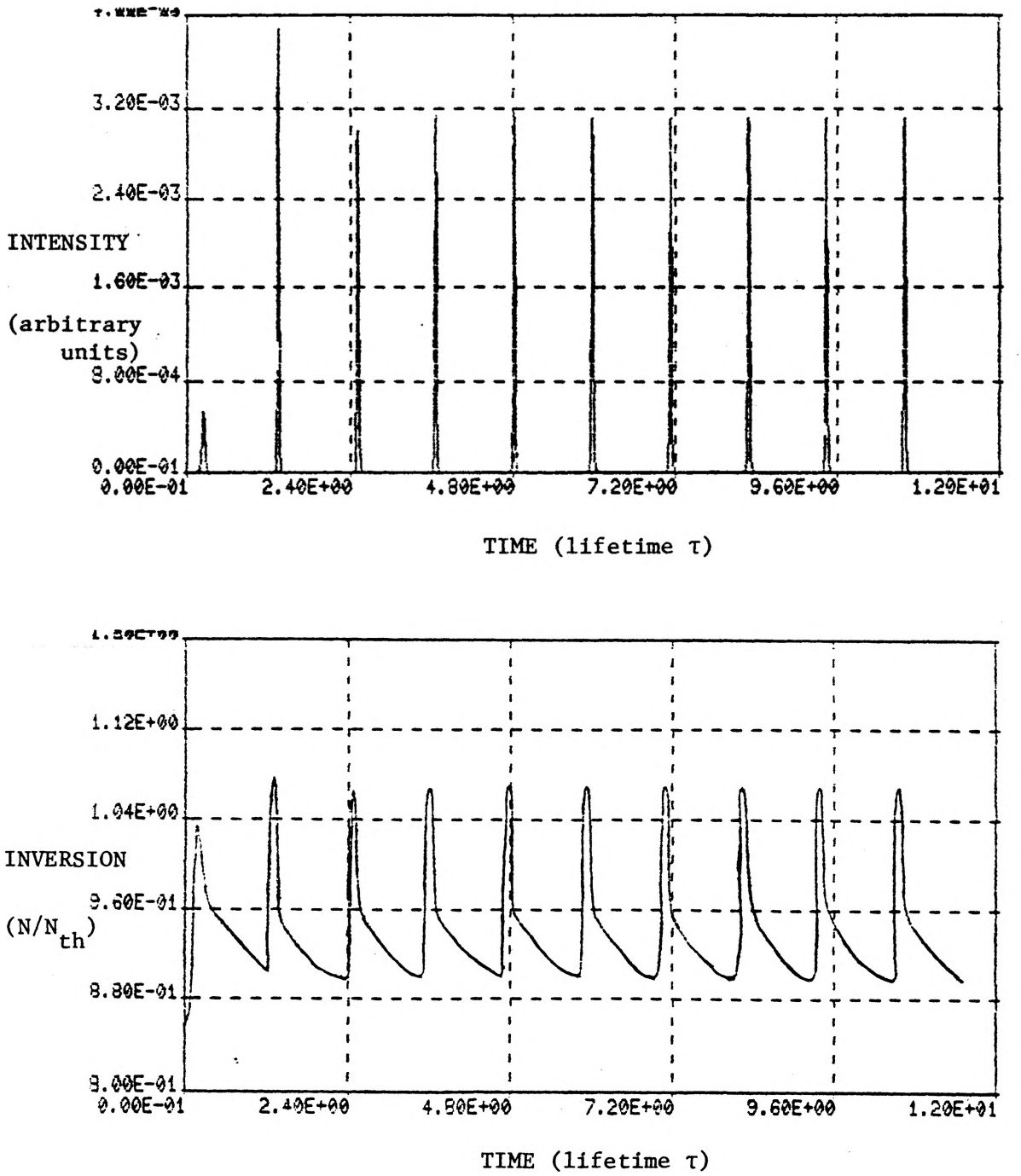

FIGURE 7.4 Evolution of intensity and inversion in time at a modulation frequency of 465 MHz.

obtained by using a 500 MHz comb generator to modulate a diode laser coupled to a 30 cm long mirror external cavity. The cavity length is chosen so that the injected current pulses are synchronous with the optical pulses in the external resonator.

The experimental optical arrangement used here is the same as that described in Chapter 4 where the effect of optical feedback on the CW linewidth of the diode laser was discussed. The optical feedback from the external mirror gives a threshold reduction of 10 mA, which corresponds to an effective loss reduction of about 42 cm^{-1}. Just above the external cavity threshold current of 34.5 mA, the laser emits essentially a single longitudinal chip mode which is broadened by a number of unresolved compound cavity modes. As the bias current (gain) is increased, more chip modes and compound cavity modes lase. This gives the linewidth and envelope broadening with increasing current shown in Figure 7.5. The maximum linewidth broadening due to CW optical feedback was measured to be about 0.85 Å in Chapter 4.

The output pulse FWHM and peak power obtained by injection locking the external cavity coupled diode is dependent on the frequency of the comb generator pulses. The tuning behaviour is similar to that shown for sinusoidal modulation in Chapter 6, but much shorter pulses of greater intensity are possible using the comb generator. The much more rapidly increasing inversion given by the short risetime current pulse leads to more significant pulse shortening effects. At a modulation frequency below the cavity round trip frequency the rapidly increasing inversion

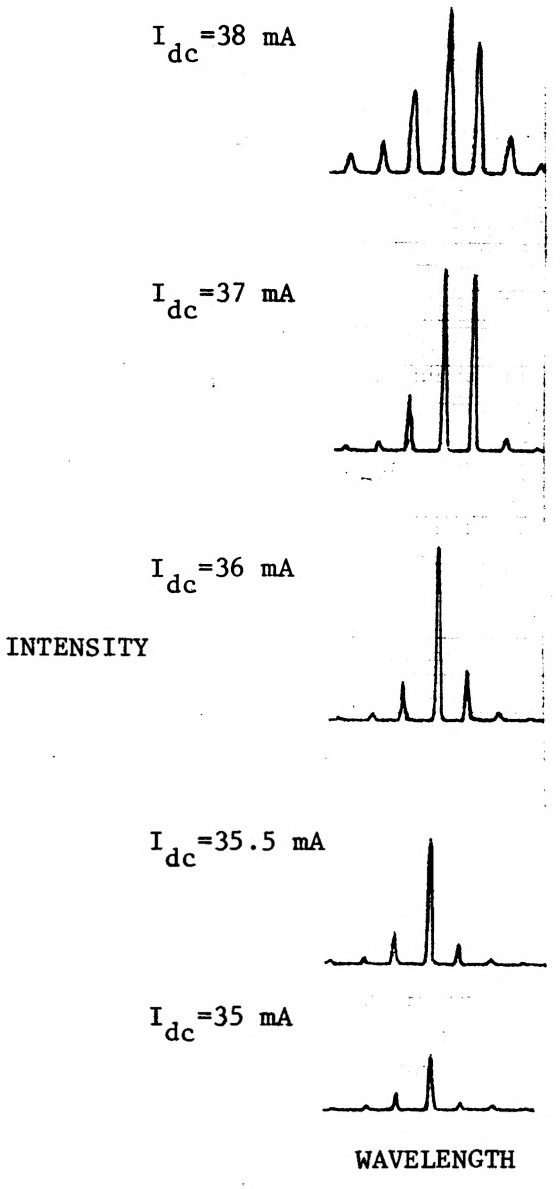

FIGURE 7.5 Increasing linewidth and spectral envelope for increasing bias current when coupled to a plane mirror external cavity. (I_{the}=34.5 mA, L=30 cm)

will amplify the trailing edge of the optical pulse much more than the leading edge. The phase shift to later in time, which compensates for the difference between the modulation and cavity resonance frequencies, and associated pulse shortening continues until a steady state FWHM and phase shift are reached. Modulation frequencies below the cavity round trip frequency yield the shortest optical pulses because of the pulse shortening effects which occur in this region.

The measured FWHM and peak power of the optical pulse versus current pulse peak is shown in Figure 7.6 for the optimum tuning in each case. The experimental uncertainty becomes large for the shortest pulses since the small optical signal level through the 10 percent transmitting mirror required the use of a 115 ps FWHM avalanche photodetector at low gain (10 x). Both the dc current and current pulse peak are varied to maintain a constant average optical power of about 2 mW. The maximum power of 180 mW and minimum pulse FWHM of 20 ± 10 ps is obtained with current pulse peak I_p = 228 mA and a dc current I_{dc} = 27.5 mA. The low dc bias prevents gain recovery and therefore avoids multiple pulsing. The results of direct modulation (Figure 7.2) show that the inversion of the isolated diode does not reach threshold for this bias current level. The isolated diode must not lase without the feedback in order to maintain the short optical pulses due to injection locking, rather than the longer pulses given by direct modulation. The minimum pulse FWHM obtained by injection locking with a plane mirror cavity is at least a factor of two lower than was measured for direct modulation of the isolated diode, while the peak pulse power is four

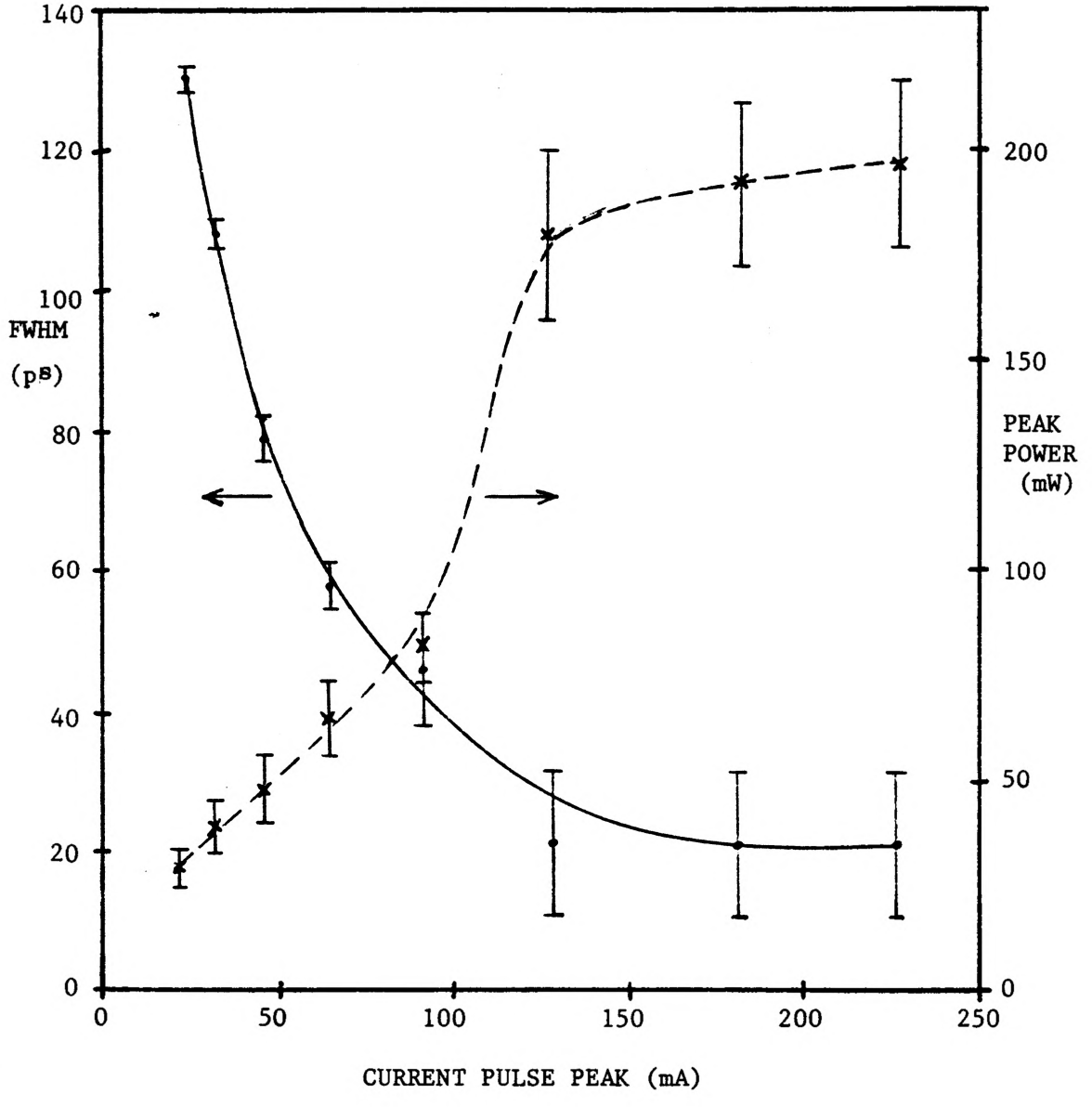

FIGURE 7.6 Optical pulse FWHM and peak power versus current pulse peak for plane mirror cavity injection locking. The average optical power is approximately constant in each case.

times that of the isolated diode case. The improvement in pulse FWHM and power attained with injection locking is due to a larger and more rapid decrease in inversion during the optical pulse than is possible without optical feedback. The optical pulse which is fed back to the diode on each round trip increases the photon density in the cavity, which decreases the lasing threshold and gives more rapid saturation of the gain. Since the output pulse risetime is essentially given by the time required for the inversion to switch from its peak to its threshold value, the more rapid gain saturation will result in shorter optical pulses.

The large decrease in inversion during the pulse associated with shorter, more intense pulses results in a large wavelength chirp of the individual Fabry-Perot modes. The magnitude of the chirp and of the spectral envelope broadening are shown to increase with increasing peak inversion in Figure 7.7. The pulse peak and bias conditions given in Figure 7.7 are the same as for the tuned cases whose FWHM and peak power are given in Figure 7.6. For the smallest current pulse used, the chirp is about half of the chip longitudinal mode spacing. For the maximum current pulse, the broadening due to the chirp is greater than the 4 Å mode spacing. The narrower spectral envelope width of 33 Å compared to the 53 Å width measured for the isolated diode is an anticipated property of injection locking. Since part of the output pulse returns to the diode on each round trip in the cavity, each output pulse need not build up from the spontaneous noise as in the case of an isolated diode. The feedback therefore results in a narrowing of the dynamic spectral envelope.

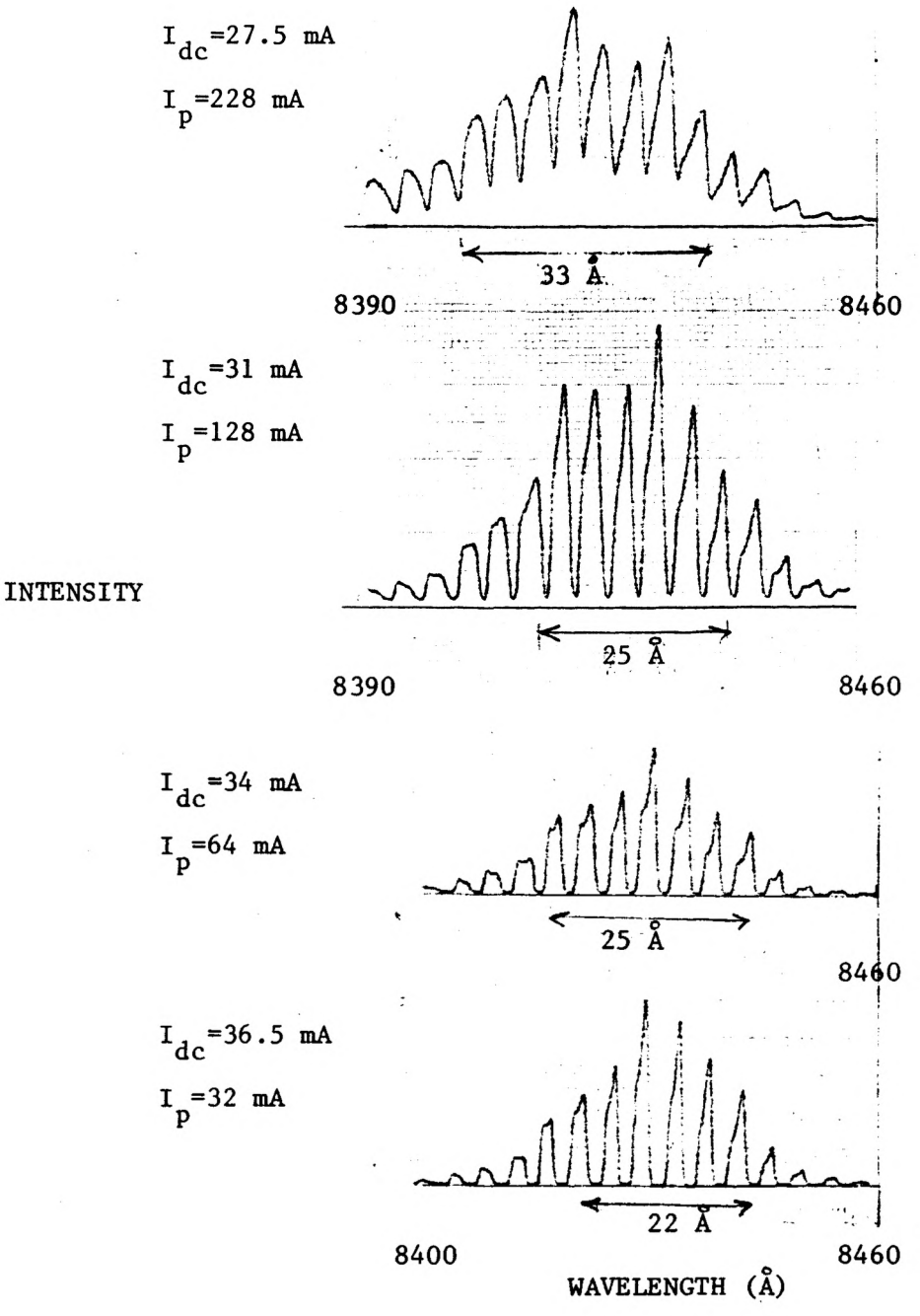

FIGURE 7.7 Dynamic spectrum (time averaged) for mirror external cavity injection locking with increasing peak inversion.

7.4 Grating External Cavity Injection Locking

Injection locking of a diode laser coupled to a mirror external cavity has been shown to give minimum pulse width of about 20 ps and peak power of close to 200 mW. However, the dynamic spectrum is broadened significantly relative to the CW lasing spectrum by the large wavelength chirp of the individual Fabry-Perot modes and the excitation of about 10 longitudinal chip modes for the case of the most intense optical pulses. By using a dispersive element in the external feedback, the spectral content of the pulses can be significantly reduced while retaining an output pulse FWHM and peak power comparable to the case of injection locking with a mirror external cavity. In this section, a diode laser coupled to a 30 cm long grating external cavity (as described in Chapter 5) is modulated with a comb generator at a 500 MHz repetition frequency to produce short, spectrally narrow optical pulses which approach the time-bandwidth product given by the Fourier transform limit. Bias current regimes above and below the external cavity CW threshold are investigated to find the necessary conditions for obtaining the shortest and most intense output pulses.

The CW characteristics of the grating optical feedback were discussed in Chapters 4 and 5 of this thesis. It was shown that single chip longitudinal mode lasing could be selected in a $\sim$ 100 Å range by rotating the grating. The maximum threshold reduction of 10 mA, or effective loss reduction of 42 cm^{-1}, is similar to the best achieved for the plane mirror cavity coupled diode. The CW spectral linewidth was found to be determined primarily by the linewidth of the isolated

diode, not by optical interference effects in the compound cavity as for a plane mirror cavity. The calculated grating feedback resolution of approximately 1 Å was also shown not to be the controlling factor on the detected CW linewidth. The maximum feedback within the wavelength tuning range of 1.3 Å over a single chip mode was shown to occur near the long wavelength end of the tuning (Figure 4.6). The same grating position dependent wavelength tuning can be seen in Figure 7.8 for the pulsed case where the peak pulse output is for near the long wavelength end of the tuning range. As the feedback is adjusted toward shorter wavelength in the region of a single chip mode, the pulse amplitude decreases. The lowest threshold mode is selected for investigation here since it represents the wavelength corresponding to the lowest peak gain required for lasing with the available level of feedback.

Since the external grating (in Littrow) is rotated approximately 29° to provide first order diffraction from feedback to the diode, an increase in pulse lengths is introduced due to the varying cavity length over the spatial limits of the beam. The beam profile was measured to determine the maximum possible contribution to the pulse width from the grating path difference. To find the beam profile shown in Figure 7.9, the total intensity of the beam was measured for various apertures at the output of the cavity. The 4 mm beam width at half intensity gives a calculated maximum time delay of 15 ps. This value is the result of an extreme simplification of the effect of the grating angle. It is expected that the dynamics of the laser diode will interact with the feedback optical pulses in order to adjust the phase front of the

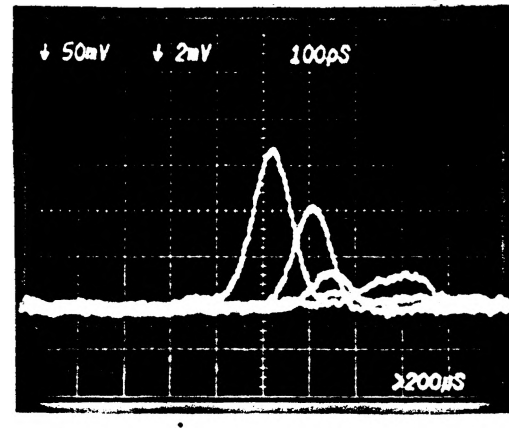

FIGURE 7.8 Feedback dependence on grating position in the pulsed case. Peak pulse intensity occurs near the long wavelength end of the 1.3 Å tuning range over one chip mode.

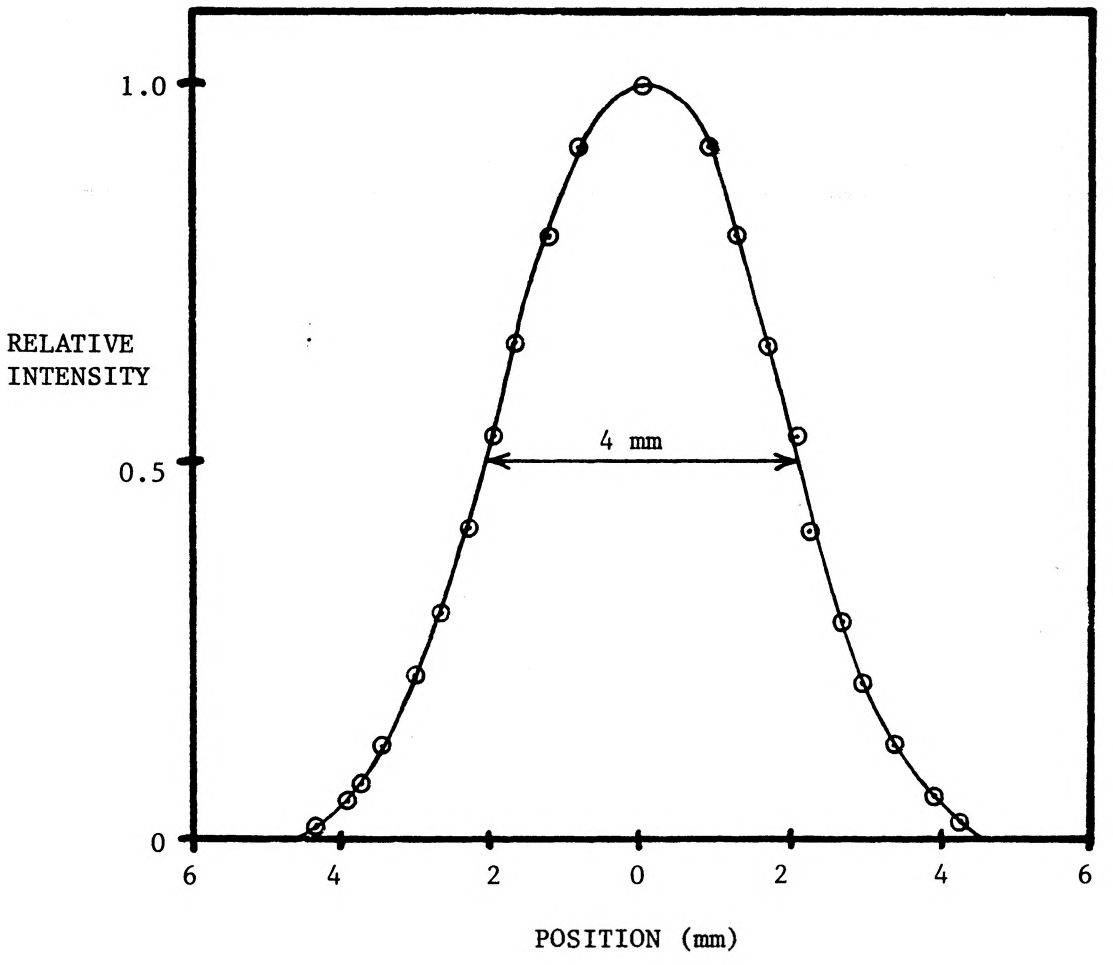

FIGURE 7.9 Profile of the output intensity for the grating external cavity.

pulses and reduce the effective time delay due to the grating angle. The 76 ps FWHM pulse response of the direct modulation scheme used in this work does not allow for closer experimental examination of the pulse width increase due to the grating.

Both small and large comb generator modulation regimes were investigated experimentally. For small peak current pulses (I_p = 32 mA), dc bias in the vicinity of the external cavity threshold was required for significant injection locking to occur. The frequency tuning characteristics with the grating tuned to the most intense mode for I_p = 32 mA and I_{dc} = 37 mA are shown in Figure 7.10. Pulse shortening at modulation frequencies below the cavity round trip frequency results in a minimum pulse FWHM of about 46 ps. This is the same pulse width as was achieved using large comb generator pulses (I_p = 228 mA) in a direct modulation scheme. The pulse shortening reaches an optimum for a modulation frequency below that which gives the most intense pulses. The higher inversion available at slightly higher modulation frequency as the peak of the optical pulse approaches the peak of the inversion results in more intense pulses, but not as significant pulse shortening. At lower frequencies, the inversion can no longer support short pulse lengths with the large phase shift required to compensate for the difference between the modulation frequency and the round trip frequency.

Because the risetime of the inversion between optical pulses is determined by the injected carrier lifetime and the dc bias level, the CW feedback conditions are not attained between optical pulses.

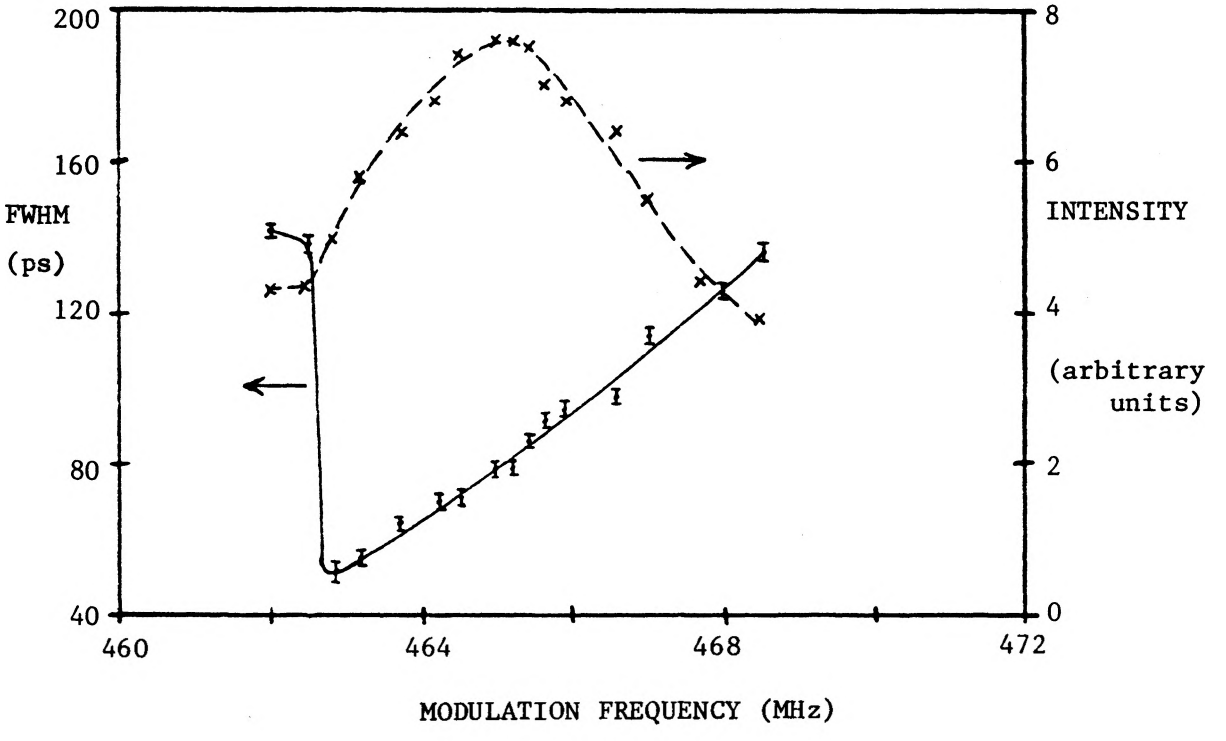

FIGURE 7.10 Tuning characteristics for small pulse modulation (I_p=32mA) biased above the grating external cavity threshold current (I_{dc}=37mA, I_{the}=35mA).

The inversion would be required to return to the no-feedback threshold level for gain recovery to cause lasing between pulses since the optical feedback is only present at short intervals whose frequency is determined by the round trip time of pulses in the external cavity. Since the dc bias level is $\sim$ 8 mA below the no-feedback threshold, no secondary pulses occur in the pulse train due to gain recovery between the injection locked pulses.

Several aspects of the tuning behaviour of the grating cavity locked diode laser will be discussed. The higher average inversion in the pulsed case relative to the CW case gives a change in the position in wavelength of the chip modes. The lower refractive index associated with higher injected carrier density reduces the mode spacing. The difference between the CW and pulsed tuned feedback wavelengths seen experimentally is a maximum of 2 Å for the case of large modulation with dc bias below threshold. An increase in dc injection current also induces a lower refractive index. The negative index change reduces the effective length of the diode chip, and slightly increases the optimum tuning frequency. The dependence of wavelength and frequency tuning on the pulsed and CW levels of carrier injection suggests that the tuning frequency is dependent on the selected wavelength. All of these tuning effects are seen experimentally and must be considered if optimum tuning is to be achieved when one or more of the dependent parameters is changed.

In the previous section of this chapter, it was shown that injection locking of a laser diode coupled to a mirror external cavity produced 20 ps FWHM optical pulses of nearly 200 mW peak power when large peak current pulses were superimposed on a below threshold dc bias. The same pulse regime can be used for grating-cavity locking to produce pulses of similar FWHM and peak power, but with a much narrower dynamic spectral width. The optical pulse dependence on the size of the modulation is shown in Figure 7.11 for approximately constant average optical power. The output FWHM decreases rapidly with increasing pulse peak to a minimum pulse width of 22 ± 5 ps with 180 mW peak power. A signal averaged sampling oscilloscope trace of the shortest detected pulse is shown in Figure 7.12. The ringing in the trace is a property of the ultrafast photodiode used. The detected FWHM of 79 ps measured by the microprocessor controlled signal averaging unit is a convolution of the 76 ps Gaussian detection system response and the actual optical pulse.

The measured frequency tuning characteristics for grating cavity locking with large modulation and below threshold dc bias are shown in Figure 7.13. The tuning displays essentially the same behaviour as was discussed for the small modulation case. The flattening of the optical pulse FWHM and intensity in the region of optimum tuning suggests that the pulses have reached the detection limit of the system response. If this is the case, the deconvolved pulse FWHM given is a significant overestimate for the shortest duration pulses obtained. An alternative explanation of the flat region in the tuning is that the effect of the

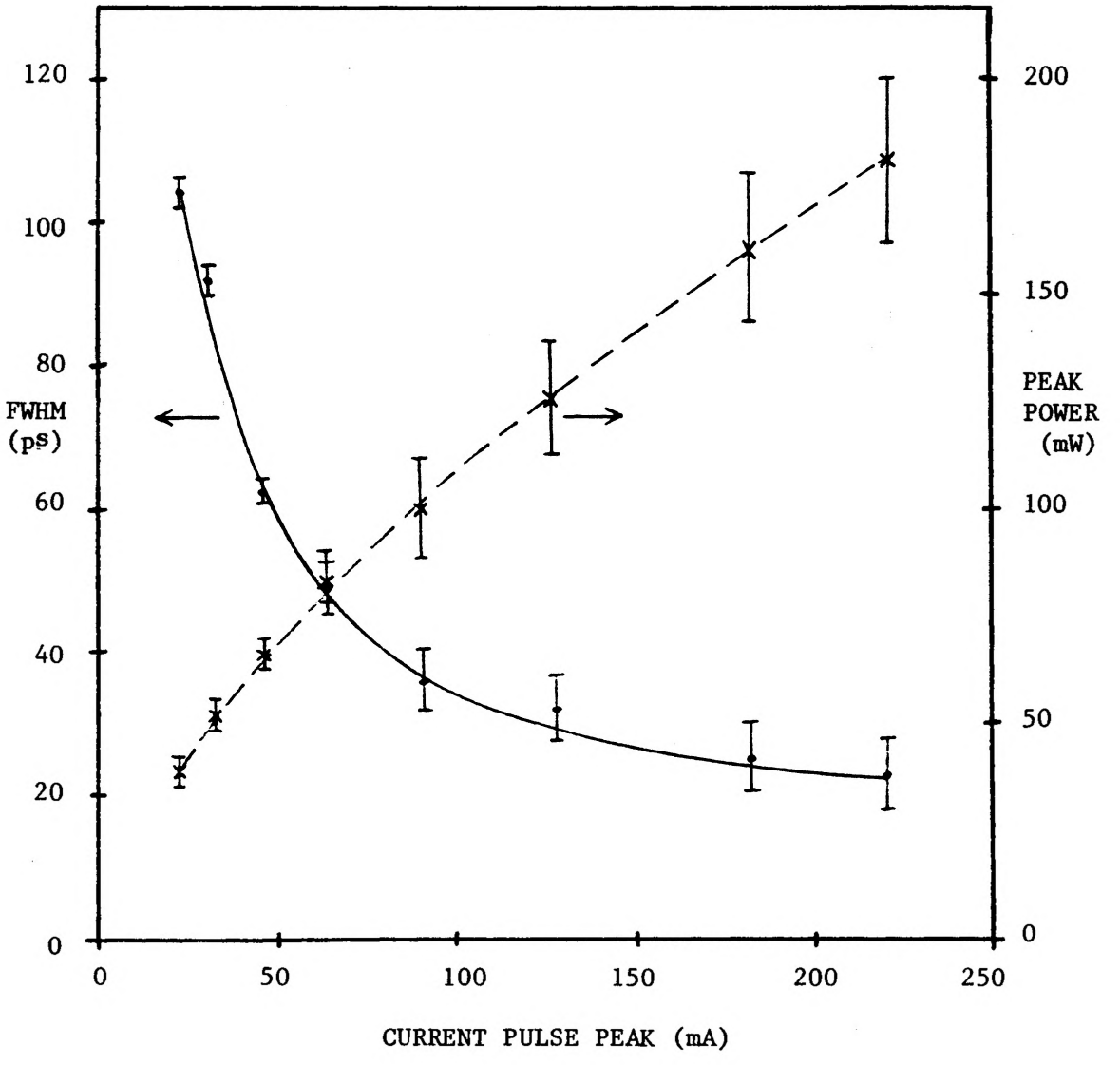

FIGURE 7.11 Optical pulse FWHM and peak power versus current pulse peak for grating cavity injection locking. The average optical power is approximately constant in each case.

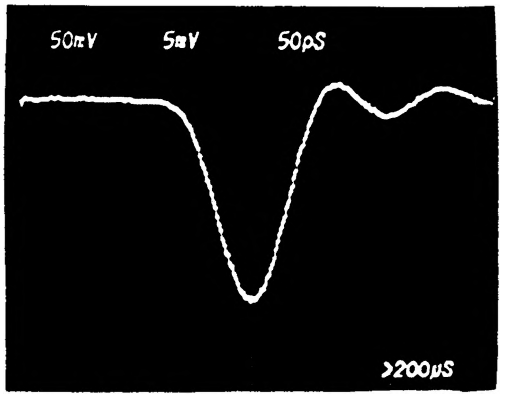

FIGURE 7.12 Detected optical pulse convolved with the 76 ps FWHM system response. The measured FWHM is 79 ps, yielding a 22±5 ps FWHM optical pulse assuming gaussian pulses. (I_{the}=35 mA, I_{dc}=30 mA, I_{p}=228 mA)

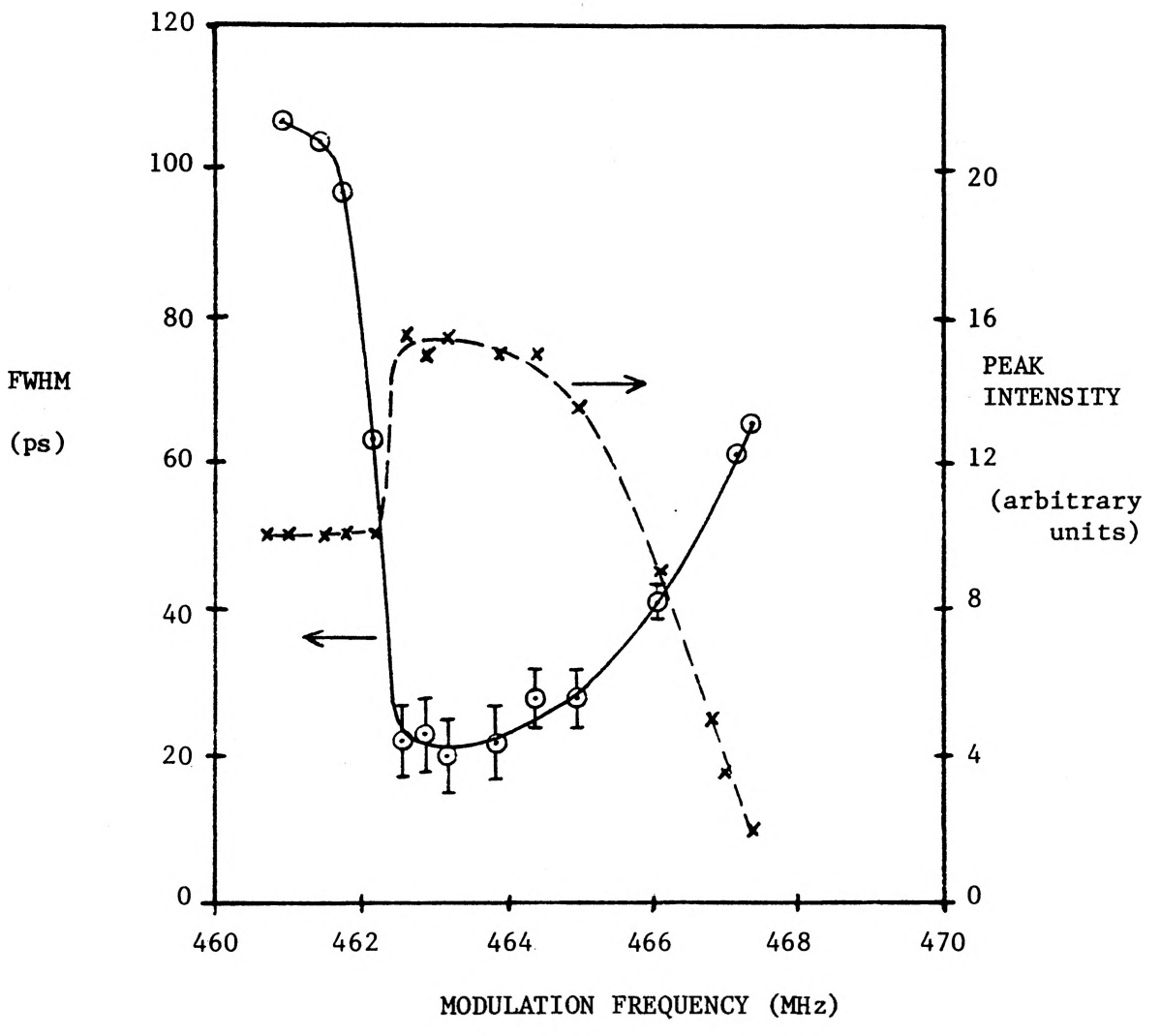

FIGURE 7.13 Tuning characteristics for large comb generator modulation (I_p=228mA) of a grating cavity coupled diode laser biased below the external cavity threshold current (I_{dc}=30mA, I_{the}= 35mA).

variable path length at the grating becomes more significant for the shortest pulses detected. These alternatives cannot be distinguished with the current direct detection scheme due to the limits on temporal resolution.

Since the frequency tuning range which results in the most intense optical pulses corresponds to the largest decrease in inversion during the pulse, dynamic broadening of the single chip FP mode should be largest for the most intense pulses. The time averaged spectral width is measured using a 0.5 m grating monochromator with 0.25 Å resolution and an avalanche photodiode with high gain (40x) at the exit slits. The dynamic spectral width versus modulation frequency for both small and large modulation of the diode in the grating cavity is shown in Figure 7.14. In both cases, the spectral width is greatest in the region of the most intense optical pulses. For small modulation, the maximum spectral width measured is 1 Å, which is significantly less than the maximum 1.4 Å spectral width resulting from large modulation. Comparing the dynamic spectral width for grating cavity locking to that resulting from either direct modulation or mirror cavity locking shows that the wavelength dependent feedback has a significant effect on the extent of the wavelength chirp caused by the high injected carrier density. A time averaged spectral scan of the grating cavity output for large modulation at the frequency which gives the greatest chirp along with sampling oscilloscope traces of the wavelength resolved optical pulse are shown in Figure 7.15. A time average of the output pulse is shown for approximately equal wavelength steps through the 1.4 Å spectral

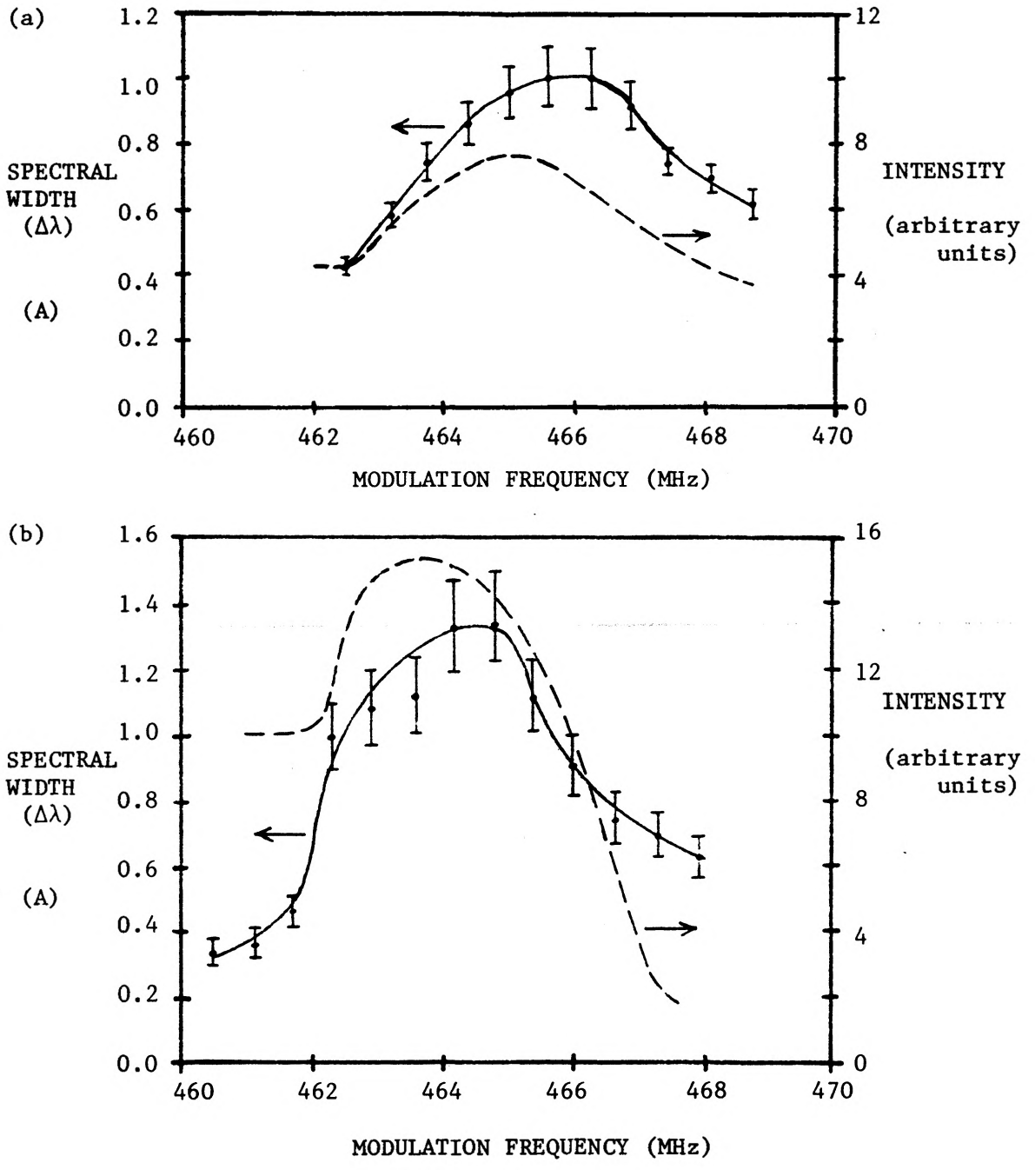

FIGURE 7.14 Spectral width and intensity versus modulation frequency for small pulse above threshold bias conditions (a) and for large pulse below threshold bias conditions (b).

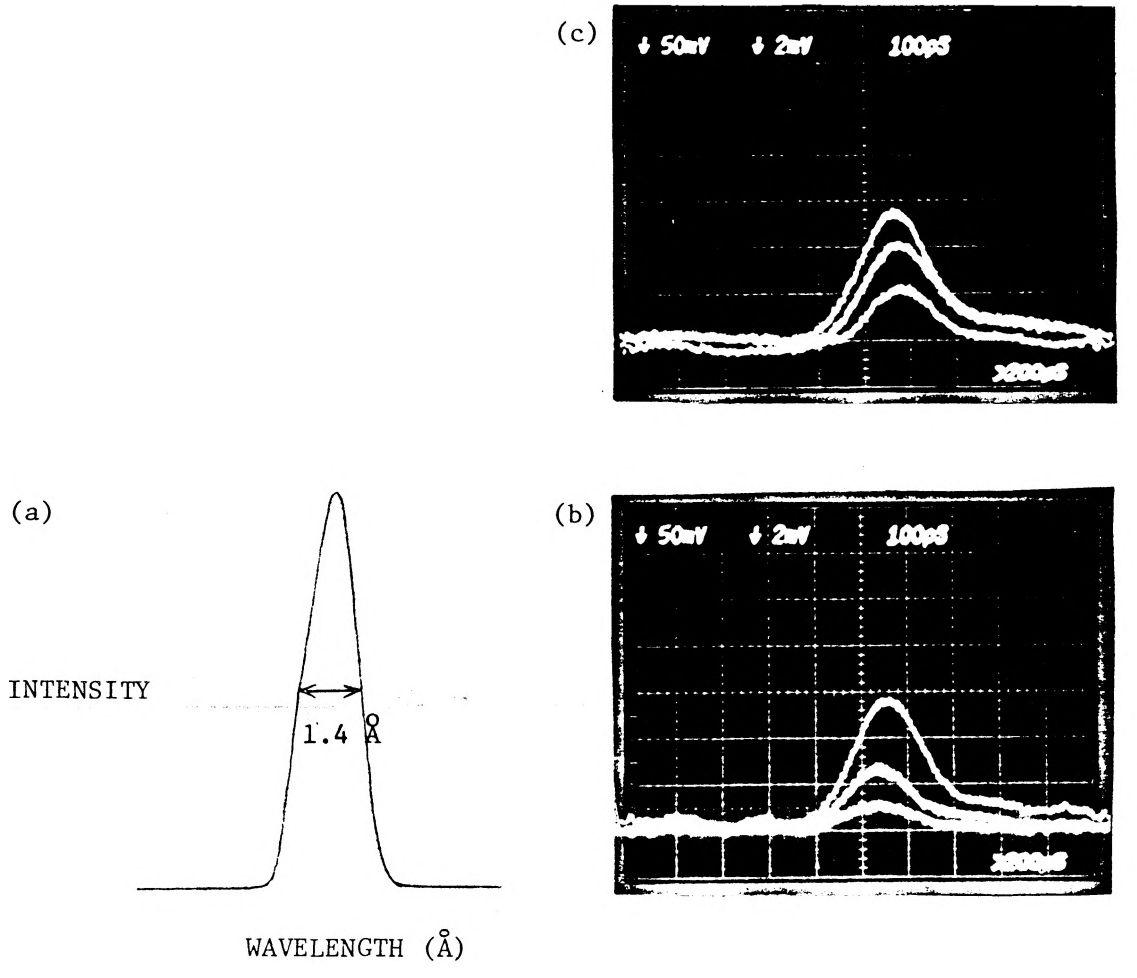

FIGURE 7.15 The maximum dynamic spectral width measured for large pulse operation is shown in (a). The wavelength resolved pulsed is shown for the short wavelength (b) to the long wavelength (c) end of the chirp at approximately equal wavelength steps. The current pulse peak I_p=228 mA, bias current I_{dc}=30 mA.

width of the pulse. The avalanche photodiode used gives the large detected pulse FWHM at its high gain setting. The peak of the detected pulse moves to longer wavelength at later time because of the chirp of the output pulse. The extent of the chirp in time is given by the roughly 30 ps shift of the detected pulse peak with wavelength. The pulse FWHM for the maximum chirp is therefore approximately 30 ps, which corresponds to the output at a modulation frequency slightly above resonance.

The bandwidth limitation imposed by the grating external cavity can be discussed qualitatively by considering the effect of the wavelength resolution of the feedback on the spectral dynamics of the diode. For the case of non-wavelength selective optical feedback, the magnitude of the inversion decrease during the optical pulse determines the size of the change in refractive index. The increasing refractive index in the active region results in movement of the chip modes to longer wavelength because of the effective length increase of the chip FP cavity. The lasing mode moves to the new wavelength as the refractive index increases since the FP losses are minimized there. Optical feedback from the external grating reduces the extent of the chirp since it changes the wavelength range for which minimum losses in the diode chip occur. At some point during the rapidly increasing inversion, the short wavelength end of the optical feedback induces lasing of a chip mode of the same wavelength. As the photon density builds up in the chip cavity, the gain begins to saturate causing an inversion decrease which in turn results in an increase in the refractive index of the cavity.

The FP losses in the chip cavity favour a shift of the lasing mode to longer wavelength. However, the optical feedback present from the external grating reduces the chip losses at a slightly shorter wavelength than that selected by the new FP conditions. Since the loss reduction induced by the optical feedback is large, the wavelength selective feedback causes a significant pulling of the lasing mode to shorter wavelength than given by the changing chip FP conditions. The extent of the wavelength chirp can therefore be limited to the wavelength resolution of the optical feedback. The resolution of the grating feedback has been calculated to be 1.0 ± .2 Å in Chapter 4, in good agreement with the maximum 1.4 Å chirp measured experimentally.

The time bandwidth product for Fourier transform limited pulses is $\Delta\omega\Delta t = 0.42$ assuming Gaussian pulses and $\Delta\omega\Delta t = 0.11$ for single sided exponential pulses. The minimum detected pulse lengths of 22 ± 5 ps correspond to a time bandwidth product of 0.95 ± .2. Further bandwidth restriction due to the feedback may therefore result in transform limited optical pulses.

7.5 1 GHz Injection Locking

It has been illustrated in [25] that it is possible for the pump pulse frequency to be an integral multiple of the round trip frequency for an injection locked laser. The necessary conditions for obtaining an output pulse at a repetition frequency twice that of the 500 MHz comb generator modulation are investigated here for the case of grating cavity feedback. The 1 GHz pulse train is produced by

shortening the grating cavity to 15 cm, resulting in a current pump pulse for every two round trips of the optical pulse in the external cavity. Biasing of the diode laser near the external cavity threshold is necessary so that optical pulses which are fed back to the diode between pump pulses do not experience too much loss. A significant fraction of the initial output pulse must be present after two round trips in the resonator to give injection locking of the diode.

Two important parameters for injection locking at a multiple of the modulation frequency are the dc current level and the current pulse peak. The importance of these parameters can be shown by considering the dynamic characteristics of the isolated diode biased above threshold. For increasing current pulse peak, the time required for the inversion to recover to its threshold value increases (Figure 7.16(a)). This time lag can be reduced by increasing the dc current (Figure 7.16(b)). The combination of appropriate dc current and current pulse peak necessary for obtaining a train of almost equal optical pulses is dependent on whether the inversion has recovered sufficiently between pump pulses to maintain unity optical gain for every two round trips in the compound cavity.

An example of the pulse train obtained experimentally for I_{dc} = 37.5 mA and I_p = 64.3 mA is shown in Figure 7.17(a). The effect of reduced feedback on the relative peak of the synchronously pumped and echo pulses is shown in Figure 7.17(b). Greater optical feedback causes the echo of the initial optical pulse to saturate the gain more

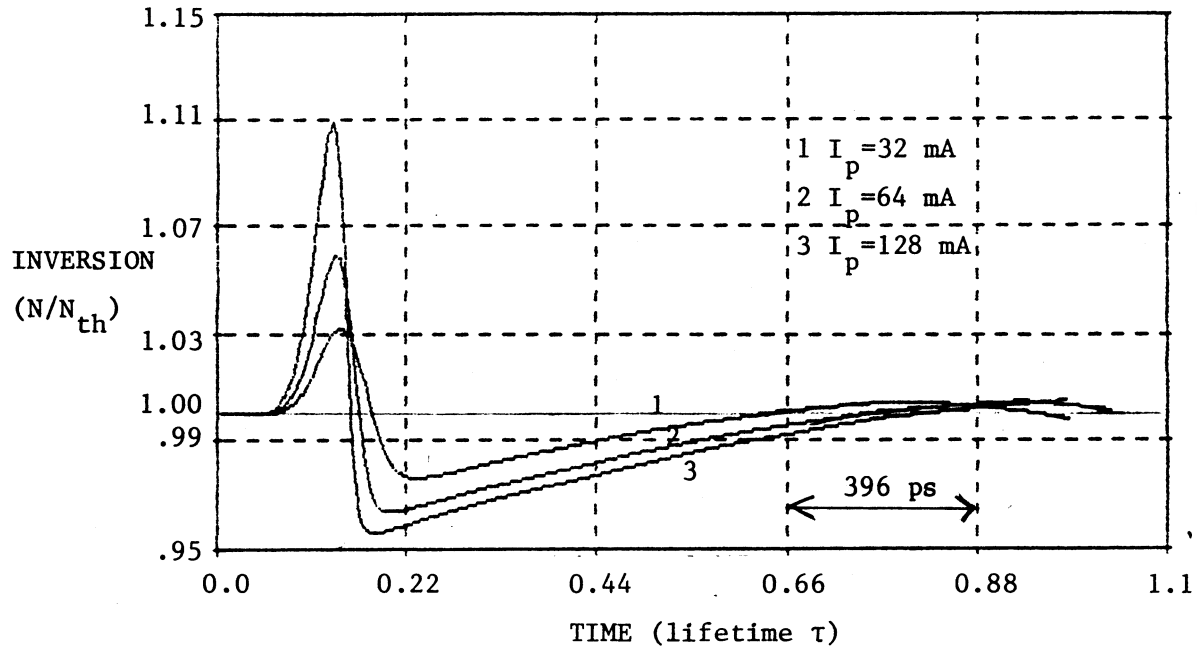

FIGURE 7.16(a) Gain recovery is slower for increasing current pulse peak I_p. (I_{th}=35 mA, I_{dc}=37 mA)

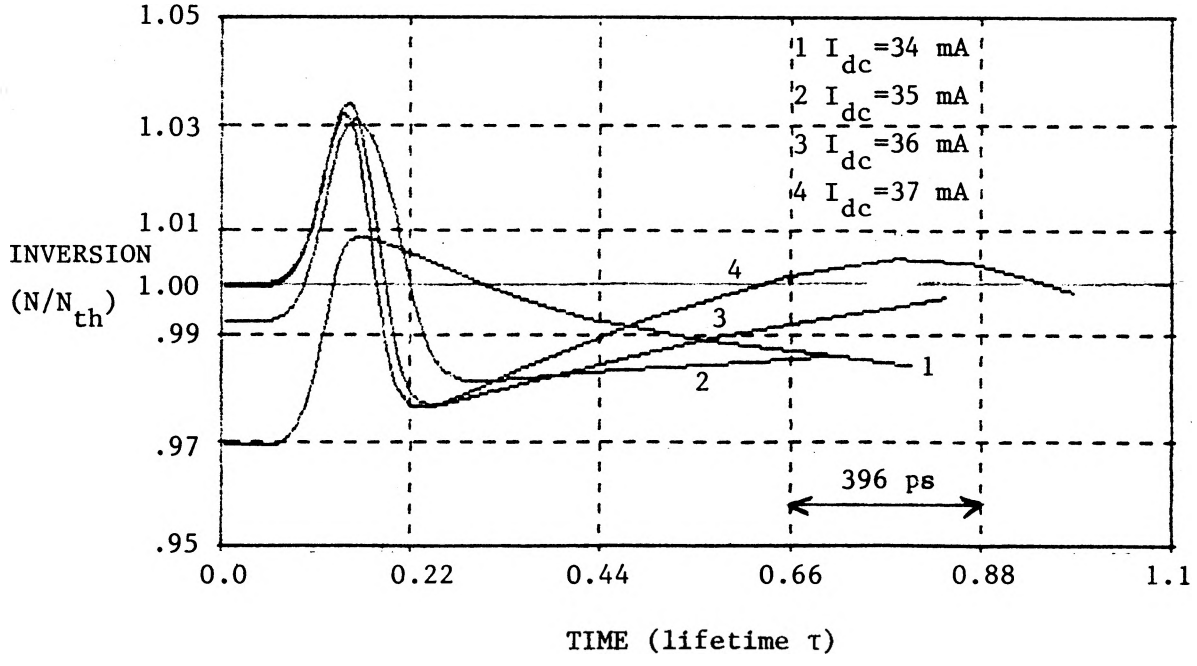

FIGURE 7.16(b) Gain recovery is faster for higher bias current I_{dc}. (I_{th}=35 mA, I_p=32 mA)

(a)

(b)

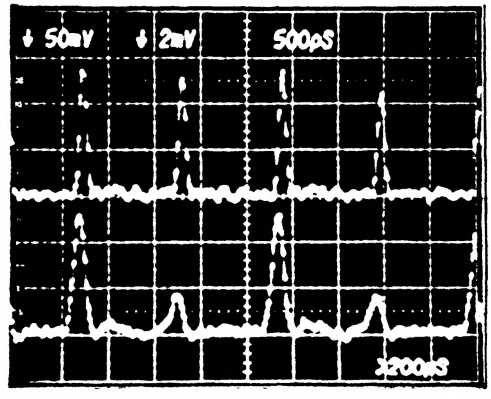

(c)

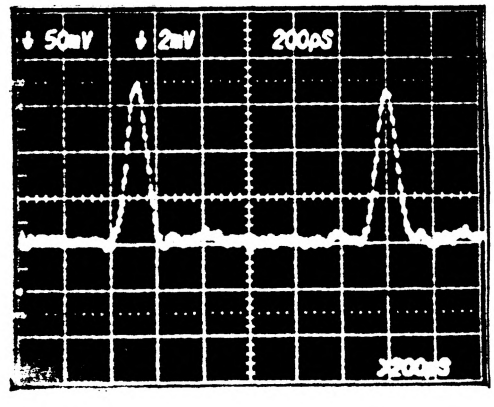

FIGURE 7.17 The two pulse trains obtained with a 15 cm long grating cavity are shown in (a) and (b). Case (b) is for lower feedback at the short wavelength end of the tuning (over a single chip mode) while (a) is the tuned case at the long wavelength end. Case (a) is shown on an expanded scale in (c). (I_{the}=35 mA, I_{dc}=37.5 mA, I_{p}=64 mA)

than for a small feedback pulse. This gives a larger decrease in the inversion, which in turn reduces the initial inversion available for the next pumped pulse. When steady state is reached, the peak inversion for both the pumped pulse and the echo is maintained at nearly the same level, producing nearly equal optical pulses.

7.6 Injection Locking Simulations

A modification to the rate equation model discussed earlier in this thesis was made in order to include the effect of external optical injection into the active region. A Gaussian pulse shape was chosen to represent an optical pulse which is injected back into the diode laser from an external reflector. This requires addition of an injection term (7.1) to the equation for the rate of change of photon density in the diode (7.2).

$$R(\lambda) = P_o \exp\{-\frac{1}{2}[(t-t_o)/\sigma]^2\} \tag{7.1}$$

$$\frac{dS(\lambda)}{dt} = gNE(\lambda) + [A\sigma(\lambda)\ (N-N_o) - (\alpha+\Gamma)]\ S(\lambda)\ N\sigma(\lambda) + R\ (\lambda_o) \tag{7.2}$$

To eliminate the infinite tails of the Gaussian pulse which would contribute to the background photon density in the chip cavity, the contribution of the optical injection term is only included when it exceeds 2 percent of its peak value. To represent optical feedback from an external grating, the optical injection is assumed to all be into a single chip mode. The input to the program includes the injected optical pulse FWHM, the peak input pulse power, and the position of the

peak of the pulse in time relative to the peak of the inversion (attained with no feedback). From the program output, the percentage change in pulse FWHM, percentage change in peak intensity (the optical gain), and the shift in time of the peak of the pulse are determined.

Simulation of the frequency tuning characteristics for large modulation of a diode laser coupled to a grating external cavity are carried out using a non-iterative technique. An iterative program in the time domain would require too many round trips to reach steady state, and therefore too much computer time to be feasible. A frequency domain solution is difficult because of the difficulty in representing the short comb generator pulses in the frequency domain. However, constraints on the relative pulse FWHM and optical gain can be imposed to yield self-consistent injection locking solutions using the rate equation model which includes external injection of an optical pulse. No change in optical pulse FWHM after each round trip in the cavity is required for the steady state solution. For simplification of the simulations, the effect of the grating on the optical pulse FWHM obtained is ignored. It is anticipated that the grating effect will not change the tuning characteristics significantly since the steady state solutions will shift to a slight pulse shortening for each round trip to compensate for the increase in pulse FWHM due to the grating. Unity optical gain in the compound cavity is also required for steady state injection locking of the diode. The effective mirror loss in the compound cavity can be considered as the factor determining the necessary optical gain from the diode on each round trip. Multiple reflections in the external

resonator give an effective reflectivity for the facet-grating pair. The inverse of the effective power reflectivity on the resonator side is essentially the required optical gain since the back facet of the diode is highly reflecting (R_1 = 0.95).

The tuning characteristics are calculated as follows. Optical pulses of various FWHM and peak power are injected at selected times relative to the peak of the rapidly increasing inversion due to the pump pulse. The inversion due to the pump pulse with no feedback present is shown in Figure 7.18. For each point in time in the inversion where the peak of the injected optical pulse occurs, there is an injected pulse FWHM and peak power which satisfies the steady state solution requirements of no change in pulse width and unity round trip optical gain. The shift in time of the peak of the output pulse relative to the input translates into the appropriate frequency offset from the cavity round trip frequency. An example of the program output leading to a steady state solution for a particular injected pulse position in time is given in Figure 7.19.

Two simulations of the tuning characteristics were done for large comb generator modulation (I_p = 228 mA) of the diode biased below the grating external cavity threshold current (I_{the} = 35 mA). The frequency tuning behaviour shown in Figure 7.20 uses an optical gain requirement of about 1.2, which corresponds to the reciprocal of the calculated effective power reflectivity due to the compound cavity. This results in a tuning range which is approximately a factor of two

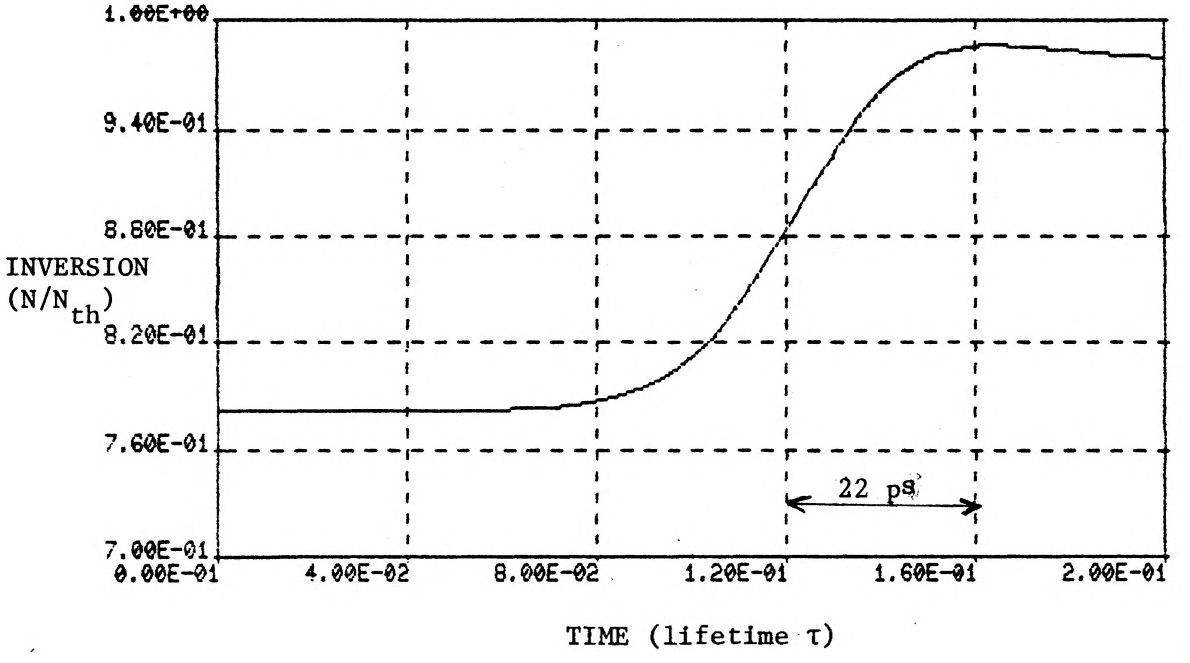

FIGURE 7.18 Rising edge of the inversion with no optical feedback.

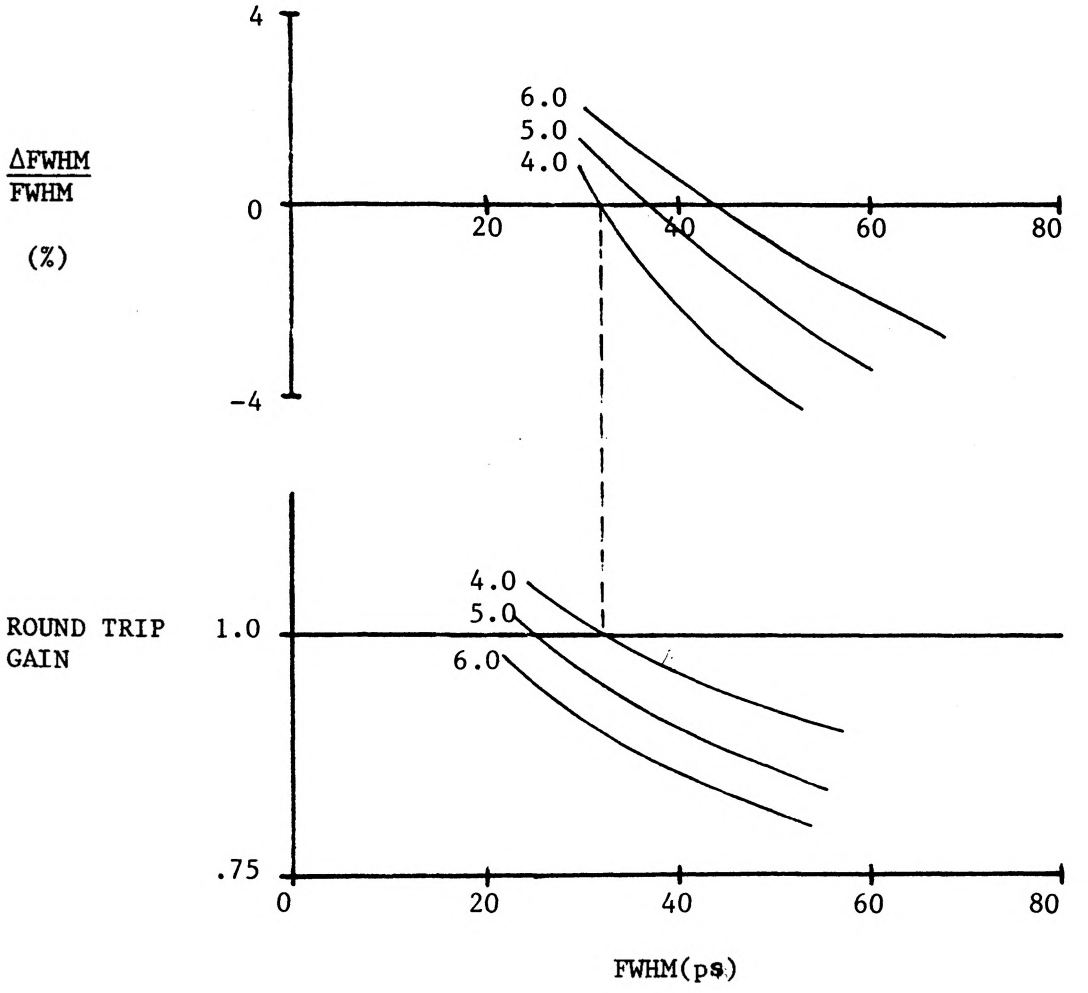

FIGURE 7.19 Program output is shown which gives the self consistent solution indicated for a unique pulse FWHM (32 ps) and pulse peak (4.0≃200 mW).

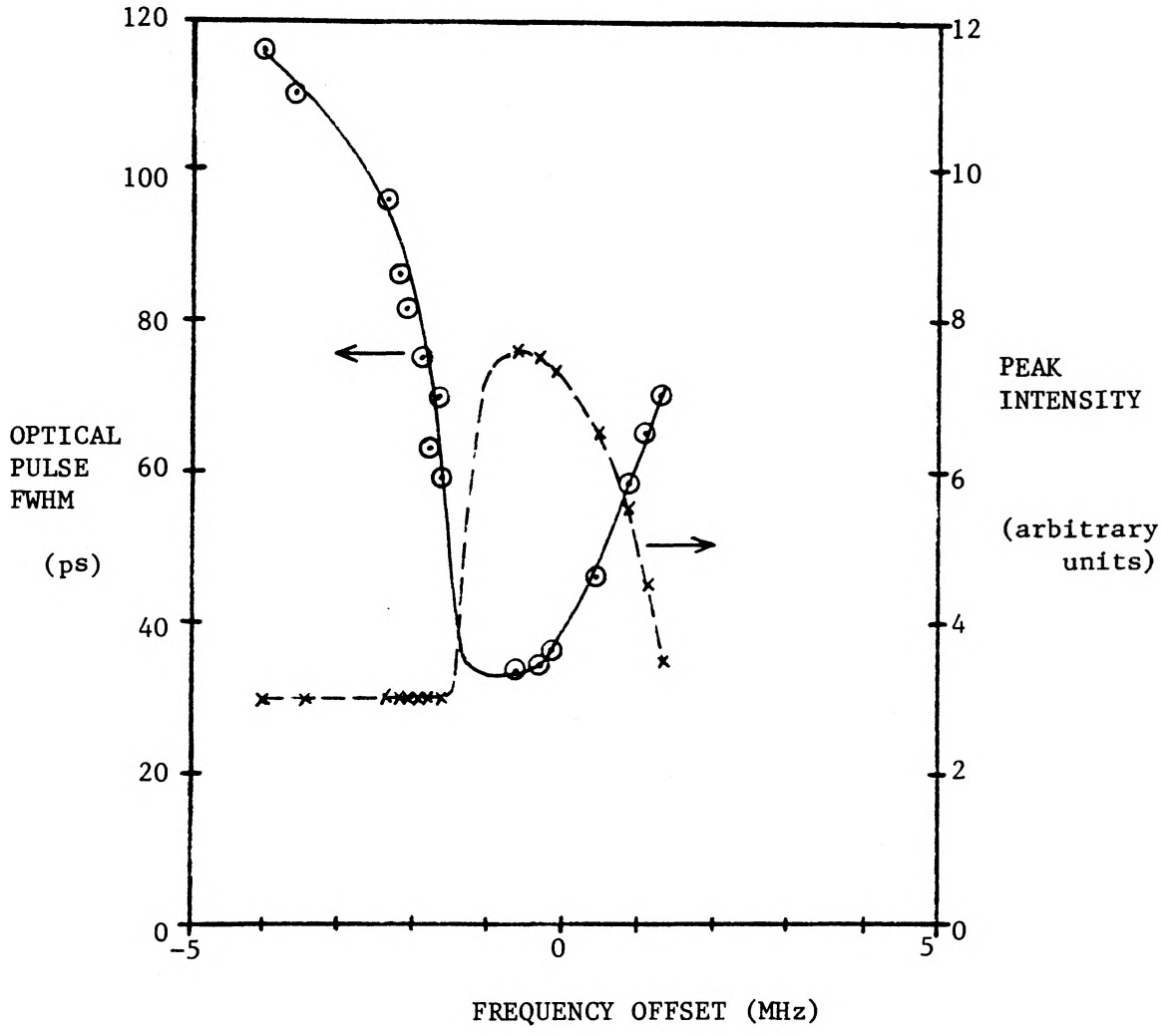

FIGURE 7.20 Simulated tuning characteristics for grating cavity injection locking assuming an optical gain requirement of 1.2. The maximum intensity corresponds to a peak power of approximately 394 mW.

narrower than that measured experimentally (see Figure 7.13), as well as a peak power which is about a factor of two greater than the 180 mW measured. Attributing the total loss reduction produced by the external reflector to a combination of a reduced effective reflectivity of the grating (50 percent lower) plus a reduction in waveguide (i.e. mode propagation) losses in the diode cavity, as discussed earlier in Chapters 4 to 6, gives the tuning characteristics shown in Figure 7.21. Reduction of the effective reflectivity of the grating results in an increased optical gain requirement of 2.0 to achieve steady state oscillation. The reduction in waveguide losses essentially reduces the bulk inversion required to reach threshold gain. The result is a tuning range and peak power much closer to those seen experimentally. Consideration of the actual sizes of the photon feedback term from the external reflector relative to the total loss reduction in the external cavity operated diode is again shown to be significant for obtaining accurate simulations of the injection locking characteristics.

7.7 Summary

Of the pulsing schemes investigated in this work, grating external cavity injection locking using a round trip frequency synchronous with the 500 MHz comb generator repetition rate produces the shortest, highest peak power optical pulses with the narrowest dynamic spectrum. The dynamic spectral broadening of a single chip FP mode due to the carrier induced change in refractive index during the optical pulse can be limited by the bandwidth of the optical feedback. The time bandwidth

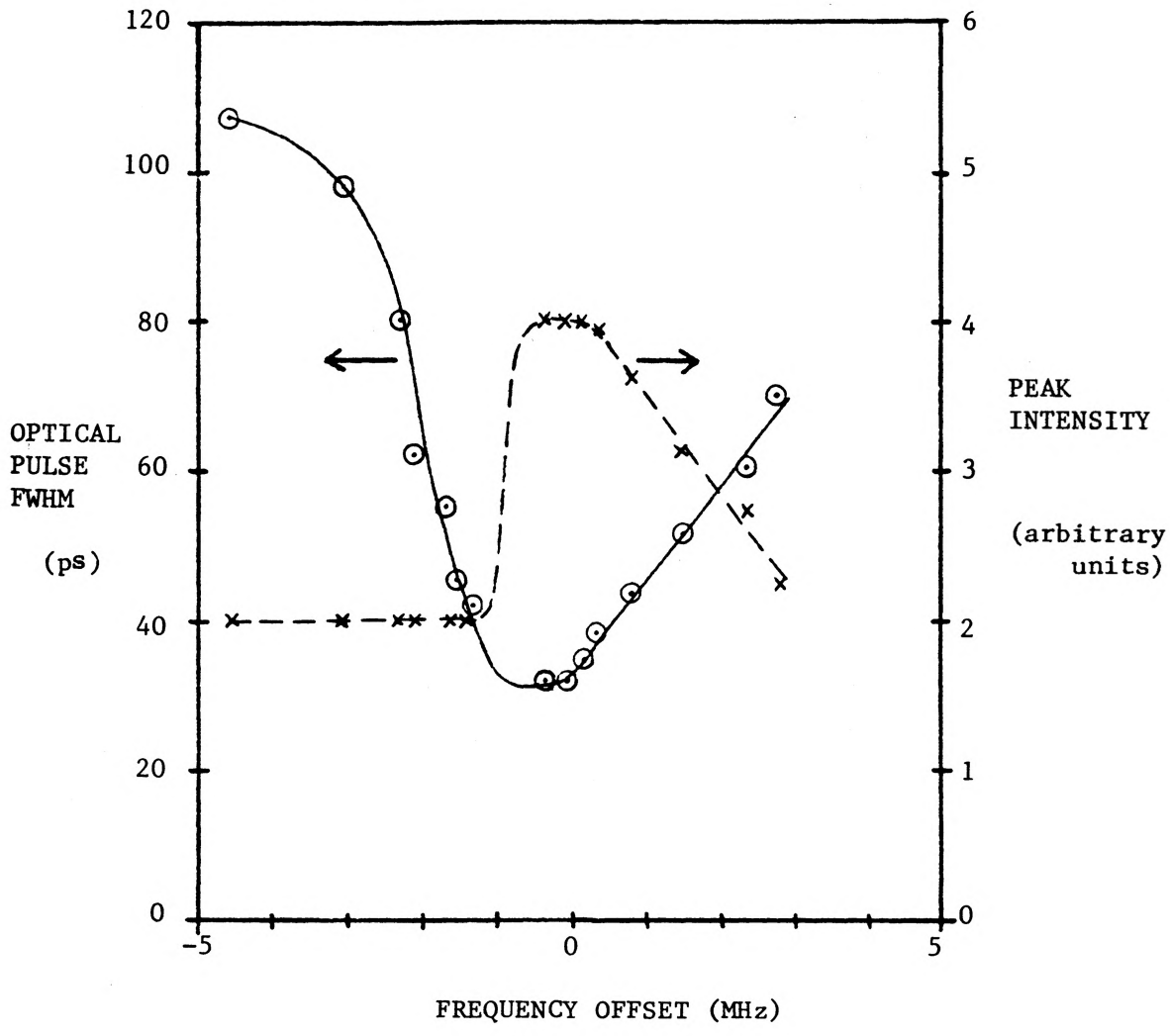

FIGURE 7.21 Simulated tuning characteristics assuming an optical gain requirement of 2.0. The maximum intensity corresponds to a peak power of approximately 207 mW.

product for the 22 ± 5 ps FWHM 180 mW peak power optical pulses obtained is 0.95 ± .2, which is close to the Fourier transform limit of 0.42 for Gaussian pulses. The shortest pulse lengths detected may be limited by a combination of the variable time delay due to the grating angle, the pulse broadening due to the finite oscillator stability (as discussed in Chapter 6), and the sensitivity of the actual pulse FWHM to the deconvolution of the measured pulse from the detection system response. The shortest optical pulses obtained have reached a limit where autocorrelation or ps streak camera techniques are necessary to resolve the pulse FWHM limitations, for grating cavity injection locking.

Simulations of the tuning characteristics for 500 MHz grating cavity injection locking are in good agreement with experiment when the effective loss reduction due to the external reflector is considered as consisting of approximately equal mirror loss reduction and waveguide loss reduction terms. Consideration of the reduction in waveguide loss due to the coupling of light back into the chip cavity is important in obtaining accurate simulation of dynamic effects in an external cavity operated diode.

CHAPTER 8

CONCLUSIONS

The effect of several external feedback schemes on the CW and pulsed operation of semiconductor lasers is investigated in this thesis. The results of this thesis are summarized in this chapter.

The regenerative pulsing scheme discussed in Chapter 3 produces a train of 55 ± 5 ps FWHM optical pulses at a repetition frequency of 10 to 100 MHz. The significant reduction in the minimum optical pulse width obtained using optoelectronic feedback is due to the use of a lower threshold laser (I_{th} = 37 mA) and difference pulse conditions than in previous work. A model which was developed to carry out simulations of the optoelectronic feedback loop using measured circuit and laser parameters gives oscillation characteristics similar to those seen experimentally. The results of simulations indicate that use of a 20 mA threshold laser to achieve higher current peak overdrive relative to threshold ($I_p = 6I_{th}$) and the use of narrower current pulses (FWHM ≈ 140 ps) will result in approximately 25 ps FWHM optical pulses using optoelectronic feedback. An approach which integrates laser, waveguide, detector, and amplifier onto a single substrate may lead to a practical source of short optical pulses with very good repetition frequency stability.

The effect of multiple reflections in a compound cavity made up of a diode laser coupled to an external reflector is evaluated in Chapter 4. The chip mode linewidth is shown to increase with dc bias to some limiting value dependent on the level of feedback from an external mirror, in agreement with a theory based on optical interference effects. The dependence of the threshold current on the optical feedback is also shown to be in agreement with the discussed theory. The spectral linewidth of a diode coupled to a grating cavity is found to be essentially that of the isolated diode, and is not dependent on optical interference effects. An important effect induced by both types of optical feedback is a reduction in the mode propagation loss in the chip cavity, possibly due to an increase in the mode size which decreases the diffraction losses, and possibly due to a spatial shift of the lasing region to a region with lower loss. The relative size of the waveguide loss reduction to the total loss reduction is important in finding the actual mirror loss reduction, whose magnitude determines the size of the delayed photon feedback term for simulations of the laser diode dynamics in an external resonator.

Grating external feedback is used as a probe of the optical gain in Chapter 5. Measurements of the dependence of the output intensity for various wavelengths on the dc bias and the level of optical feedback results in a representation of the diode gain which includes a significant wavelength dependent background loss term. This representation is shown to have no appropriate place in a discussion concerning the size of the actual mirror loss reduction relative to the

total loss reduction induced by the external feedback. It is thought to be the reduction in waveguide loss induced by the external feedback which increases the total loss reduction, and in turn causes the calculated effective external mirror reflectivity to be an over-estimate of the actual mirror reflectivity. Also, in Chapter 5, a technique for directly measuring the diode gain (using grating feedback) which avoids problems with diode temperature fluctuations encountered in other work results in a significant improvement in the agreement between tmeasured and theoretical gain curves. The use of grating feedback to measure the diode gain gives an alternative method to the standard Hakki and Paoli type gain measurement which requires a much higher dynamic range and better resolution of the measurement apparatus.

Experiments on the effect of reduced optical feedback from a mirror external cavity on the modulation tuning characteristics of a laser diode with a partially anti-reflection coated facet ($R_2 \simeq 0.11$) are compared to the results of simulations in Chapter 6. The waveguide loss reduction used in simulations is equal to the actual mirror loss reduction induced by the optical feedback. The relative size of these two terms is in agreement with values found experimentally in other work for the same type of lasers. The excellent agreement between model predictions and the measured tuning characteristics for varying feedback strongly supports calculations of the effect of different facet reflectivities on the tuning behaviour. The increased feedback coupling associated with lower facet reflectivity causes a significant increase in the rate of change of optical pulse position relative to the current

modulation, which accounts for the previously unexplained sensitivity of the modelocking process to oscillator stability.

Modulation of a laser diode at a repetition frequency in the region of 500 MHz with short, high peak current pulses was carried out to find the conditions necessary for producing very short FWHM optical pulses ($\leq$ 20 ps) with high peak power and a narrow dynamic spectrum. Since the dynamic spectrum of a pulsed diode laser is broad for high pumping, an optical feedback scheme is necessary to reduce the spectral width of the pulsed laser. Relative to injection locking within a mirror external cavity, grating cavity injection locking gives similarly narrow FWHM ($\simeq$ 22 $\pm$ 5 ps) and high peak power ($\simeq$ 180 mW) optical pulses. However, the bandwidth limitation imposed by the grating feedback determines the much narrower dynamic spectrum ($\Delta\lambda \simeq 1.4$ Å). The minimum optical pulse FWHM produced using grating cavity injection locking approaches the transform limit imposed by the bandwidth of the optical feedback. Therefore, a new method has been presented here for producing nearly transform limited pulses by injection locking a diode laser coupled to a grating external cavity.

A modification of the rate equation model used in this work for the laser dynamics which allows for external optical pulse injection into the active region makes it possible to simulate the modulation tuning characteristics of a grating cavity injection locked laser. Because of the difficulties inherent in attempting an iterative solution of the injection locking behaviour using short current pulse modulation,

a non-iterative approach is used. This approach seeks self consistent injection locking solutions which satisfy the steady state optical pulse FWHM and unity net gain requirements for each round trip in the compound cavity. This work is the first to present simulations of the tuning behaviour of an injection locked diode laser modulated with short, high peak current pulses. The good agreement between experiment and simulation again stresses the importance of the relative size of the waveguide and mirror loss reductions induced by external optical feedback.

In conclusion, this work has described the operation of laser diodes with various types of external feedback in both CW and pulsed modes of operation. It is hoped that the results described in this work will be of value to the use of semiconductor lasers in high speed optoelectronics, and in high data rate communication systems.

REFERENCES

1. J.C. Goodwin, "Diode Laser Dynamics", Ph.D. Thesis, McMaster University, Hamilton, Ontario, 1983.

2. H.C. Casey and M.B. Panish, "Heterostructure Lasers Part A: Fundamental Principles", Academic Press, New York, 1978.

3. R.N. Hall, G.E. Fenner, et al., Phys. Rev. Lett. 9, 366 (1962).

4. G.H.B. Thompson, "Physics of Semiconductor Laser Devices", John Wiley and Sons, New York, 1980.

5. H.C. Casey and M.B. Panish, "Heterostructure Lasers Part B: Materials and Operating Characteristics", Academic Press, New York, 1978.

6. J.C. Goodwin and B.K. Garside, "Threshold Variations in Diode Lasers Induced By External Resonator Feedback", IEEE J. Quant. Elec., Vol.QE-19, No.10, October 1983.

7. H. Kressel and J.K. Butler, "Semiconductor Lasers and Heterojunction LEDs", Academic Press, New York, 1977.

8. S.N. Crocker, M.Eng. Thesis, McMaster University, Hamilton, Ontario, 1984.

9. T. Paoli and J. Ripper, "Frequency Stabilization and Narrowing of Optical Pulses From CW GaAs Injection Lasers", IEEE J. Quant. Elec., Vol.QE-6, No.6, June 1970.

10. T. Damen and M. Duguay, "Optoelectronic Regenerative Pulses", Electron. Lett. 16, 166 (1980).

11. R.E. Park and B.K. Garside, "Regenerative Diode Laser Pulses", Applied Optics, Vol.21, No.1, January 1, 1982.

12. Hewlett Packard Application Note 918, "Pulse and Waveform Generation With SRD's".

13. B.K. Garside and R.E. Park, Optics and Laser Technology, April 1983.

14. A. Olsson and C.L. Tang, "Coherent Optical Interference Effects In External-Cavity Semiconductor Lasers", IEEE J. Quant. Elec., Vol.QE-17, No.8, August 1981.

15. J.H. Osmundsen and N. Gade, "Influence of Optical Feedback on Laser Frequency Spectrum and Threshold Conditions", IEEE J. Quant. Elec., Vol.QE-19, No.3, March 1983.

16. J.A. Russi, S.R. Chin, H. Heckscher, "High-Power Narrow Linewidth Operation of GaAs Diode Lasers", Appl. Phys. Lett., Vol.23, No.1, 1 July 1973.

17. N. Gade and J.H. Osmundsen, "Gain Measurements on Semiconductor Lasers By Optical Feedback From An External Grating Cavity", IEEE J. Quant. Elec., Vol.QE-19, No.8, August 1983.

18. B.W. Hakki and T. Paoli, "Gain Spectra In GaAs Double-Heterostructure Injection Lasers", J. Appl. Phys., Vol.46, No.3, March 1975.

19. J.P. van der Ziel, "Active Modelocking of Double Heterostructure Lasers in An External Cavity", J. Appl. Phys. 52(7), July 1981.

20. R.P. Salathe, "Diode Lasers Coupled to External Resonators", Appl. Phys. 20, 1-18 (1979).

21. P.T. Ho, L.A. Glasser, E.P. Ippen, H.A. Haus, "Picosecond Pulse Generation With a CW GaAlAs Laser Diode", Appl. Phys. Lett. 33(3), 1 August 1978.

22. H.A. Haus, "Modelocking of Semiconductor Laser Diodes", Jap. J. Appl. Phys., Vol.20, No.6, June 1981.

23. M.B. Holbrook, W.E. Sleat, T.J. Bradley, "Bandwidth Limited Picosecond Pulse Generation in an Actively Mode Locked GaAlAs Diode Laser", Appl. Phys. Lett. 37(1), 1 July 1980.

24. J. AuYeung, "Picosecond Optical Pulse Generation at Gigahertz Rates By Direct Modulation of a Semiconductor Laser", Appl. Phys. Lett. 38(5), 1 March 1981.

25. J. AuYeung, A.R. Johnston, "Picosecond Pulse Generation From A Synchronously Pumped Mode-Locked Semiconductor Laser Diode", Appl. Phys. Lett. 40(2), 15 January 1982.

26. Hewlett Packard Comb Generator, HP 33004A.

27. Optoelectronics Inc. Model SE-10.

28. J.P. van der Ziel, "Spectral Broadening of Pulsating $Al_xGa_{1-x}As$ Double Heterostructure Lasers", IEEE J. Quant. Elect., Vol.QE-15, No.11, November 1979.

29. C. Lin, T.P. Lee, C.A. Burrus, "Picosecond Frequency Chirping and Dynamic Line Broadening in InGaAsP Injection Lasers Under Fast Excitation", Appl. Phys. Lett. 42(2), 15 January 1983.